Vibrations from railway traffic
The Femern Belt Link

by Nikolaj Kiel

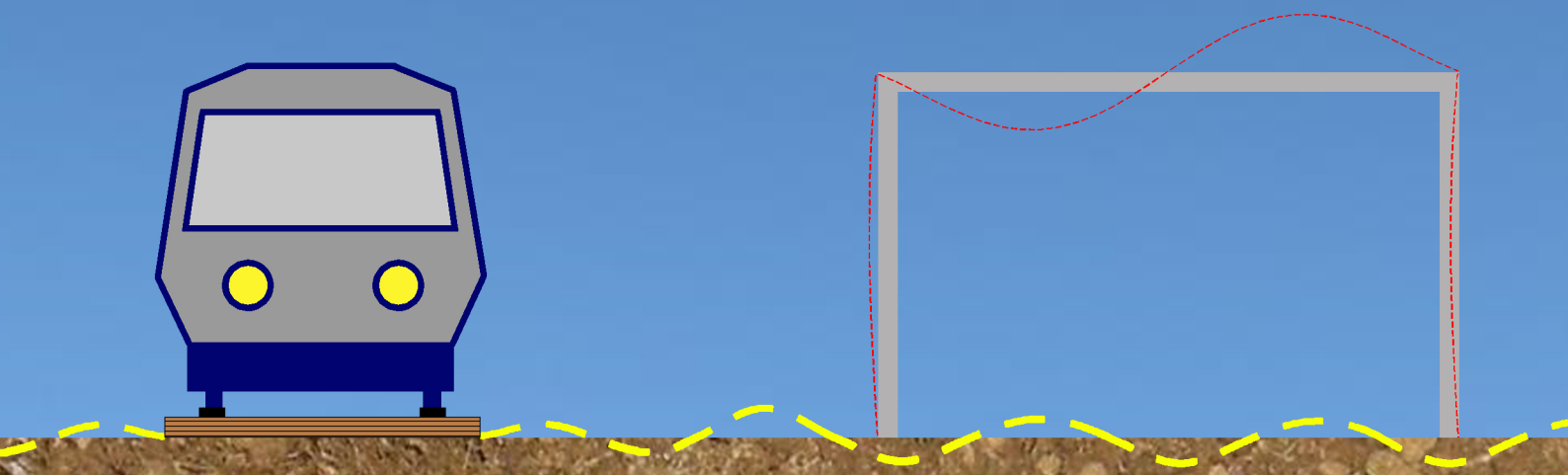

Aalborg University
School of Engineering and Science
Department of Civil Engineering
Structural and Civil Engineering
4th Semester, June 2011

Structural and Civil Engineering, 4th Semester
Department of Civil Engineering
Sohngårdsholmsvej 57, 9000 Aalborg
Telephone 9940 8530
www.bsn.aau.dk

Title:
Vibrations from railway traffic: The Femern Belt Link

Theme:
Master Thesis

Project period:
Spring 2011

Author:

Nikolaj Kiel

Supervisor:
Lars Andersen

Editions: 3

Number of pages: 96

Appendix: Appendix CD

Completed: 9th of June 2011

Synopsis:

This thesis concerns vibrations from trains running on the planned railway on the Danish side of the Femern Belt Link. The vibrations emanating from the passing trains are analyzed in relation to a reference building place 25m from a new planned railway. The amplitudes of the waves are evaluated on two soil profiles, as well as the response of two different structures, with different boundary conditions. The amplitudes are evaluate with respect to distance from the source to the reference building and frequency of the train load application, and especially the transmission of waves originated in the soil into the reference building is analyzed. The response of the soil and the structure is found in an uncoupled model, base on the Boundary Element Method and the Finite Element Method, as well as a coupled model combining BEM and FEM. It is found, that the response of the soil, is highly influenced by the response of the building near its natural frequencies. At the eigenfrequency of the structure, the response of the soil is balanced by reaction forces from the building in the coupled model. This can give rise to reductions of the soil response of up to 80% in the coupled model.

Preface

This mater thesis, under the title "Vibrations from railway traffic: The Femern Belt Link", is the documentation for the project work, at the 4th semester of the master degree, spring 2011, on the institute of Structural and Civil Engineering at Aalborg University.

Source references are made by the Harvard standard, as (writer, year of publication), with a possible specification to pages, equations etc. after the year of publication. Further information regarding the source references can be seen in the back of the report under the chapter "Bibliography", where the titles are sorted alphabetic after the writers last name.

Figures and tables are numbered in accordance with the chapter, which implies that, the first figure in chapter two for instance is called 2.1, the second 2.2 and so on. Unless otherwise is mentioned the figures and tables in the report are made by the group. The numbers are placed beneath the figure or table.

As a supplement to the main report there is an Appendix enclosed. Here elaborated informations regarding parts of the project are placed.

Documentation for the report can be found at the external CD-ROM. References to files on the DVD-ROM used in the project, are written in italic i.e. (*filename.type*). A description of the files on the CD-ROM can be found in (*Program info.txt*.

Summary in Danish

I dette afgangsprojekt, under titlen "Vibrationer fra jernbane trafik: Femern Bælt forbindelsen", er vibrationer oprindende fra menneskelig aktivitet, nærmere bestemt vibrationer fra jernbaner, blevet analyseret.
I forbindelse med en nye planlagte jernbane strækning fra Ringsted på Sjælland til Rødby på Lolland, som skal forbinde det danske tognet med det tyske via den kommende Femern Bælt forbindelsen, vil en kommende togstrækning skulle føres forbi eksisterende boligområder. I den forbindelse, ønskes det undersøgt, om en sådan vil forårsage generende vibrationer stammende fra passerende tog.
Energitabet fra togstrækningen til en reference bygning er blevet undersøgt, såvel som transmissionstabet ved bølgeovergangen fra jorden til konstruktionen er blevet undersøgt. Dette er undersøgt for forskellige konstruktioner på to jordprofiler med forskellige dynamiske egenskaber.
Via randelement metoden er bølgefeltet bestemt på jordoverfladen og i laggrænserne via en program pakke kaldet TEA. TEA er et randelement program, hvor bølgefelter kan bestemmes for forskellige geometrier. Via randelement metoden opnås en hurtig og præcis løsning, specielt for jordbundsgeometrier, grundet den begrænsede diskretisering af domænet, som kun foregår på randen. Transmitterende randbetingelser er en integreret del af randelement modellen, og dette muliggør en analyse af et bølgefelt i et endeligt domæne med en harmonisk linelast, idet energien tilført modellen kan strømme ud ved randen.
I forbindelse med brugen af randelement programmet, er der udført en konvergens analyse, hvor den nødvendige diskretisering af modellen og modellens udstrækning er bestemt. Ved diskretiseringen er det blevet bestemt hvor mange randelementer, der skal til at repræsentere en bølge for at få en konvergerende resultater med en given præcision. Det er yderligere fundet i hvor høj grad modellen bliver forstyrret af randen i modellen - både med hensyn til diffraktion omkring endepunktet af jordoverfladen, men også mht. refleksion på randen ved en lagdelt jord.
Reference bygningen er blevet modelleret i et finite element program konstrueret af forfatteren. Ved at påføre de fundne flytninger, langs fundamentet af reference bygningen, er bygningens dynamiske respons undersøgt for den ikke-koblede model. Konstruktionens dynamiske egenskaber vil vise sig ved dynamisk forstærkning ved visse frekvenser, hvor også den indbyrdes faseforskydning mellem de to fundamentpunkter ved formur og bagmur vil spille ind.
I hvor høj grad responset fundet i jorden hhv. bygningen, fundet ved en ikke-koblet tilgang, afviger fra en koblet model er desuden undersøgt. Dette er gjort ved at udnytte muligheden for at implementere finite elementer i randelement modellen, hvorved det koblede respons af jorden og konstruktionen er opnået. Det er fundet, at afvigelsen særligt for jord responset, afhænger af bygningens egenfrekvens, da den største reaktionskraft opnåes ved krafigt response af konstruktionen. Denne effekt er generelt stigende for en stigende egenfrekvens.

Table of Contents

Chapter 1

Introduction

In this chapter, the problem, which will form the basis of this thesis, will be presented. Additional a 2-dimensional plane strain model setup, used to evaluate the problem, will be described.

1.1 Presentation of the problem

The focus of this project lies around the evaluation of energy transmission/loss in the form of vibrations created by human activities, in this case from trains.
The starting point is the new planned railway on the Danish side of the Femern Belt Link, where the neighbors of the future railway are the potential victims of vibration inconveniences. The Femern Belt Link is as well as the new planed railway from Ringsted to Rødby marked on the map in Figure 1.1.

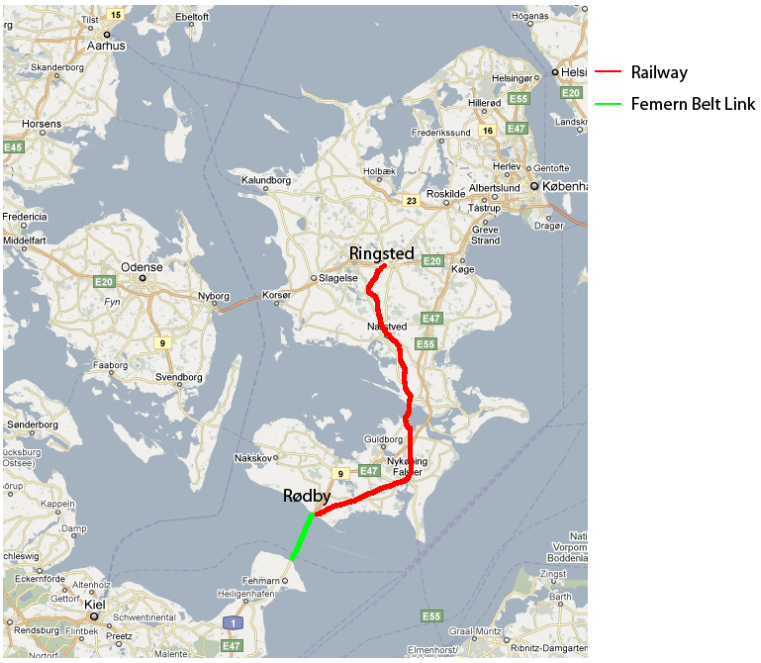

Figure 1.1 – *Position of the Femern Belt Link, connecting Denmark and Germany, marked with green. The new planed railway in connection to the Link marked with red.*

The waves of interest are generated by the trains, when they are passing by the buildings, and could cause inconveniences inside the existing buildings in the form of vibrations or noise. The vibrations inside the building will be created by the load of the train passing by, which will introduce vibrations traveling in the subsoil towards a selected reference building. The energy loss of these waves will be evaluated via the wave amplitudes, with respect to distance as well as frequency and especially in connection with the transmission of energy into the nearby building.
The wave transmission and essential results from the soil-structure interaction will be evaluated and assembled in an "easy-to-use program", which will be referred to throughout this report.

The vibrations originate in the way the train is "coupled" to the ground. If for instance the rails of the track is assumed "almost" infinite stiff, a passing train would give rise to a quasi-static movement of the rails leading to a slightly increasing load until, the train gets closer to the reference building after which, it will decrease again. If the rails instead were infinite stiff, the load would be constant over time, unless some trains are removed from the grid connected to this track.
Since this is not the case, the train will follow a vertical path with spikes for every sleeper, creating a harmonic varying load (at constant velocities), dependent on the speed of the train, the distance between the sleepers and to a certain degree also of the width of the sleeper (which will affect the assumed sinusoidal harmonic load). The frequency, for the load on sleepers along the railway, will in this case be the train velocity divided by the distance between the sleepers, $f = v_{train}/l_{sleeper}$. The frequency at one sleeper, will depend on the distance between the axles and the velocity of the train. This axle distance will in addition vary depending on, if two axles from the same carriage are passing the sleeper.
Another issue, which will influence the frequency of the train load, is the wheels on the train, as imperfections will cause harmonic loads as the train drops at the same spot and hits the rail creating another harmonic load. The frequency will in this case depend on the diameter of the wheel and off course the velocity of the train ($f = v_{train}/(2\pi r)$). A similar case could occur for imperfections on the rails itself, here the frequency will again depend on the distance between the succeeding wheel axles.

The main frequencies of interest for the vibration problem lie between approximately 10-30Hz and 80-100Hz, which is the frequency range, where the train is expected to generate perceptible response in the surrounding soil (P. Galvín, 2007) (F. Kirzhner, 2005) (X. Sheng, 2003). This corresponds to a train velocity between approximately 22-65 and 173-220km/h, if the sleeper distance is looked upon, which seems fair, as most of the train traffic in Europe runs with a maximum speed just below 200km/h, see Appendix A (Media, 2009). For this reason the soil model will be using the frequencies between 1 and 100Hz spaced with a step of 1Hz and additionally the one-third octave band centre frequencies 1 and 200Hz is used (1.0, 1.25, 1.6, 2.0, ..., 125, 160, 200). In this way the frequencies of interest is covered, framed with an extra margin.

It is now interesting to find the response of the building, when it is excited by the moving soil. It is expected, that the waves at or near the eigenfrequencies of the building or parts of it (e.g. walls and floors) will provide significant response, and even amplified response compared with the corresponding response of the soil. The response will be found both in

an uncoupled model, where no soil-structure interaction will be present, and in a coupled model, where the responses will be influenced by the interaction.

1.2 Model description

The reference building is placed 25m from the center of the track, has a width of 8m and is selected to be 2.5m high.
The problem is sketch in Figure 1.2, where the track, the train load, the reference building and their respective dimensions and internal distances are shown.

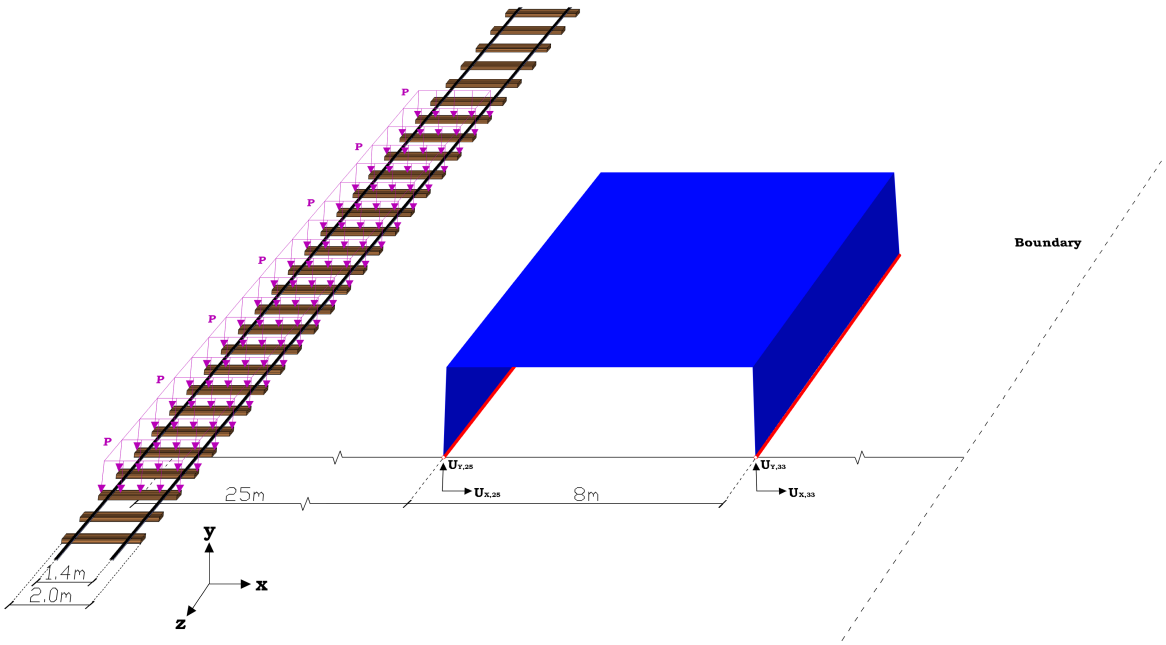

Figure 1.2 – *Sketch of full 3D mode.*

Apart from the assumption of the load being harmonic, it is assumed that the load, P, will act in phase all along the railway. In this way, the wave front will travel parallel to the railway, creating a linear wave front, opposite the case, where a point load is applied, creating a circular wave front emanating from the point of application, see Figure 1.3.

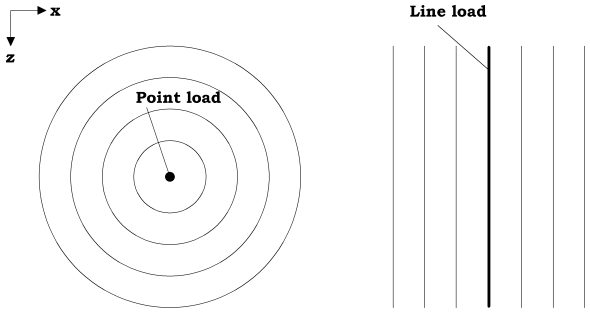

Figure 1.3 – *Wave front propagation on soil surface, for a point load (left) and a line load (right).*

These parallel wave fronts will make it possible to simplify the 3-dimenisonal problem into a 2-dimensional plane strain problem. This simplification is allowable, as the soil material is selected as a homogeneous linear elastic isotropic material, and when the load is in phase of equal magnitude along the railway and only applied in the xy-plane, as this will ensure no generated response in the z-direction.
The line load from the train is not actually working as a line load, it is working over a certain width creating a surface load. In this project, it is assumed, that the load is distributed uniformly over the length of the sleepers (width of the track) which is 2m wide, from which the load is transferred from the rails, placed 1.4m from each other. As will be explained later, the elements in the soil model is made with 3-noded elements, which means that the load is applied with the relative values per elementnode 1/6, 4/6, 1/6 representing a uniform distribution of the load (Clausen, 2009). In addition to this, it is chosen to use two elements around the load application, leading to the load distribution on the five involved nodes, as shown in Figure 1.4.

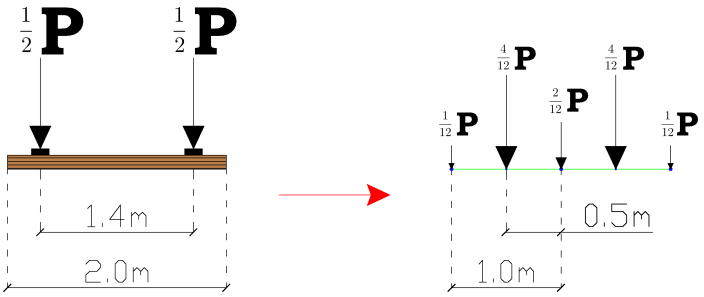

Figure 1.4 – *Train load applied to two 3-noded elements at the soil surface.*

The simplification of the model correspond to a cut in the xy-plane of the model, shown in Figure 1.2. With the load application as explained above, see Figure 1.5.

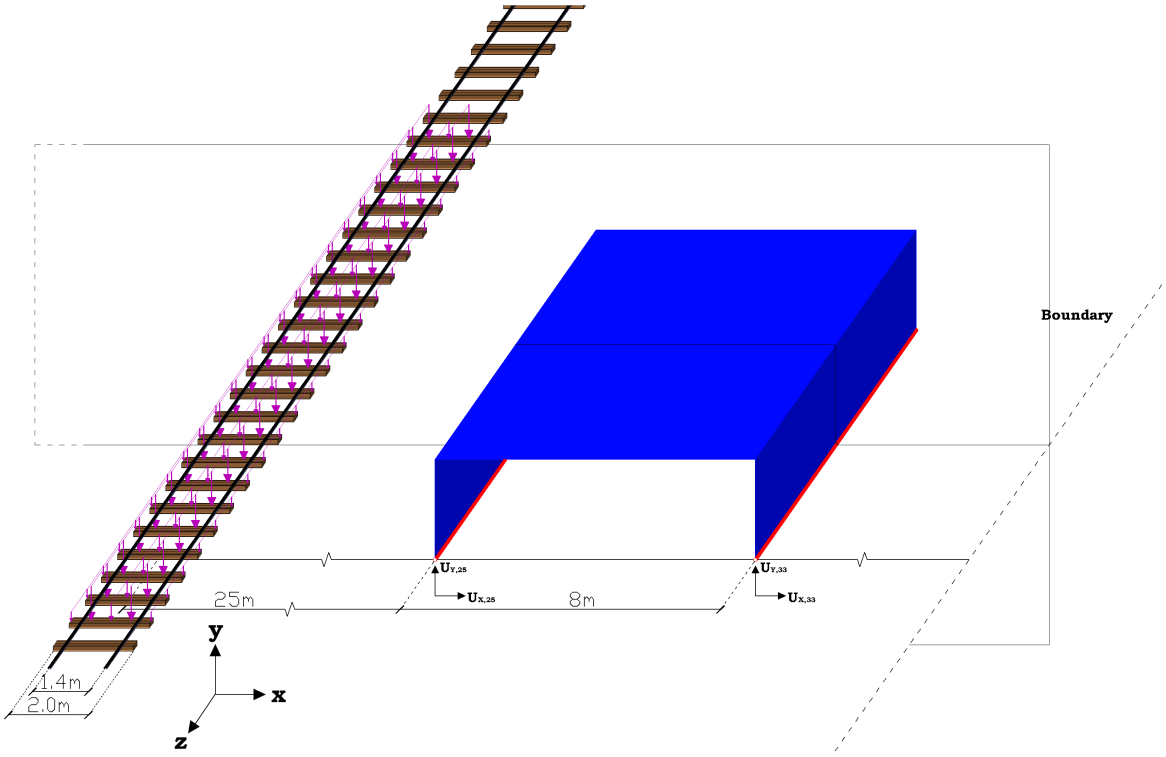

Figure 1.5 *– Sketch of full 3D mode with cut in xy-plane.*

This correspond to the final plane strain model, shown in Figure 1.6.

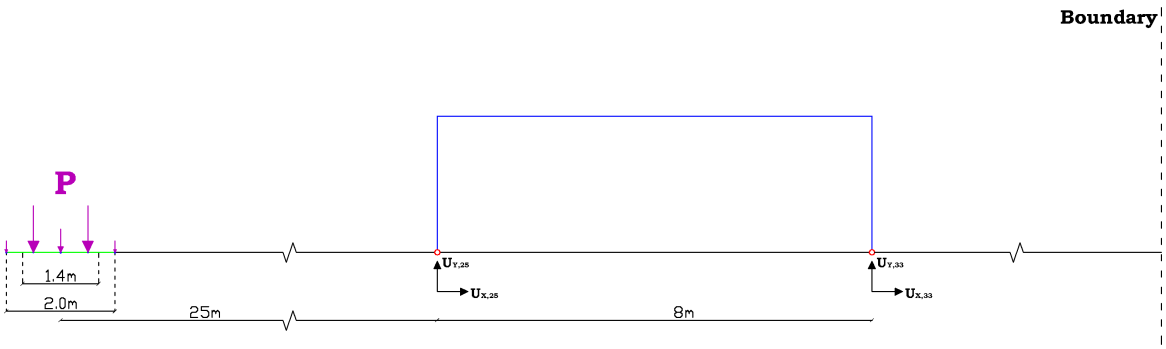

Figure 1.6 *– 2D plane strain model of the full soil and structure model.*

The model consists of different parts involving different sub-programs. First and foremost the software package TEA has been used (C. J. C. Jones, 1999a), where the Boundary Element Method (BEM) is utilized.
The Boundary Element Method provides the possibility of modeling wave propagation within a full-space, a half-space or a layered half-space. The individual domains is divided by boundary elements, discretizing the interfaces in between the different materials, see Figure 1.7.

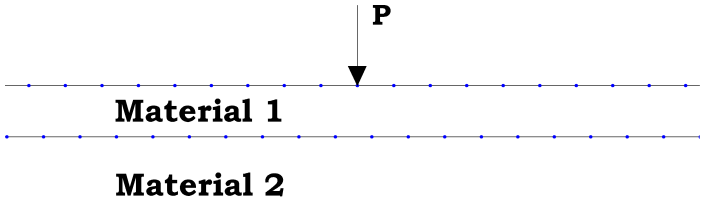

Figure 1.7 *– Discretized surface and interface between two materials, where material 2 is occupying the half-space.*

The properties of the BEM makes it possible to find the wave amplitudes in the entire domain via the so called Green's funcion.
In the BE formulation the implementation of transmitting boundaries are included, which allows the supplied energy (at the source = track) to leave the model. This is an essential application of the BE model used, since reflected waves at the boundary, would disturb the wave field emanating from the source, with either constructive or destructive interference as a result (see Section 2.4). Additionally the TEA software package can include FE within the BE model, which will be used for a combined FE-BE model, where soil-structure interaction hereby will be taken into account.

As mentioned above, the soil will be assumed homogeneous, isotropic and will further be assumed to behave linear elastic, as only small stresses are expected in the soil, due to the emanating waves. The stiffness of the soil is defined by Young's modulus, E. Additionally the density of the soil and the Poisson's ratios is defined by ρ and ν respectively. As for the damping a hysteretic material damping model is used, where η is a fraction representing the damping in the material per cycle.
Two soil stratifications, which are representative for the soil near the planned railway, is used for the vibration analysis. The stratifications are found in (Andersen, 2010).

The structure will first be modeled in a separate FE program, setup by the author, where the ground motions, from the BEM, at the base of the wall will be the only input for the model. Since only relatively small movements are generated, it is assumed, that the building can be modeled with a linear elastic FEM.
The buildings will be modeled with simply supported beams, where the deflections from the BE model are introduced, as force deflections. As explained above a model including both the soil and the structure will also be setup inside the TEA software package, where the importance of the soil-structure interaction is judged upon.

The combined models, for which the vibration analysis will be made, is listed in Figure 1.8. The combination marked with red will be the reference case, consisting of structure 1 combined with soil 1, where the wave field and the response of the structure is found in two different models, where no soil-structure interaction is allow for.

Uncoupled models

Coupled models

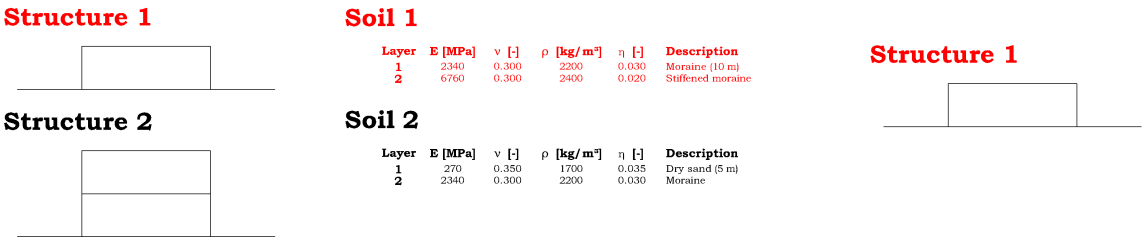

Figure 1.8 – *Model matrix, with the structural systems of the uncoupled model listed to the left, the structural system of the coupled model to the right and the soil strtifications in the middle.*

Chapter 2

Convergence analysis

To ensure a both fast and accurate model, several parameters of the model have to be evaluated to ensure a converging model (with a given level of precision).
The element size of the Boundary Elements have to be evaluated to find the maximum size at which the model is converging and delivering the desired accuracy at as low computational effort as possible. It is also necessary to see, if the results delivered near the boundary of the model are independent of the location of the edge where the waves are transmitted out of the model, see Figure 1.6. In the "Convergence regarding multiple layers" Section 2.4, the material parameters for the reference soil profile number one is used, see Figure 1.8.
Another factor, which could lead to differing results, is the method of applying the load, which could be done directly on the soil surface or at a plate representing railway sleepers (where the first option is chosen, see Section 1.2).

As the analysis is evaluated in the frequency domain, the results from the BE model, see Chapter 3, will be complex values of the deflection in the horizontal (x-dir) and the vertical direction (y-dir) at the discrete nodal values of the model. With this data structure, all the amplitudes are available, as well as the absolute amplitude, i.e. the maximal experienced amplitude during one period, and the phase shift, see Equation (2.1).

$$\begin{aligned} A(\omega,t) &= Re\left(x \cdot e^{i\omega t}\right), \quad \text{where} \quad t = \left[0; \frac{2\pi}{\omega}\right[\\ A_{abs} &= \sqrt{Re(x)^2 + Im(x)^2} \\ \Psi &= tan^{-1}\left(\frac{Re(x)}{Im(x)}\right) \end{aligned} \tag{2.1}$$

where x is the amplitude from the TEA program, A and A_{abs} is the amplitude and absolute amplitude respectively, or actually the half amplitudes, but they will be denoted the amplitudes throughout the report. $Re(x)$ and $Im(x)$ represent the real and the imaginary part of the amplitude x.

2.1 Convergence model

The soil model use in the convergence analysis, and throughout the report, is a Boundary Element model, using three-noded elements, with quadratic shape functions (C. J. C. Jones,

1999b). The model is evaluated in frequency domain with the specified frequencies given in Section 1.2.

The first two parts of the convergence analysis, use a (non-layered) half-space of one homogeneous isotropic linear elastic material. The stiffness is defined by Young's modulus and is set to 1.0 GPa, while the Poisson's ratio is set to $\nu = 0.20$. The density of the soil is selected to $\rho_{soil} = 2000\text{kg/m}^3$. Furthermore the hysteretic damping (see Section 4.1) of the soil is set to 10% ($\eta = 0.10$).

The geometry of the model used for the convergence analysis is shown in Figure 2.1, with 1 element per 100Hz wavelength.

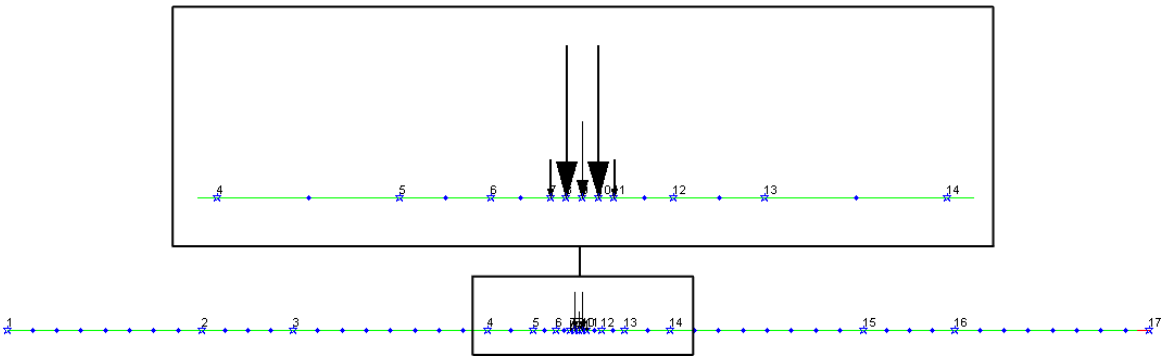

Figure 2.1 – *Geometry of a half-space consisting of uniform homogeneous soil with a uniformly distributed load applied at five nodes (2 elements) between -1.00m and +1.00m from the centerline.*

The model consists of a plane surface with bounds 50m away from the center of the track. Nodes are assigned in the middle of the track and at ±1.00m from this representing the railway sleepers. Additionally nodes are assigned at ± 2, 4, 8, 25 and 33m, which are used as reference points.
The load is applied as described in Section 1.2.

2.2 Convergence regarding the element length

In this subsection the element size will be evaluated with the given geometry described above, in Section 2.1.

In the program (*geosimmod.m*), the geometry of the model is defined. An important part of this definition is to prescribe the number of elements per wavelength, since this factor defines the accuracy of the model. But obviously the number of elements per wave will vary relative to the frequency. Therefore it is necessary to know the maximum frequency of interest which is estimated to 100Hz, see Section 1.1. A factor determining the number of elements in this 100Hz wave is introduced, $n_{ele,wav}$.
To be able to apply the correct number of elements, it is necessary to know the wavelength for this maximum frequency of interest. To find this wavelength the wave velocity is needed. Since the wave amplitudes of interest are at the boundary of the half-space, namely on the

soil surface, the possibility of captured waves along the surface arise. These waves are called Rayleigh waves, and as they will travel slower than both P- and S-waves, the critical element length will be shortest for these surface waves ($L_{wave} = c_{Rayleigh}/f$). For this reason the Rayleigh wave speed is needed, which is found in Equation (2.2). (Andersen, 2006, Sec. 1.4).

$$\left(\frac{c_R}{c_S}\right)^2 - 8\left(\frac{c_R}{c_S}\right)^4 + (24 - 16\alpha^{-2})\left(\frac{c_R}{c_S}\right)^2 - 16(1 - \alpha^{-2}) = 0 \tag{2.2}$$

where $\alpha = c_P/c_S$.
This equation requires the primary and secondary phase wave speeds, which, for plane strain, is found via Equation (2.3).

$$c_P = \sqrt{\frac{\lambda + 2\mu}{\rho}}, \quad c_S = \sqrt{\frac{\mu}{\rho}} \tag{2.3}$$

which are determined with use of the Lamé constants, where the material parameters E and ν from Section 2.1 is used. The Lamé constants are given in Equation (2.4).

$$\lambda = \frac{\nu E}{(1+\nu)(1-2\nu)}, \quad \mu = \frac{E}{2(1+\nu)} \tag{2.4}$$

The wave speeds are shown in Table 2.1.

	Wave speed [m/s]
c_P	745
c_S	456
$c_{Rayleigh}$	431

Table 2.1 *– Wave speeds for the primary, the secoundary and the Rayleigh wave.*

These values seem reasonable, as they correspond to the expected value for a soft/clayey moraine (Andersen, 2006, Fig. 1-7).

By displaying the real part of a wave radiating from the source, the waves are visualized as they would appear at the instance of time where the load is applied. In Figure 2.2 the waves for the frequencies 1, 3.15, 10, 31.5 and 100Hz with one element per 100Hz wavelength (i.e. $n_{ele,wav} \equiv 1$) are shown.

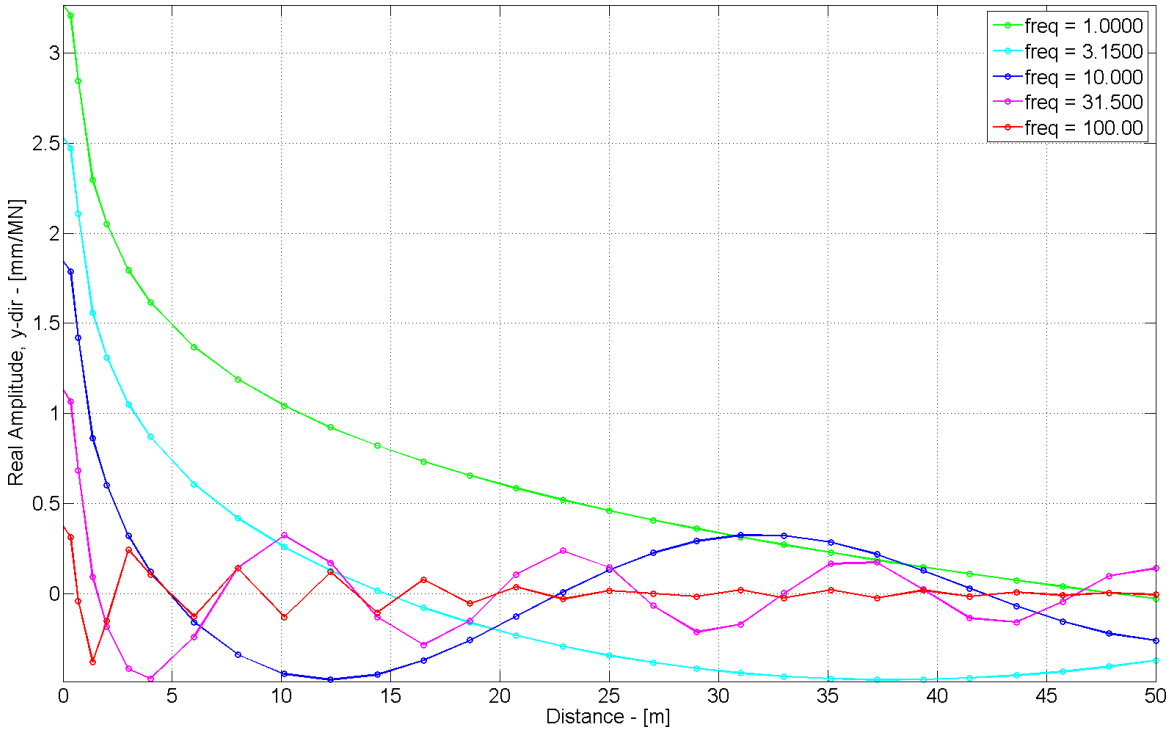

Figure 2.2 – *Real amplitude of the vertical response at* $n_{ele,wav} = 1$.

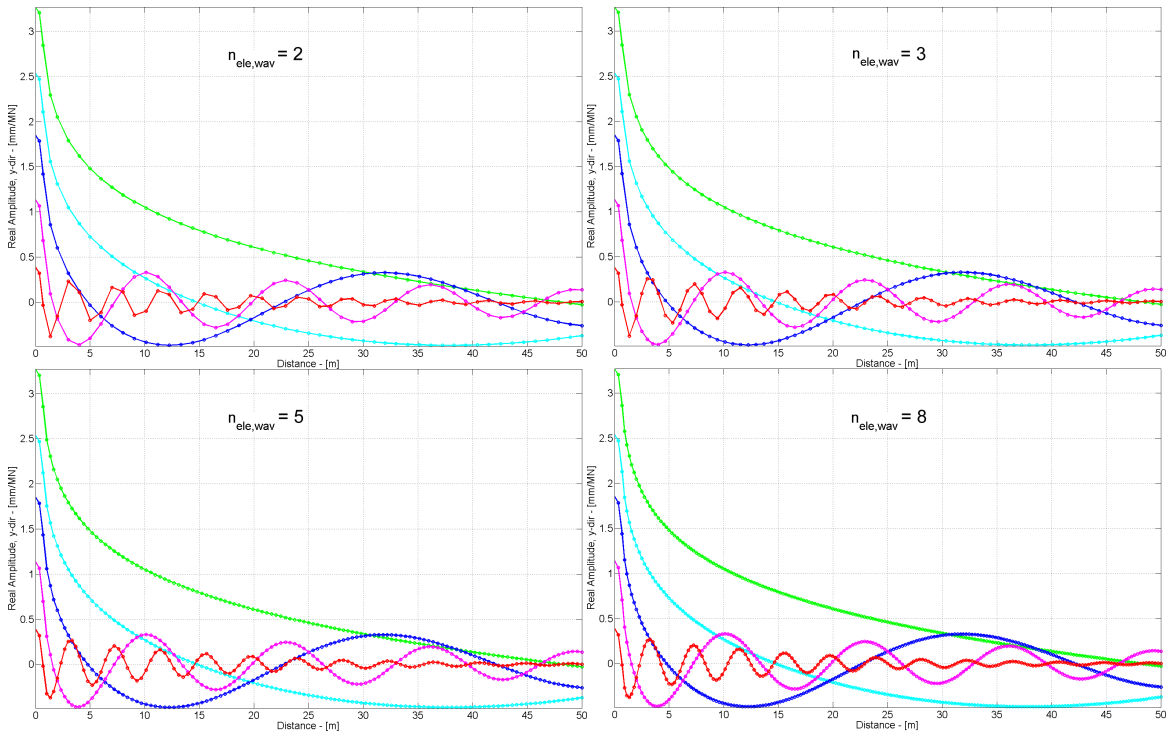

Figure 2.3 – *Real amplitude of the vertical response at* $n_{ele,wav}$ *equal 2, 3, 5 and 8.*

As expected the 100Hz wave is not recognized as a wave, since only one element per wavelength is not enough to recreate the shape of the wave. But focusing on the wave with the frequency of 31.5Hz, which would approximately correspond to 3 elements per wavelength ($1 \cdot 100/31.5 \approx 3$), it is seen that at least the shape of the wave is becoming more clear. And the 10Hz wave has a curvy shape with 10 elements per wave.

In Figure 2.3 the same plot is shown for $n_{ele,wav}$ equal to 2, 3, 5 and 8.

As mentioned above, the shape of the 100Hz wave begins to show already at three elements per wavelength (as for the 31.5Hz wave). But as it is not possible to judge the behavior of the waves directly based on the smoothness of the wave, it will only indicate where a given number of elements may lead to incorrect results.
As the Green's function is derived for an infinite space (the so called full-space), the response of all waves inside the entire domain can be found with use of this Green's function, where all the elements will contribute to the determination of the response at a given point, see Figure 2.4.

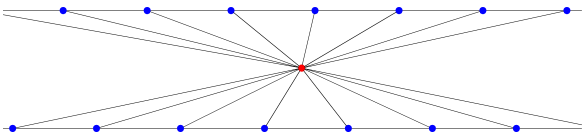

Figure 2.4 *– The response in the red point, is weight via the Green's function, from all other nodes of the surrounding BE.*

In contrast a response in between two nodes in a finite element formulation has to rely on the adjacent nodes and the selected shape function. To find the necessary amount of elements needed to provide first and foremost a converging model and secondly the needed accuracy, the absolute amplitude at five reference points are used. Two of these five point lie relatively far away, namely 25m and 33m from the track (the location of the reference building). Additionally three reference points are placed close to the track, to check if the BE model is having trouble close to the points at which the loads are applied. The data, which are looked upon are the absolute amplitudes in the vertical direction as function of the frequency evaluated at the five points. A plot of the situation is shown in Figure 2.5, where $n_{ele,wav}$ is set to 8. This model and its results will be a reference, in the search of the appropriate number of elements.

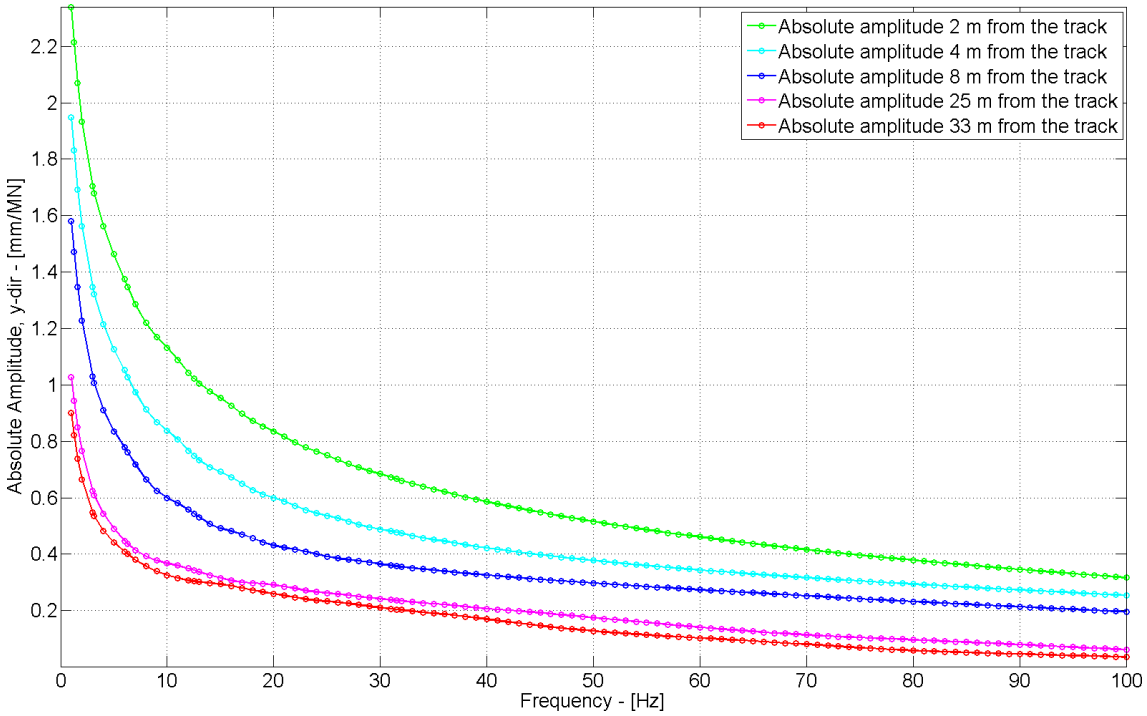

Figure 2.5 – *Absolute amplitude for the reference model with 8 elements per 100Hz wavelength.*

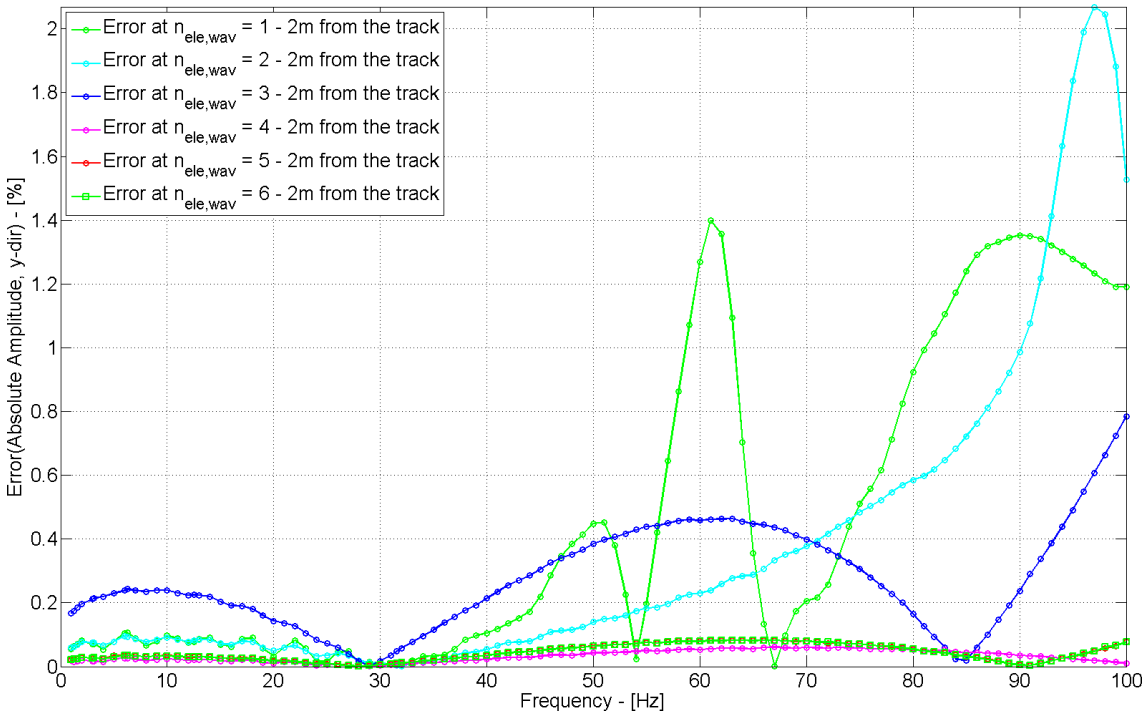

Figure 2.6 – *Relative errors for $n_{ele,wav}$ set to 1, 2, 3, 4, 5 and 6, for the reference point 2m away from the center of the track.*

The amplitudes are decreasing as the waves spread out and especially as the high frequency waves are damped away. To identify the number of elements for a converging model the absolute errors relative to the results obtained with a BE model with $n_{ele,wav} = 8$ are calculated at the five reference locations. The first plot is shown in Figure 2.6.

It is seen that with $n_{ele,wav}$ set to both 1 and 2 and partly 3 are equally bad at representing the amplitude 2m from the center of the track and hereby 1.0m from the railway sleepers. The results from the models with 4, 5 and 6 elements have a much more consistent behavior and support the initial assumption by using a model with relatively many elements as a reference model. All though the errors obtain with the 1, 2 and 3 element models are relatively high compared with the refined models, the absolute error is not particularly large compared with the results 4, 8, 25 and 33m from the track, see Figure 2.7. The error just exceed 2% for the 2 elements model, which is low compared with the results further away from the track where the same model provide errors as big as 8% and 15% for high frequent wave 25m and 33m away from the track.

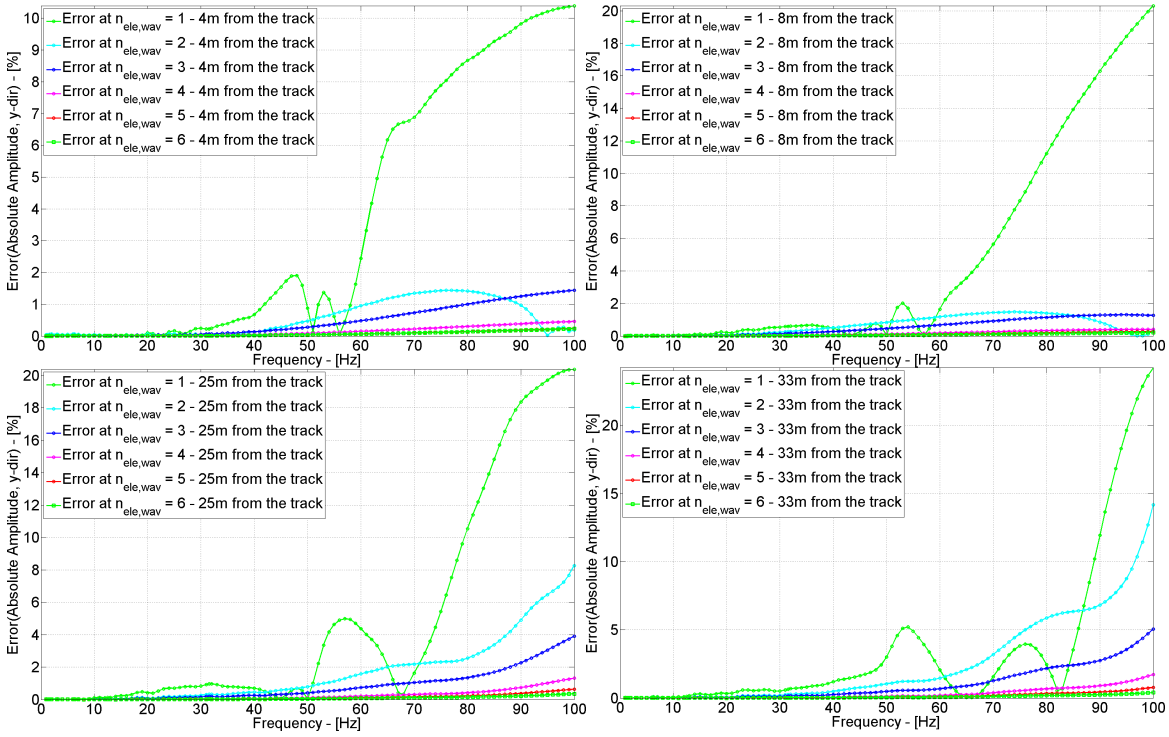

Figure 2.7 – *Relative errors for $n_{ele,wav}$ set to 1, 2, 3, 4, 5 and 6, for the reference points 4, 8, 25 and 33m away from the center of the track.*

The results indicate an increasing error with the distance to the track, which can be seen in Figure 2.8, where the mean error from Figure 2.6 and Figure 2.7 have been used.

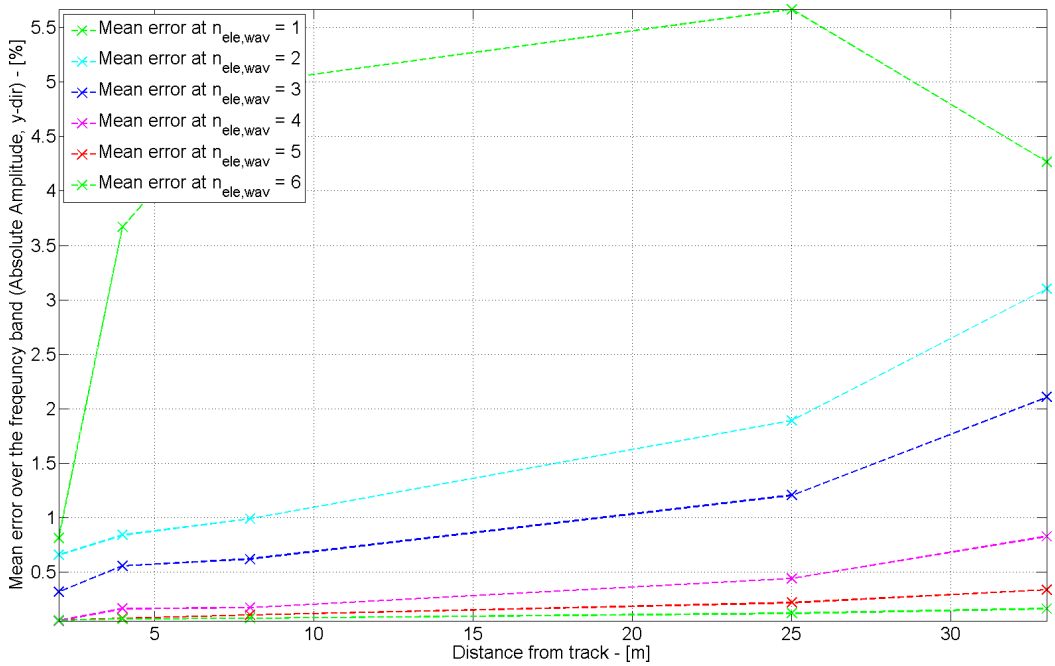

Figure 2.8 – *Mean error over the frequency band of the relative errors for $n_{ele,wav}$ set to 1, 2, 3, 4, 5 and 6, as function of the distance to the track.*

A considerable amount of accuracy is gained by increasing $n_{ele,wav}$ from 3 to 4, where the averaged error goes from 2.1% to 0.8 %, 33m from the track. After this point the error is roughly halfed for every increase of $n_{ele,wav} = 1$, which becomes more clear from Figure 2.9, where the mean value of the error from the five reference points in Figure 2.8 has been used.

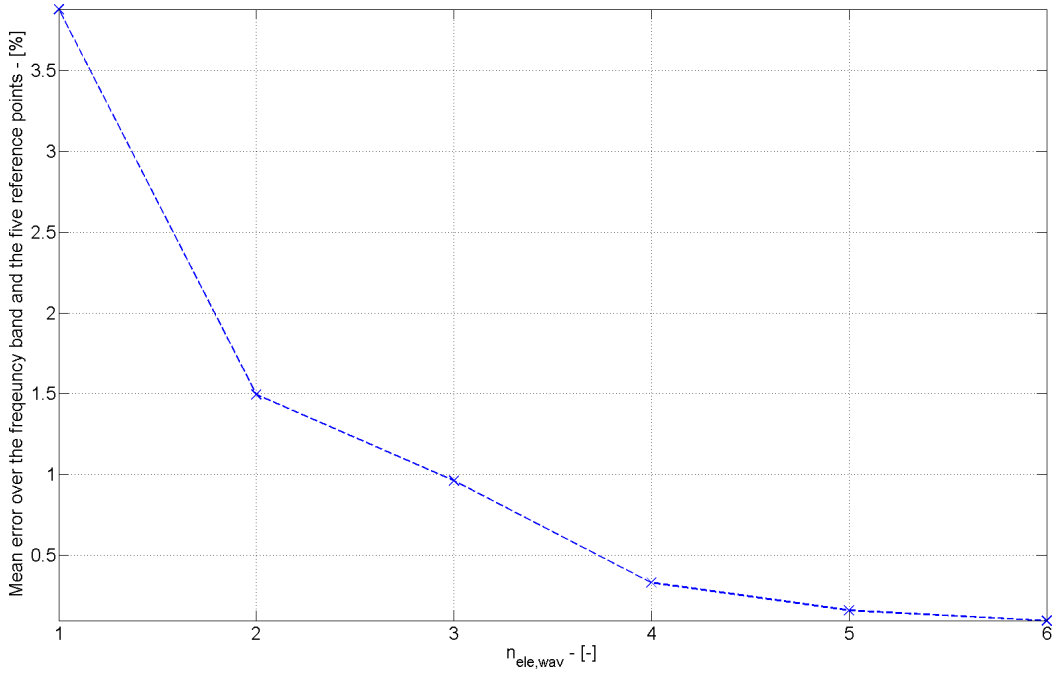

Figure 2.9 – *Mean error over the frequency band and the reference point, as function of $n_{ele,wav}$.*

It is chosen to use $n_{ele,wav} = 4$, representing four elements per 100Hz wavelength for a Rayleigh wave, since this will provide a converging model with a relatively high accuracy compared with the calculation time.

2.3 Convergence at the boundary

Another issue, which has to be taken into account, is potential errors introduced at the boundary of the model. Since the model is a BE model, it will behave advantageous directly compared with an equivalent FE model, as transmitting boundary conditions is included. But even though a BE model is considerably better, it may still introduce some errors locally around the boundary of the model.
These errors arise from diffraction around the "end-point" of the surface, with either constructive or destructive interference as a result, see Figure 2.10.

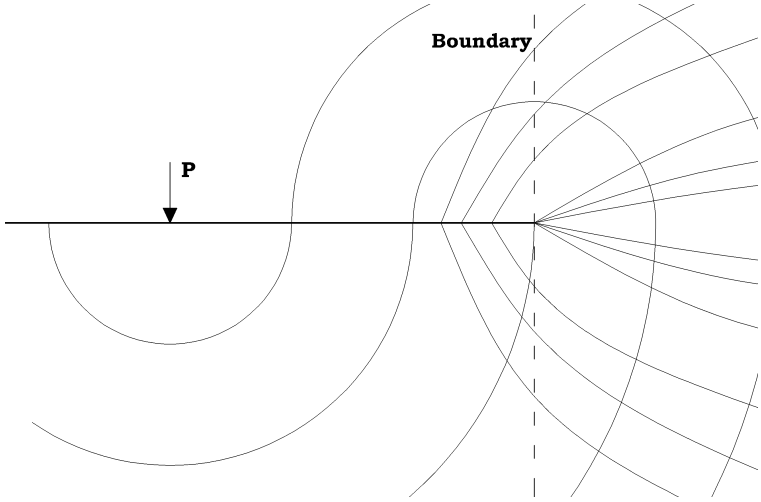

Figure 2.10 *– Diffraction around "end point" of surface.*

To identify the order of magnitude of this kind of error, the model from the previous section is extended at the right edge by 0.5, 1, 2, 5, 10, 15 and 25 meters, where the 25m will be the reference point at which it is assumed, that the model is providing the correct results.
In Figure 2.11 the absolute amplitude in the vertical direction is show. It is clear that, at the right edge of the model at around 45 to 50m, the absolute amplitude is dropping relatively fast providing a wrong answer at or near the boundary.

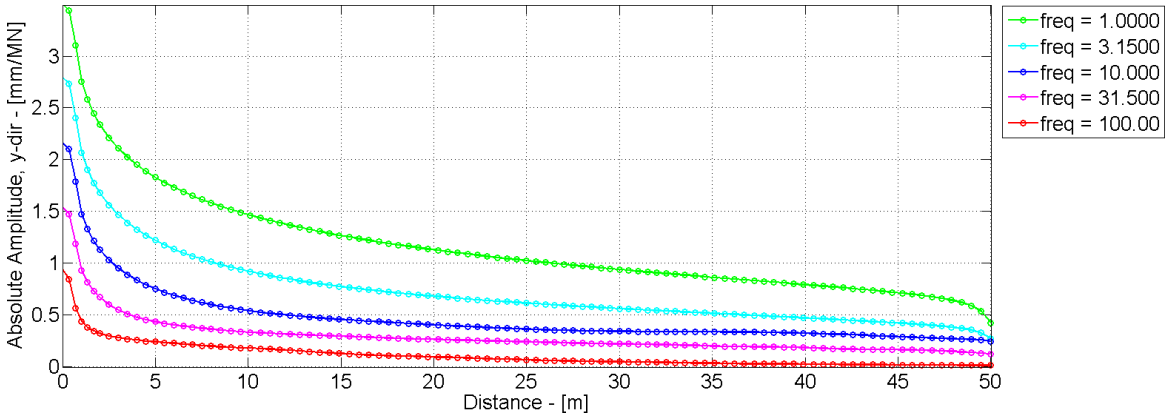

Figure 2.11 – *Absolute amplitude in the vertical direction as function of the distance to the track at 5 selected frequencies.*

The error seems to be largest for low frequencies. This can be explained by the longer wavelengths for these low frequent waves, which requires a wider model and hereby more elements to represent the next wave further to the right, see Figure 2.12. One could say that the aim is to find how many waves (or which fraction of a wave) is necessary, to the right of furthers point from the center of interest, to provide the desired accuracy for the lowest frequency of interest (around $10 - 30$Hz, see Section 1.1).

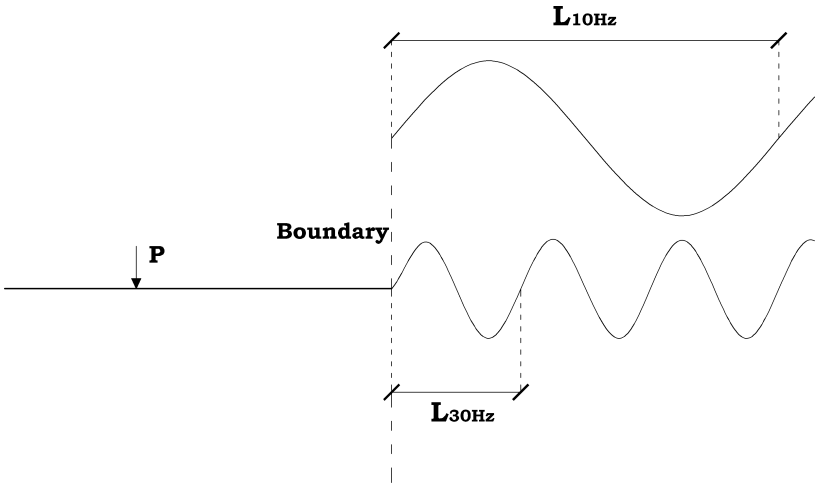

Figure 2.12 – *Principle sketch of model extend necessary, to include one additional wave length.*

In Figure 2.13 the absolute amplitude 50m from the center of the track is shown, with the model from the previous section, where the 50m mark was the edge of the model. Additionally the new models, with edge extensions of 0.5, 1, 2, 5, 10 and 15m from the comparison point 50 meter from the center of the track are plotted as well.

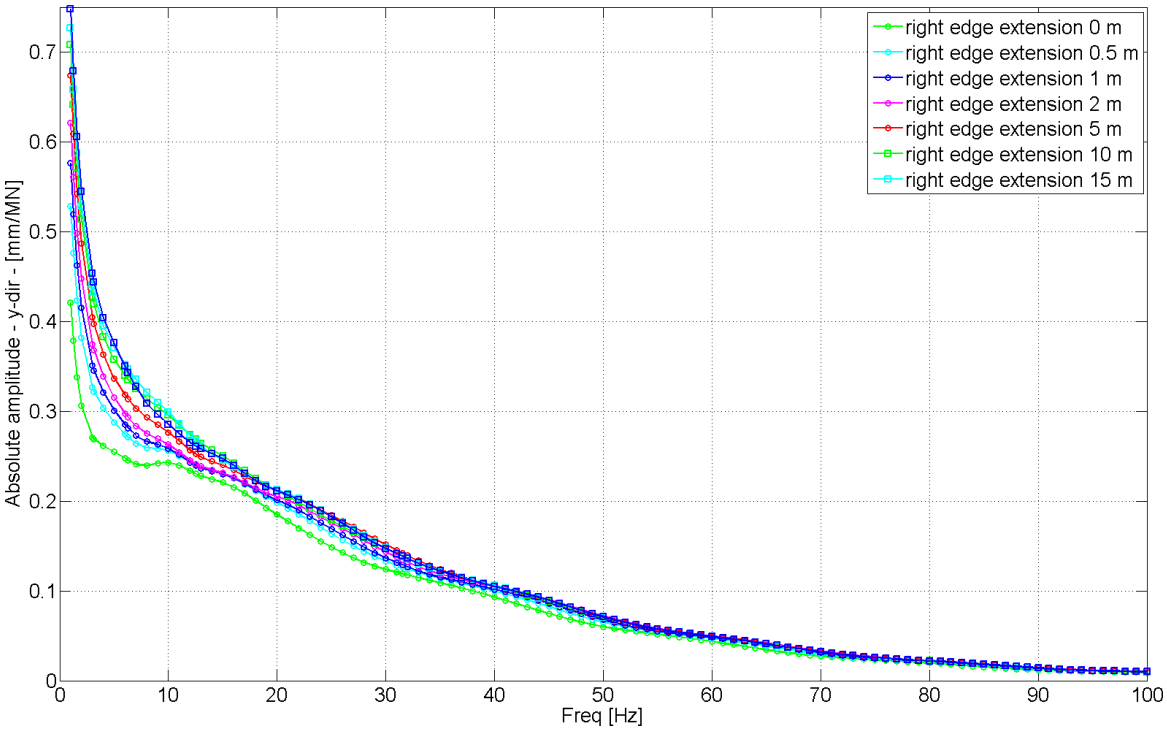

Figure 2.13 – *Absolute amplitude 50m from the center of the track. Model edges at 50, 50.5, 51, 52, 55, 60, 65m from the center of the track.*

The relative error is now estimated via the reference point 75m from the center of the track, see Figure 2.14. It can be seen, as mentioned before, that the error introduced near the boundary is relatively big at low frequencies, followed by a decrease as the frequency increases and the error stagnates at $10-25$Hz with a given level of accuracy dependent of the extension of the model. For instance in the model with no extension, the error goes towards a value around 14 % almost independent of the frequency. In the model with 2m extension, the error stagnates around 10Hz for the critical low frequencies. After this frequency it remains below $3.5-4.0\%$, with a tendency to decrease.

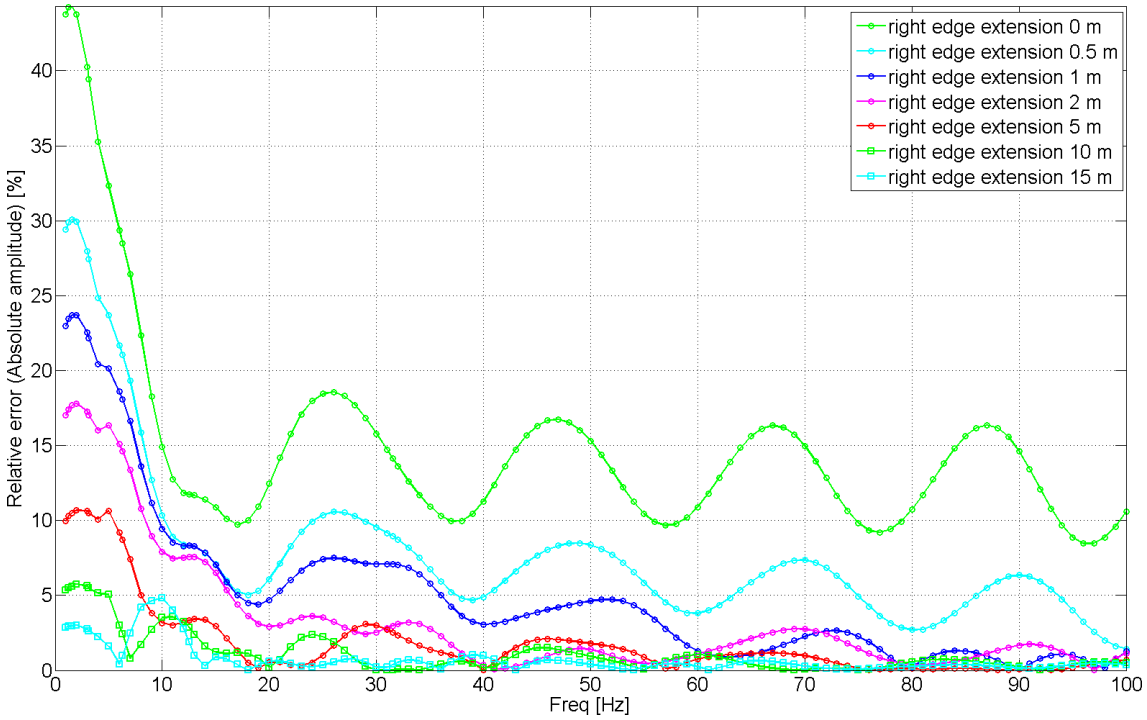

Figure 2.14 – *Relative errors for the 7 models, estimated relatively to results obtained from the model with the edge placed 75m from the center of the track.*

A plot of the mean error over the frequency band is shown in Figure 2.15.

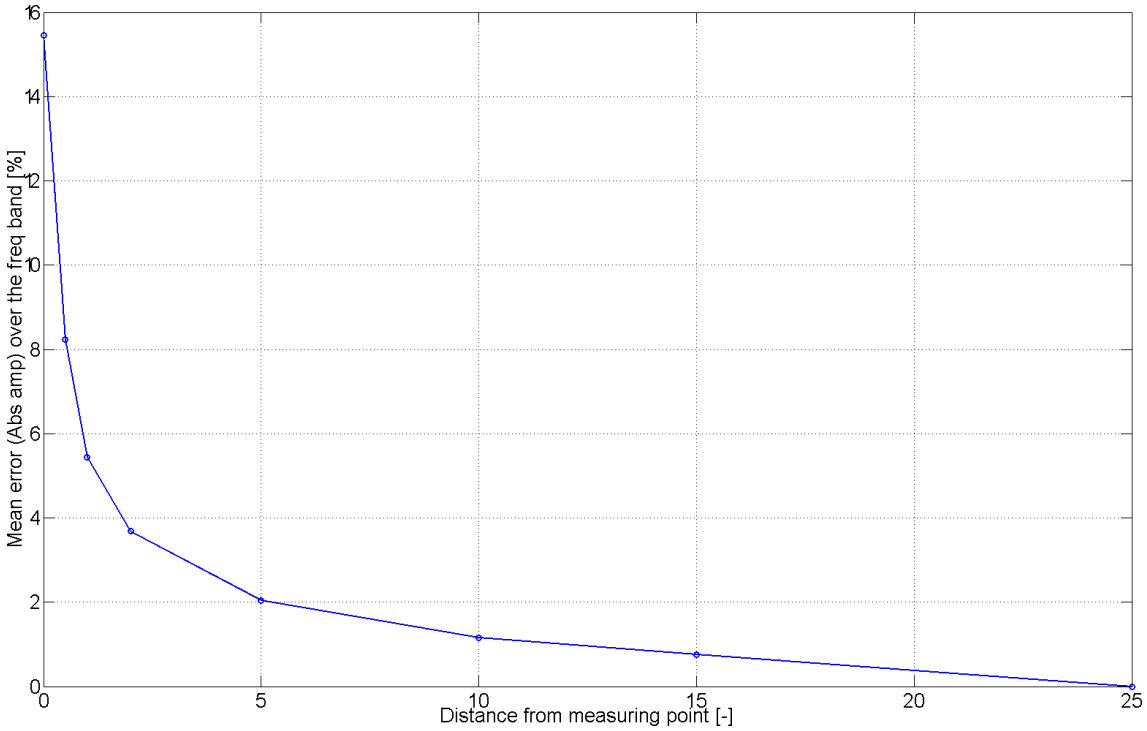

Figure 2.15 – *Mean error over the frequency band shown as function of the extension length in meters [m].*

As discussed before, the fraction of a wavelength necessary to the right of the comparison point providing the necessary accuracy is sought. It would therefore be expected, that the error is halfed for every double of the frequency. This tendency is illustrated in Figure 2.16.

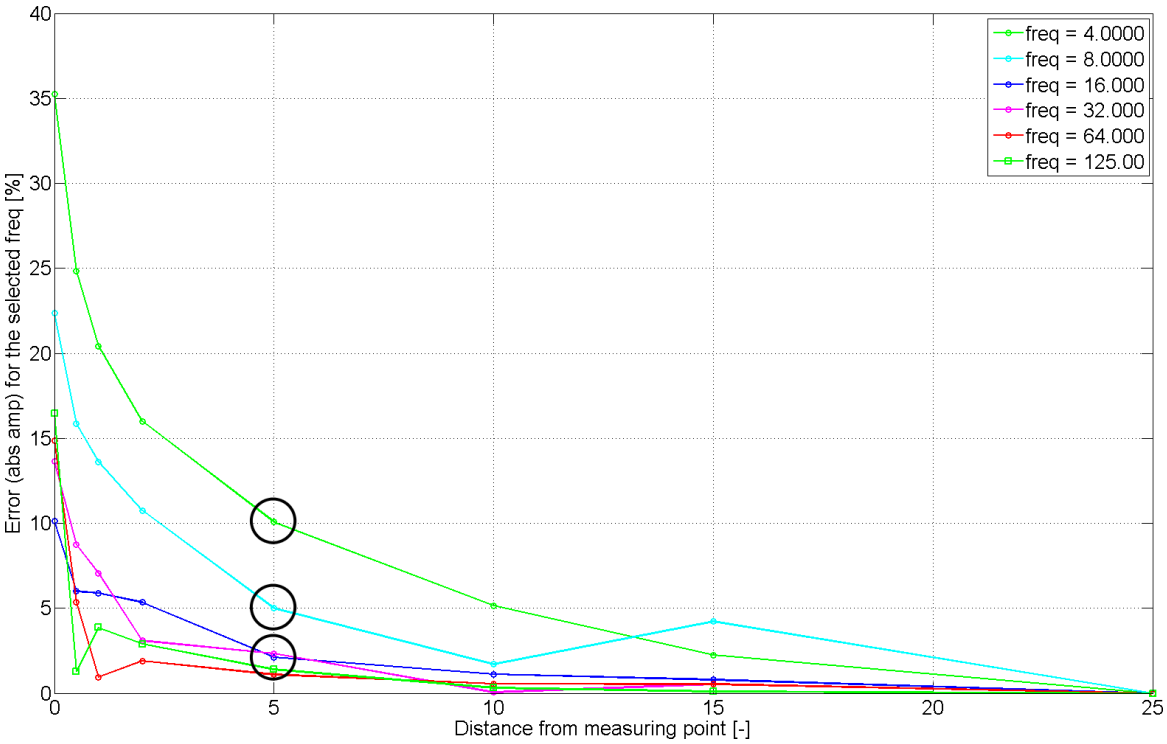

Figure 2.16 *– Error for the selected frequencies 4, 8, 16, 32, 64, 125Hz.*

The tendency is clearest shown 5m (and 10m) from the measuring point. At 5 m the error is 10% for 4Hz, 5% for 8Hz, 2.5% for 16Hz.
So if the desired level of accuracy at the comparison point is 2.5%, the distance to the right of this point should be approximately 0.2 wavelengths which should be used for the lowest frequency of interest, see Equation (2.5) and Figure 2.16.

$$\frac{5m \cdot 16Hz}{c_{Rayleigh}} = \frac{10m \cdot 8Hz}{c_{Rayleigh}} \approx 0.2 \tag{2.5}$$

where $c_{Rayleight} = 431$m/s, see Table 2.1.
This means that for this accuracy the extension of the model should approximately be $L_{extend} = c \cdot f^{-1} = 431$m/s / 30Hz $\approx$ 14m and the triple ($L_{extend} = 42$m) if the accuracy should apply for 10Hz waves.

2.4 Convergence regarding multiple layers

It is again noted, that the material properties in this section, is set to the reference values, marked with red, in the modelmatrix, see Figure 5.1.
Until now, only surface waves have been looked upon, since no reflection takes place in an

infinite half-space. But with the introduction of a layer on top of the half-space, wave reflection and refraction will be present at the interface between the two materials. This means that another factor than the 0.2 times the wavelength, found in the previous subsection, could be critical for accurate results near the edge of the model.
The reason for this, is that reflected waves at the interface will influence the wave field and hereby amplitudes at the surface when it "returns". Near the boundary there is a risk of the wave field feeling the full-space outside the model, leading to an only partly transmitting boundary. The reflected waves will in this way influence the whole wave field as it travels "back" into the domain, but will produce largest deviation near the boundary of the model (due to damping). For this reason it is expected that the convergence is satisfied with an extend of the model measured in layer thicknesses. On Figure 2.17, a situation with a reflected wave disturbing the wave amplitude near the boundary is sketched.

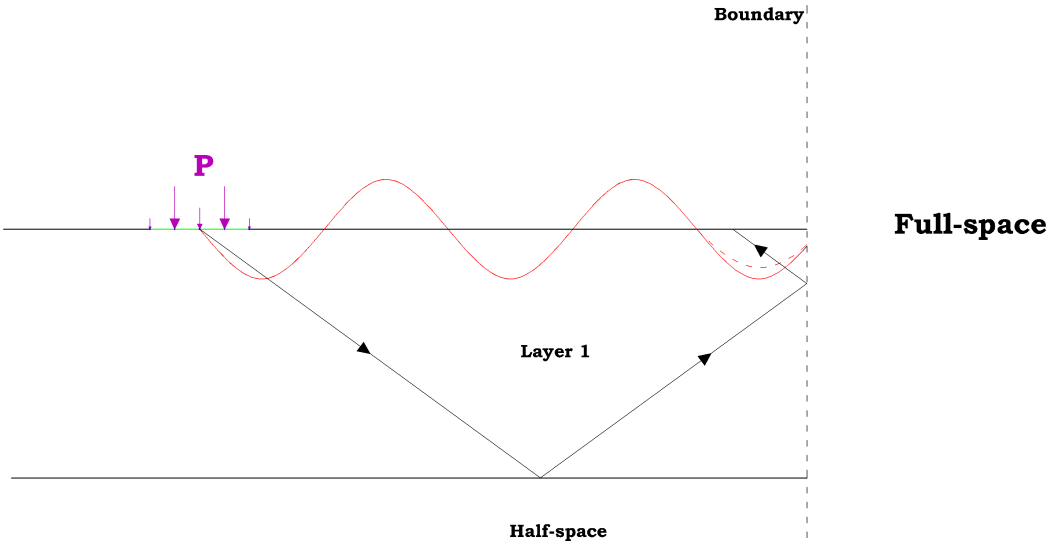

Figure 2.17 – *Principle sketch of amplitude disturbance near the boundary.*

The reason for this partly transmitting boundary, found in the impedance mismatch in the top layer and the felt material outside the model, which can occur when a stiff material is superimposing a soft material or vice versa. Generally the top material overlaying the material in the half-space tend to feel the superimposed material as if was present in the full space just outside the boundary of the model, see Figure 2.18.

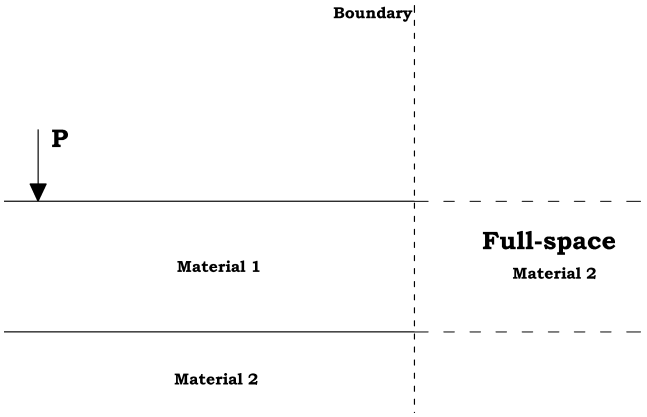

Figure 2.18 – *Sketch of felt material outside the model. Material 1, inside the model, feels, the material 2 outside the model, as if it was occupying the full-space outside the boundary.*

This means that the advantageous behavior of the boundary is partly absent, as full transmission only occur at identical impedances (equivalent to the half-space case). The impedance of a material, z, is defined by the material density multiplied by its phase velocity, see Equation (2.6). It is not necessarily correct to state that an impedance mismatch will increase for materials with increasing deviation on the stiffness. But as the phase velocity in the respective materials increase, for an increased stiffness, see Equation (2.3) and Equation (2.4), and the fact that stiff soil deposits tend to be more dense, than loss/soft materials, the terminology is adopted.

$$z = \rho c \tag{2.6}$$

where the impedance mismatch is defined by the fraction, ϱ:

$$\varrho = \frac{z_2}{z_1} \tag{2.7}$$

where z_1 and z_2 refers to the impedance of the two materials.
In the case of a stiff material overlaying a soft material, in the half-space, the stiff material will not be particular influenced by the soft material outside the model (in the Full-space), as its stiffness is small compared with the top material inside the model. This will create a free end at the boundary of the model, letting the stiff top material move unaffected. The case is analogous to a stiff beam with a soft fixed beam at the end, see Figure 2.19.

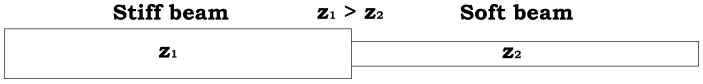

Figure 2.19 – *Beam stiffness mismatch analogous to impedance mismatch.*

Here the stiff beam to the left, will vibrate unaffected by the smaller beam fixed at the end (at least in the case of a impedance mismatch going towards zero).

The opposite is the case when the wave is traveling along the small beam (the soft soil) and hits the much stiffer material. Here the stiff material will act as a fixed boundary ($\varphi \to \infty$). In either way, the waves will be reflected, as full transmission only occurs for equal impedances (Andersen, 2006, Sec. 1.3).

As for the boundary convergence analysis in the half-space situation, the relative error near the boundary depends on the frequency. In Figure 2.20 the relative error of the vertical amplitude at 50 meter from the centerline of the track is shown as function of the frequency. For reference a model with an extension of 4 layer thicknesses is used (in this case $4 \cdot 10\text{m} = 40\text{m}$).

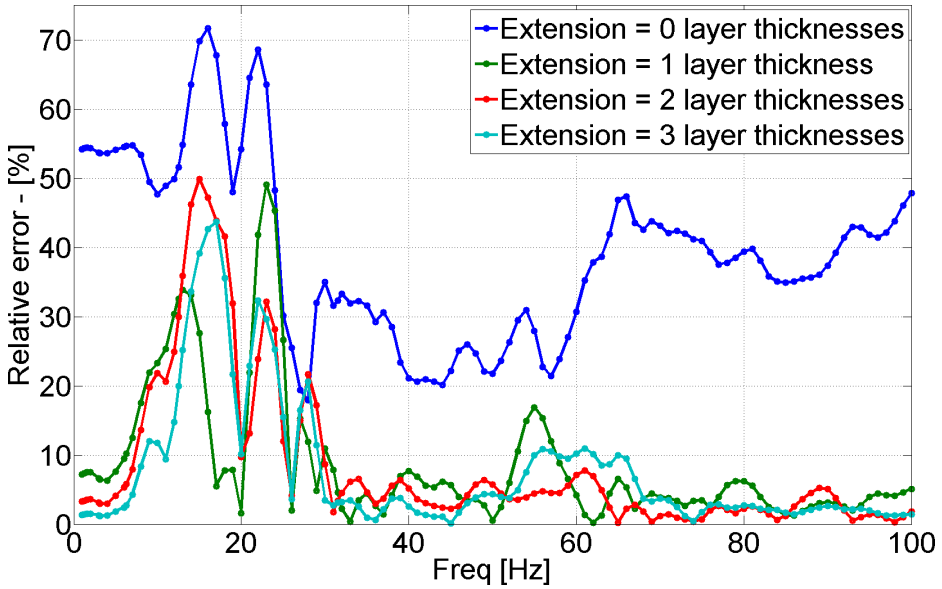

Figure 2.20 – *Relative errors over the frequency band for models with extensions of 0, 1, 2 and 3 layer thicknesses compared with a reference model with 4 layer thicknesses.*

As seen, relative large errors occur in the interval $10 - 25\text{Hz}$, even for a relatively large extension of the model. But as the main focus lies just above these frequencies; this issue will not be further addressed.

The mean error of the absolute amplitude over the frequency band is shown in Figure 2.21.

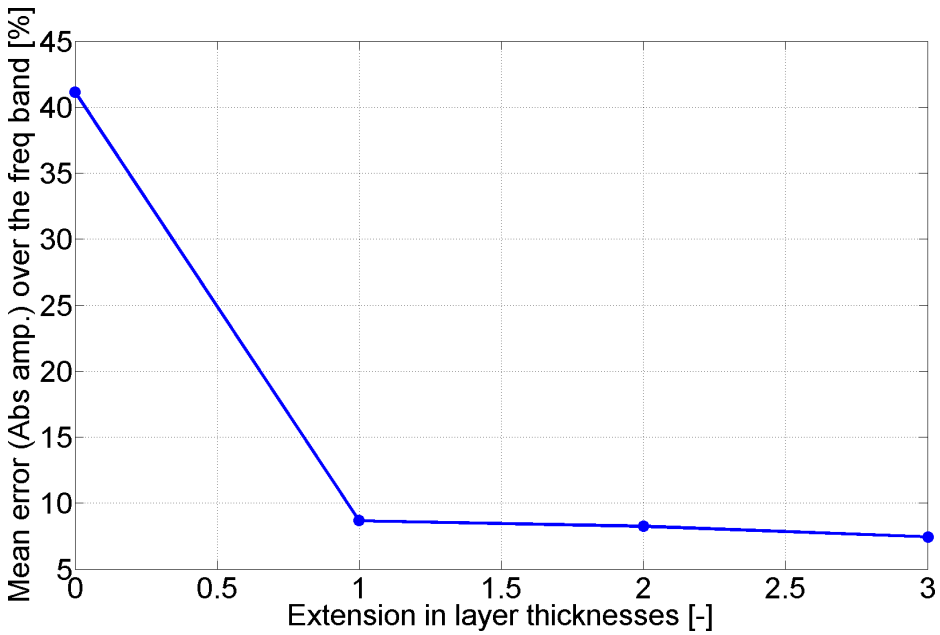

Figure 2.21 – *The mean errors over the frequency band for models with extensions of 0, 1, 2 and 3 layer thicknesses compared with a reference model with 4 layer thicknesses.*

As seen the error quickly drops as the extend of the model goes towards approximately 2 layer thickness from the points of interest. The errors introduced, due to this reflection at the boundary, for a layered half-space, is relatively large, compared with the disturbance encountered by diffraction. This holds true, even for extensive model extensions.

Chapter 3

Boundary Element Method

The overall model, described in Section 1.2, consists of two main parts. The first part, which will be described in this section, is the boundary element model, where the waves in the sub-soil are generated from a surface load applied at specified frequencies. The second part uses the output from the BEM as input for the finite element structure to find and identify loss and transmission of vibrations from the soil into the nearby structure.
A BE formulation, called TEA (two-dimensional elastodynamic analysis), is borrowed from C. J. C. Jones, D. J. Thompson and M. Petyt from "Institute of Sound & Vibration Research" without any kind of modification. Only the application of this model is used. The model with its applications is described below. (C. J. C. Jones, 1999a) (C. J. C. Jones, 1999b) After this, the BEM is described in Section 3.1.

Before the BEM is described the overall structure of the programs, starting from the geometry generation to the post processing of the response of the structure is described and listed below for a convenient overview. The layout is sketched in Figure 3.1.

Before the applications of BEM can be utilized via TEA, the geometry of the model must be specified. For this, some knowledge of the allowed input in the TEA software is needed, which can be found in the program manual, see reference (C. J. C. Jones, 1999a). The geometry of the different models will be generated in various geometry files, which lies in the main directory of the MatLab programs on the Appendix CD. The files are named "geo" followed by a expressive name relevant for the given model (*geo_ _ _.m*). A complete list of the geometry files with a short description is given in Appendix B.
When the geometry is configured, a .dat-file containing the materials used, the frequencies for which the load is applied, the BE nodes, the BE domains and obviously the load, which has to be applied in the BEM is generated.
TEA will now evaluate the input and compute amplitudes to the individual nodes for every frequency of interest creating a .res-file, containing the results for every node under a header showing the frequency.
This .res-file is now loaded by (*loadfile.m*) and the headers and the amplitude data's are split and saved in a structure containing all data for each frequency in a variable called output. The (*loadfile.m*) also provide post processing of the soil-only data, e.g. plots of the amplitudes in the horizontal (x-dir) and vertical (y-dir) direction as function of the frequency or the distance.
Finally the output variable from the (*loadfile.m*) is accessible in the FE model, (*FEM.m*). In this file the whole procedure of setting up a FEM is carried out. The outputs of this

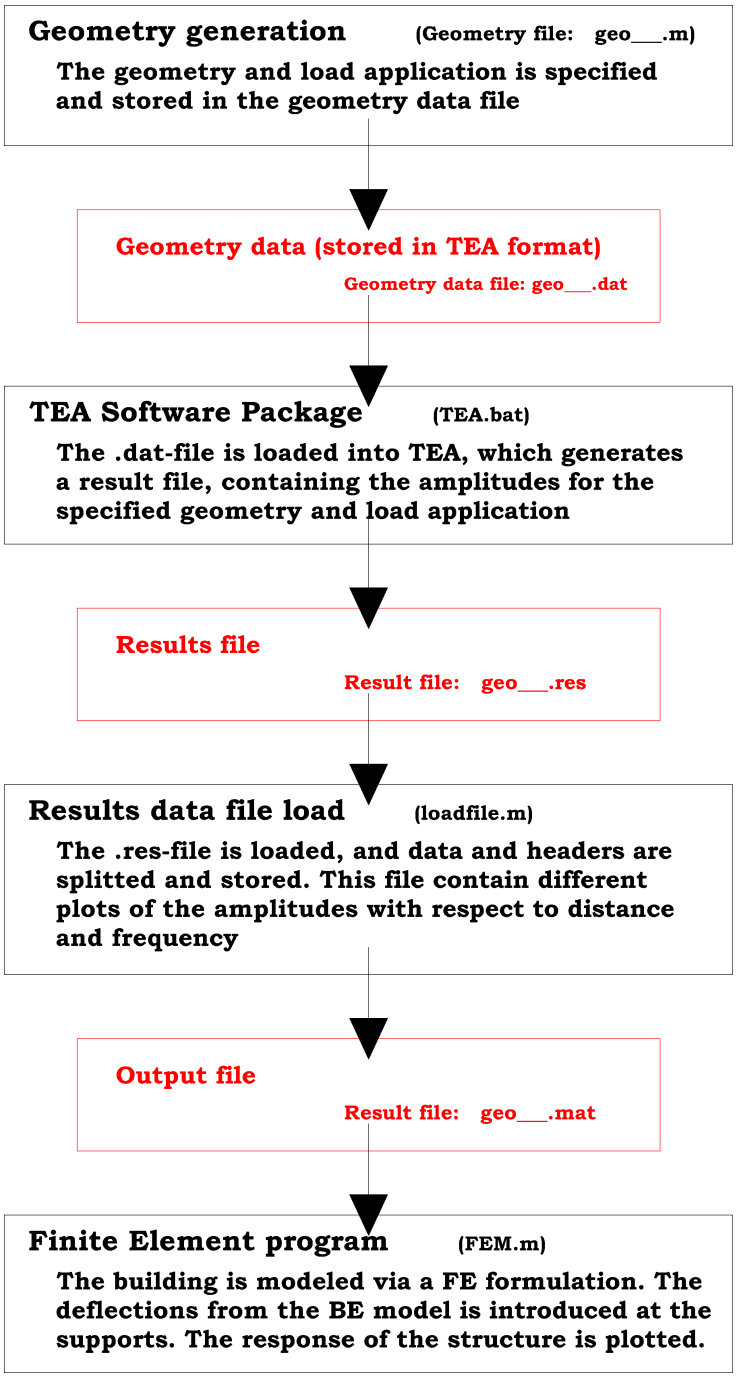

Figure 3.1 – *Sketch of program structure. The content marked with red, represent an output (file) generated by the overlying program.*

FE model will be the responses of a building, with a specified geometry on the selected soil profiles (specified in the geometry file), as function of the frequency. The evaluation of the results from the BE model is evaluated in Section 3.3, after the need knowledge regarding the BEM is summarized below. The setup of the FEM is gone through in Chapter 4.

The BE model, TEA, is used for the determination of the wave field in the soil model. It is also used for the coupled model, where the FE structure is included in the model. This requires a conversion of the BE matrices into equivalent FE matrices, as the BE formulation is relating surface tractions and deflections, while the FE formulation is relation stresses and strains (forces/moments and deflections). (C. J. C. Jones, 1999b)

3.1 Boundary Element Method

The theory behind the boundary element model and the used applications of the software package will be explained below in the relevant subsection, based on (Andersen, 2006).

The main reason for using the boundary element method for the description of the waves in the soils are the advantageous implementation of transmitting boundaries, see Section 2.4, and the reduced DOFs due to the discretization of the boundaries instead of the entire domain.

The BE formulation is basically a discretization of the Boundary Integral Equations. The basic Boundary Integral Equations (BIE) is described below.

3.1.1 Boundary Integral Equation

As for the finite element method, the principle used for obtaining the deflections in the prescribed soil domain, Ω, is a stress-strain relation derived with use of Newton's second law of motion. In this case the Cauchy Equation, which for the plane strain wave propagation problem in time domain looks like Equation (3.1).

$$\frac{\partial \sigma_{ij}(\mathbf{x},t)}{\partial x_j} + \rho b_i(\mathbf{x},t) = \rho \frac{\partial^2 u_i(\mathbf{x},t)}{\partial t^2} = \rho \ddot{u}_i(\mathbf{x},t) \quad i,j = 1,2 \tag{3.1}$$

where σ_{ij} are the Cartesian components of the Cauchy stress tensor, $b_i(\mathbf{x},t)$ is the load per unit mass in coordinate direction i, $u_i(\mathbf{x},t)$ are the components of the displacement field and $\ddot{u}_i(\mathbf{x},t)$ is the second time derivative of the displacement namely the acceleration, see Figure 3.2.

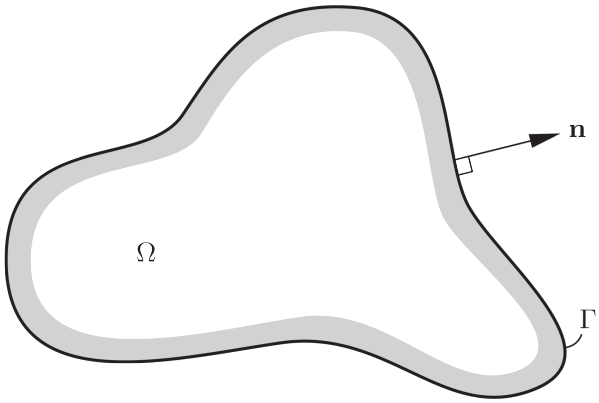

Figure 3.2 – *The elastic body* Ω*, bounded by the surface* Γ*, with the outward unit normal vector* $\mathbf{n}$*. (Andersen, 2006, Fig. 3-1)*

In order to solve the Cauchy equation boundary and initial conditions has to be selected. The boundary conditions are prescribed deflections or, as in this case, surface tractions along the surface Γ. The initial conditions are the deflection and velocity of the entire domain encircled by the surface Γ, see Equation (3.2).

$$\begin{aligned} p_i(\mathbf{x},t) &= p_i^{bc} \; for \; \mathbf{x} \in \Gamma \\ u_i(\mathbf{x},0) &= v_i^{ic} \; for \; \mathbf{x} \in \Omega \\ \dot{u}_i(\mathbf{x},0) &= \dot{v}_i^{ic} \; for \; \mathbf{x} \in \Omega \end{aligned} \tag{3.2}$$

where $p_i(\mathbf{x},t) = \frac{\partial \sigma_{ij}(\mathbf{x},t)}{\partial x_j} n_j(\mathbf{x})$ are the components of the surface traction vector related to plain strain.

The unknown deflection is now solved via a paraphrased Cauchy equation, called the Betti-Rayleigh theorem, see Equation (3.3).

$$\begin{aligned} &\int_0^t \int_\Gamma p_i^{(1)}(\mathbf{x},\tau) u_i^{(2)}(\mathbf{x},t-\tau) d\Gamma d\tau - \int_0^t \int_\Gamma p_i^{(2)}(\mathbf{x},t-\tau) u_i^{(1)}(\mathbf{x},\tau) d\Gamma d\tau \\ &+ \int_0^t \int_\Omega \rho b_i^{(1)}(\mathbf{x},\tau) u_i^{(2)}(\mathbf{x},t-\tau) d\Omega d\tau - \int_0^t \int_\Omega \rho b_i^{(2)}(\mathbf{x},t-\tau) u_i^{(1)}(\mathbf{x},\tau) d\Omega d\tau \\ &= \int_\Omega \rho \left[\dot{u}_i^{(1)}(\mathbf{x},t) v_i^{(2)}(\mathbf{x}) - u_i^{(2)}(\mathbf{x},t) \dot{v}_i^{(1)}(\mathbf{x}) \right] d\Omega \\ &+ \int_\Omega \rho \left[u_i^{(1)}(\mathbf{x},t) \dot{v}_i^{(2)}(\mathbf{x}) - \dot{u}_i^{(2)}(\mathbf{x},t) v_i^{(1)}(\mathbf{x}) \right] d\Omega \end{aligned} \tag{3.3}$$

where the superscript $^{(i)}$ refers to two states, at time $t_1 = \tau$ and $t_2 = t - \tau$.

One of the major differences between the FE and the BE formulation is the interpolation method of the field quantities of the individual elements in the respective models. In a FE model the field quantities is weighted hence interpolated via the shape functions, while for the BE a Green's function is selected for the weighting. Via the Green's function all elements

on the boundary are now related, connecting all elements at once unlike the FEM, where only elements containing coincident nodes are directly dependent on each other.

The Green's function has the general form $g(\mathbf{x}, t; \mathbf{y}, \tau)$. The output is the response at an observer, $\mathbf{x}$, to the time, t, due to a unit unit magnitude load at $\mathbf{y}$ applied at the time, τ, see Figure 3.3.
The Green's function is strongly dependent on the boundary conditions. In Figure 3.3, this is illustrated in a full (unbounded domain) and a half-space, where the response at the observer is influenced by the presence of the boundary, where the observer will be affected by the direct response (in a straight line) and a bit later by the reflected response from the boundary.

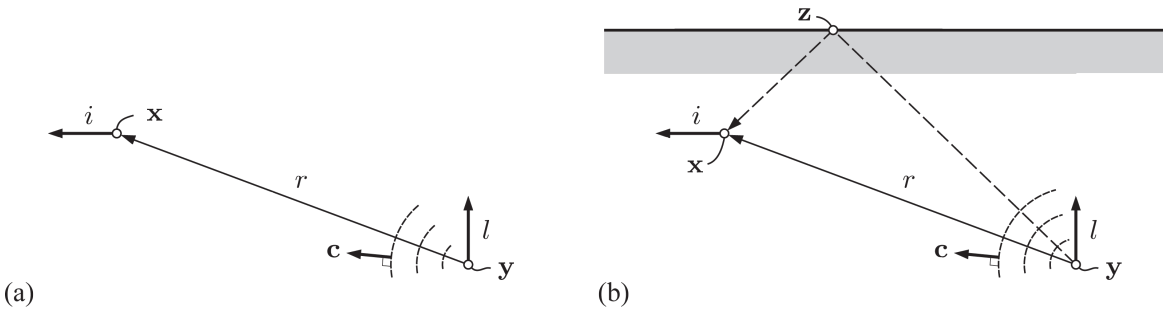

Figure 3.3 – *The figure illustrates the Green's function $g_{il}(\mathbf{x}, t; \mathbf{y}, \tau)$, which provide the response in direction i at point $\mathbf{x}$ to a load in direction l at $\mathbf{y}$. In both the full space (a) and the half space (b), a response is observed at the time $t - \tau = r/c$. Additionally a reflection response is seen in the half space due to the boundary (at point $\mathbf{z}$). (Andersen, 2006, Fig. 3-3)*

In the full space case, with wave propagation in an unbounded homogeneous elastic domain, the Green's function for the displacement in time domain is found via the Cauchy equation in Equation (3.1). It is noted that the Green's function is a tensor field $\mathbf{u}^*(\mathbf{x}, t; \mathbf{y}, \tau)$ with the double indiced components $u^*_{il}(\mathbf{x}, t; \mathbf{y}, \tau)$. An impulse in direction l in point $\mathbf{y}$ will introduce a response in direction i at point $\mathbf{x}$). The displacement field $\mathbf{u}(\mathbf{x}, t)$ is a vector field with the components $u_i(x, t)$. This lead to the see Equation (3.4).

$$\frac{\partial}{\partial x_j}\sigma^*_{ijl}(\mathbf{x}, t; \mathbf{y}, \tau) + \rho b^*_{il}(\mathbf{x}, t; \mathbf{y}, \tau) = \rho \frac{\partial^2}{\partial t^2} u^*_{il}(\mathbf{x}, t; \mathbf{y}, \tau) \tag{3.4}$$

where the body forces per unit volume now are defined with respect to the location and time via the Dirac delta functions

$$\rho b^*_{il}(\mathbf{x}, t; \mathbf{y}, \tau) = \delta_{il}\delta(\mathbf{x} - \mathbf{y})\delta(t - \tau) \tag{3.5}$$

3.1.1.1 Green's function for elastic waves in plane strain

In case of a homogeneous linear elastic isotropic material with a line load applied along the z-direction acting in phase and with no loads applied in the z-direction, a plane strain

model is allowable, since no response is generated in the z-direction. This corresponds to the combined P- and SV-wave propagation, which in the full space is governed by the Navier equation. The Navier equation is found via Hooke's law, see Equation (3.6).

$$\sigma_{ij}(\mathbf{x},t) = \lambda\Delta(\mathbf{x},t)\delta_{ij} + 2\mu\varepsilon_{ij}(\mathbf{x},t) \tag{3.6}$$

where λ and μ are the Lamé constants and $\Delta(\mathbf{x},t) = \varepsilon_{kk}(\mathbf{x},t)$ is the dilation.
The Navier equation is now appearing by inserting Hooke's law into Cauchy equation (Equation (3.1)), see Equation (3.7).

$$(\lambda+\mu)\frac{\partial^2 u_j(\mathbf{x},t)}{\partial x_i \partial x_j} + \mu\frac{\partial^2 u_i(\mathbf{x},t)}{\partial x_j \partial x_j} + \rho b_i(\mathbf{x},t) = \rho\frac{\partial^2 u_i(\mathbf{x},t)}{\partial t^2} = \rho\ddot{u}_i(\mathbf{x},t) \tag{3.7}$$

The governing equation for the Green's function is now found by inserting the Green's function u^*_{il}, see Equation (3.8).

$$(\lambda+\mu)\frac{\partial^2 u^*_{jl}(\mathbf{x},t;\mathbf{y},\tau)}{\partial x_i \partial x_j} + \mu\frac{\partial^2 u^*_{il}(\mathbf{x},t;\mathbf{y},\tau)}{\partial x_j \partial x_j} + \rho b^*_{il}(\mathbf{x},t;\mathbf{y},\tau) = \rho\ddot{u}^*_{il}(\mathbf{x},t;\mathbf{y},\tau) \tag{3.8}$$

where $\rho b^*_{il}(\mathbf{x},t,\mathbf{y};\tau)$ can be written

$$\rho b^*_{il}(\mathbf{x},t,\mathbf{y};\tau) = \delta_{il}\delta(\mathbf{x}-\mathbf{y})\delta(t-\tau) = \delta_{il}\delta(x_1-y_1)\delta(x_2-y_2)\delta(t-\tau) \tag{3.9}$$

The governing equation for the Green's function can be written in frequency domain similarly to Equation (3.8), see Equation (3.10).

$$(\lambda+\mu)\frac{\partial^2 U^*_{jl}(\mathbf{x},\omega;\mathbf{y})}{\partial x_i \partial x_j} + \mu\frac{\partial^2 U^*_{il}(\mathbf{x},\omega;\mathbf{y})}{\partial x_j \partial x_j} + \delta_{il}\delta(\mathbf{x}-\mathbf{y}) = -\rho^2 U^*_{il}(\mathbf{x},\omega;\mathbf{y}) \tag{3.10}$$

where the body force has been replaced by a harmonic varying function of the kind $B^*_{il}(\mathbf{x},\omega;\mathbf{y})e^{i\omega t} = \delta_{il}\delta(\mathbf{x}-\mathbf{y})$.

The Green's function corresponding to the solution of Equation (3.10) is given by Equation (3.11).

$$\begin{aligned} U^*_{il}(\mathbf{x},\omega;\mathbf{y}) &= \frac{1}{4i\rho c_P^2}\left[\frac{\varrho_i\varrho_l}{\varrho^2}H_0^{(2)}(k_P\varrho) + \left(\frac{\delta_{il}}{k_P\varrho} - \frac{2\varrho_i\varrho_l}{k_P\varrho^3}\right)H_1^{(2)}(k_P\varrho)\right] \\ &+ \frac{1}{4i\rho c_S^2}\left[\left(\delta_{il} - \frac{\varrho_i\varrho_l}{\varrho^2}\right)H_0^{(2)}(k_S\varrho) - \left(\frac{\delta_{il}}{k_S\varrho} - \frac{2\varrho_i\varrho_l}{k_S\varrho^3}\right)H_1^{(2)}(k_S\varrho)\right] \end{aligned} \tag{3.11}$$

where $k_P = \omega/c_P$ and $k_S = \omega/c_S$ are the wavenumbers for the primary and the secondary waves, ϱ is the distance vector and H_n^2 is the Hankel function of the second kind and order n.

Before the formulation of the Boundary Element Method can be established, Equation (3.3) is rewritten among other things with the use of reciprocity relations for the Green's function. The Somigliana's identity for the frequency domain is now obtained in Equation (3.12).

$$\begin{aligned} C(\mathbf{x})U_i(\mathbf{x},\omega) \quad &+ \quad \int_\Gamma P^*_{il}(\mathbf{x},\omega;\mathbf{y})U_l(\mathbf{y},\omega)d\Gamma(\mathbf{y}) \\ = \int_\Gamma U^*_{il}(\mathbf{x},\omega;\mathbf{y})P_l(\mathbf{y},\omega)d\Gamma(\mathbf{y}) \quad &+ \quad \int_\Omega U^*_{il}(\mathbf{x},\omega;\mathbf{y})\rho B_l(\mathbf{y},\omega)d\Omega(\mathbf{y}) \end{aligned} \tag{3.12}$$

where $U^*_{il}(\mathbf{x},\omega;\mathbf{y})$ and $P^*_{il}(\mathbf{x},\omega;\mathbf{y})$ are the Green's functions for the displacements and the surface traction. $C(\mathbf{x})$ is a scalar constant, which depend on the geometrically location of the evaluated point and is equal to 1, within the domain Ω, and is geometrically weighted at the boundary.

3.1.2 BEM

The Boundary Element Method is a discretization of the Boundary Integral Equation, where the basic idea is to partition the boundary, Γ, enclosing the domain, Ω, into sub-boundaries, Γ_j, where each partition, is referred to as one Boundary Element, see Figure 3.4.

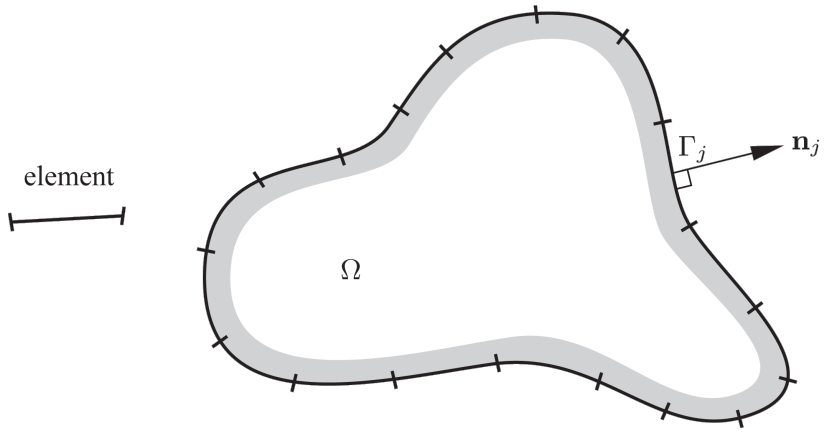

Figure 3.4 *– Discretization of the boundary, Γ, encirceling the domain, Ω, into boundary elements, Γ_j, with the outward unit normal n_j. (Andersen, 2006, Fig. 4-1)*

The Somigliana's identity is the basis for the development of the Boundary Element method, see Equation (3.13).

$$\begin{aligned} C_{il}(\mathbf{x})U_i(\mathbf{x},\omega) + \int_\Gamma P^*_{il}(\mathbf{x},\omega;\mathbf{y})U_l(\mathbf{y},\omega)d\Gamma(\mathbf{y}) \\ = \int_\Gamma U^*_{il}(\mathbf{x},\omega;\mathbf{y})P_l(\mathbf{y},\omega)d\Gamma(\mathbf{y}) \end{aligned} \tag{3.13}$$

Here $U_i(\mathbf{x},\omega)$ and $P_i(\mathbf{y},\omega)$ signify the displacements and the surface tractions in the physical state, while $P^*_{il}(\mathbf{x},\omega;\mathbf{y})$ signifies the Green's function for the surface traction with $U^*_{il}(\mathbf{x},\omega;\mathbf{y})$

signifying the displacements in the fundamental solution state.
$C_{il}(\mathbf{x})$ depends on the location, as stated above and takes the value $C_{il}(\mathbf{x}) = C(\mathbf{x})\delta_{il}$.

A discretization of Equation (3.13) provides the result in Equation (3.14).

$$\begin{aligned}\mathbf{C}(\mathbf{x}_i)\mathbf{U}_i(\mathbf{x}_i,\omega) + \sum_{j=1}^{NE}\left[\int_{\Gamma_j}\mathbf{P}^*(\mathbf{x}_i,\omega;\mathbf{y})\mathbf{\Phi}_j(\mathbf{y})d\Gamma_j(\mathbf{y})\right]\mathbf{U}_j(\omega)\\ = \sum_{j=1}^{NE}\left[\int_{\Gamma_j}\mathbf{U}^*(\mathbf{x}_i,\omega;\mathbf{y})\mathbf{\Phi}_j(\mathbf{y})d\Gamma_j(\mathbf{y})\right]\mathbf{P}_j(\omega)\end{aligned} \tag{3.14}$$

where NE represent the number of elements in the domain, while $\mathbf{\Phi}_j$ contains the shape functions used for the interpolation between the nodal quantities and

$$\mathbf{U}(\mathbf{x},\omega) = \mathbf{\Phi}_j(\mathbf{x})\mathbf{U}_j(\omega), \quad \mathbf{P}(\mathbf{x},\omega) = \mathbf{\Phi}_j(\mathbf{x})\mathbf{P}_j(\omega) \tag{3.15}$$

Equation (3.14) contain two summations over the number of elements, NE. The inner integrals are stored in two matrices, for convenience, see Equation (3.16).

$$\int_{\Gamma_j}\mathbf{P}^*(\mathbf{x}_i,\omega;\mathbf{y})\mathbf{\Phi}_j(\mathbf{y})d\Gamma_j(\mathbf{y}) = \widehat{\mathbf{H}}_{ij}, \quad \int_{\Gamma_j}\mathbf{U}^*(\mathbf{x}_i,\omega;\mathbf{y})\mathbf{\Phi}_j(\mathbf{y})d\Gamma_j(\mathbf{y}) = \widehat{\mathbf{G}}_{ij} \tag{3.16}$$

Letting $\mathbf{H}_{il}(\omega)$ be defined by

$$\mathbf{H}_{ij}(\omega) = \begin{cases} \widehat{\mathbf{H}}_{ij} + \mathbf{C}(\mathbf{x}_i) & \text{for} \quad x_i = j \\ \widehat{\mathbf{H}}_{ij} & \text{for} \quad x_i \neq j \end{cases} \tag{3.17}$$

Equation (3.14) can now be written in the form

$$\sum_{j=1}^{NE}\mathbf{H}_{ij}(\omega)\mathbf{U}_j(\omega) = \sum_{j=1}^{NE}\mathbf{G}_{ij}(\omega)\mathbf{P}_j(\omega) \tag{3.18}$$

The global system of equations for the entire domain can now be assembled in Equation (3.19).

$$\mathbf{H}(\omega)\mathbf{U}(\omega) = \mathbf{G}(\omega)\mathbf{P}(\omega) \tag{3.19}$$

Here $\mathbf{U}(\omega)$ and $\mathbf{P}(\omega)$ are vectors storing the nodal values of the displacements and the traction.

The BEM has some advantages over the FEM by virtue of the Green's function. Obviously the boundary element method only has to discretize the boundaries, e.g. the surface and interfaces in between different soil layers. This strongly minimizes the computational time, since it is avoided to discretize the whole domain. This minimizes the DOFs and hereby the system matrices **H** and **G**, but this does not mean a reduction in computational time of $\left(\frac{n_{DOF}}{n_{DOF}^{red}}\right)^2$ compared to the corresponding FEM, since all entrances of the system matrices are occupied, (unlike the stiffness matrix, where only the diagonal is occupied).
In addition to that, it is possible to use open boundaries, where a certain transmission will take place, i.e. "transmitting boundaries". This is a useful tool, when a constant oscillating load is creating a response into finite soil profile like in this case. If the boundary was reflecting, the waves back into the domain of interest, the incident and the reflected waves would create larger waves than expected due to energy conservation.

3.2 Soil stratifications

Two soil profiles are used for the analysis in Chapter 5. They are selected from the existing soil investigations available on the Femern Belt Link homepage (Andersen, 2010). The first profile consists of 10m of moraine overlying a stiffer moraine occupying the lower half-space. The second stratification consists of 5m dry sand overlying a moraine similar to the top moraine in the first soil stratification. The material properties of the two soil profiles are listed in Table 3.1, where also Young's modulus, Poisson's ratio, the density and the hysteretic damping is given.

Soil 1	Layer	[MPa]	ν [–]	ρ [kg/m^3]	η [–]	Description
	1	2340	0.300	2200	0.030	Moraine (0-10m)
	2	6760	0.300	2400	0.020	Stiffened moraine (10m+)
Soil 2	Layer	[MPa]	ν [–]	ρ [kg/m^3]	η [–]	Description
	1	270	0.350	1700	0.035	Dry sand (0-5m)
	2	2340	0.300	2200	0.030	Moraine (5m+)

Table 3.1 *– Material properties for soil 1 and 2.*

With these properties, the wave speeds can be calculated, with use of Equation (2.4), see Table 3.2.

Wave speed [m/s]	**Stiffened moraine**	**Moraine**	**Dry sand**
c_P	1947	1197	505
c_S	1041	640	242
$c_{Rayleigh}$	989	607	231

Table 3.2 *– Wave speeds for the primary, the secondary and the Rayleigh wave for the three soil materials.*

3.3 BE soil model results

In the following section, the results from the two soil stratifications are evaluated. In Section 4.3, the corresponding results for the uncoupled building model, where the output displacements from the soil model is used as forced displacements for the structure, is shown. Finally in Section 5.1, the results from the model, where the FE structure is included in the TEA software, creating a combined FE-BE model, allowing for interactions between the soil and the structure, is evaluated.

3.3.1 Soil 1

The wave field for soil 1 is visualized in Figure 3.5 and Figure 3.6, where the absolute amplitudes on the surface in the horizontal and vertical directions are plotted against the distance to the track for a few selected frequencies. Note that, the lowest frequencies are not expected to provide converging values as the model only extends 24m further than the back most wall. This correspond to converging results for 25Hz and above for soil 1 ($c_{Rayleigh}$/24m$\approx$ 25Hz), see Section 2.3 and Section 2.4.

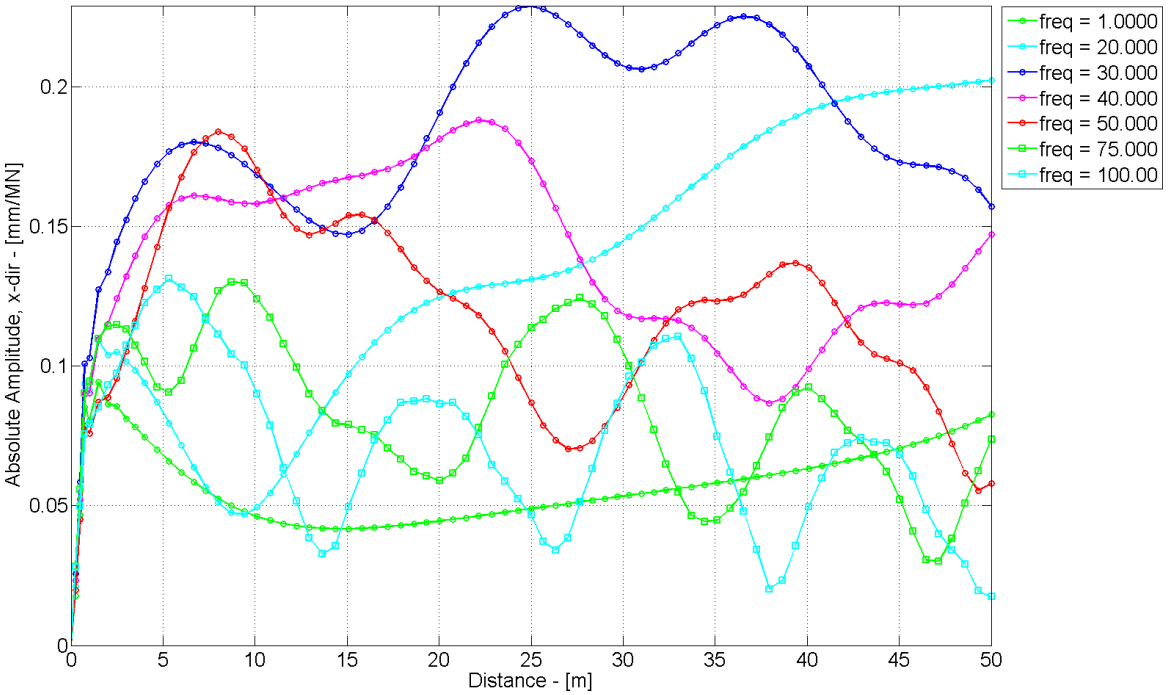

Figure 3.5 – *Absolute amplitudes for soil 1 as function of the distance to the track, in the x-direction.*

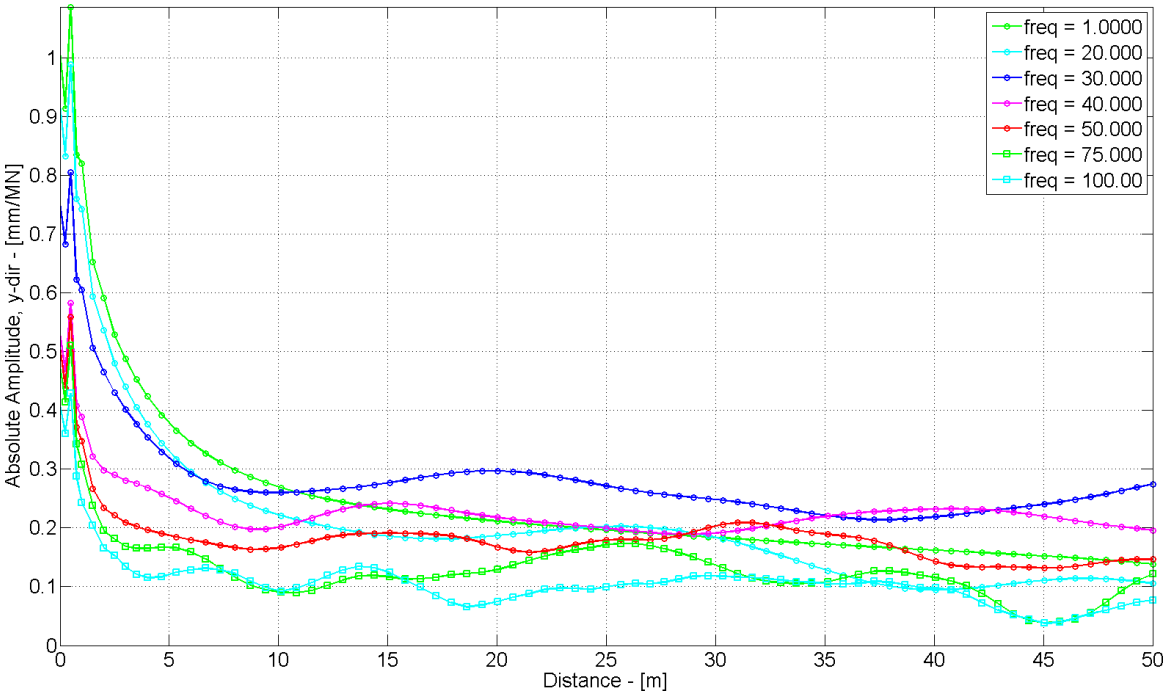

Figure 3.6 – *Absolute amplitudes for soil 1 as function of the distance to the track, in the y-direction.*

Both Figure 3.5 and Figure 3.6 shows, that the wave field is influenced by the interface between the two soil materials, as reflections have caused interference at the surface. This shows, that the absolute amplitudes vary more or less randomly along the first axis (compared with the half-space model, where the amplitudes decrease with a certain amount per wavelength, see for instance Figure 2.11). The peaks and the local minimums arise, due to interference. The tendency is for instance seen for the several peaks along the 100Hz curve, for the horizontal response, where the peaks is spaced with $\approx$ 14m. This distance correspond to one wavelength reflected at the interface between the two soil layers 10m below the surface, see Figure 3.7.

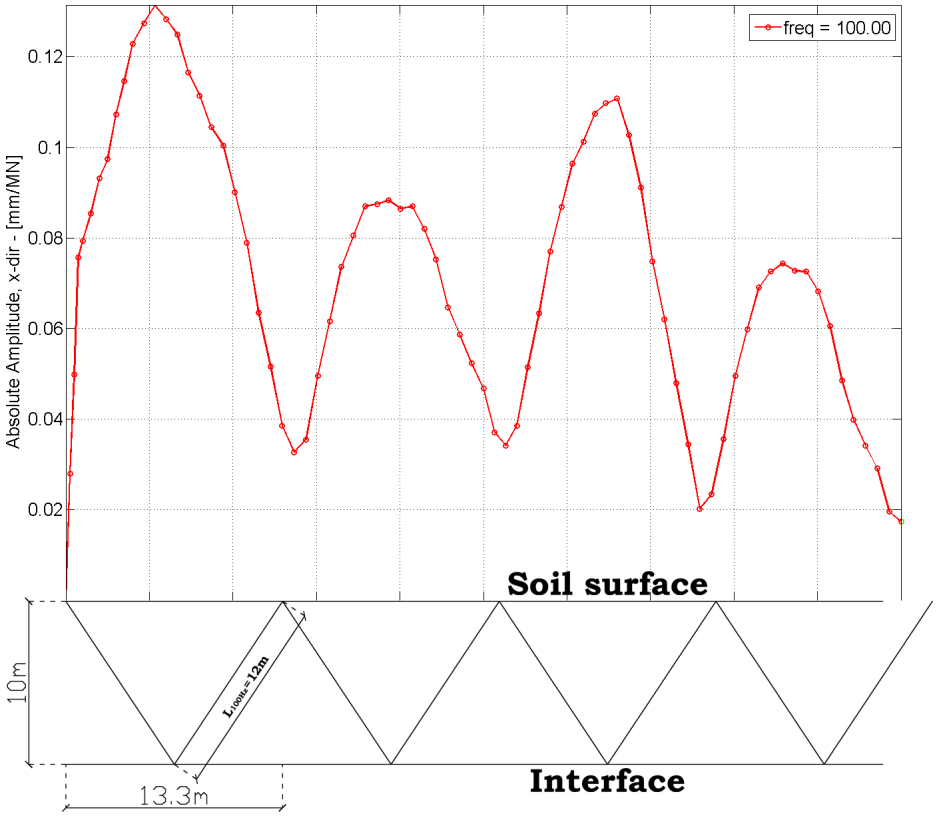

Figure 3.7 – *Interference on the soil surface, caused by the reflected 100Hz wave illustrated with the absolute amplitude for soil 1 as function of the distance to the track, in the x-direction.*

This tendency is more or less clear for the other plotted frequencies, see Figure 3.5 and Figure 3.6. The waves look more and more irregular, as the wave field gets influence by more and more different reflected waves, as waves of multiple wavelengths gets reflected, see Figure 3.8. This irregular appearance will increase for a growing distance to the source (at the track).

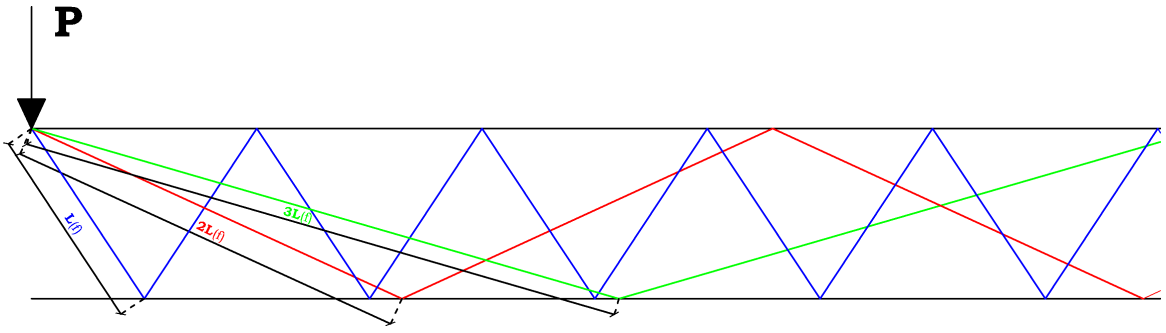

Figure 3.8 – *Wave field disturbed by reflected waves, with different "reflection lengths". The reflected waves are illustrated for 1, 2 and 3 wavelengths as the reflection length for the frequency in question.*

To find the frequencies of interest at the location of the building, the response of the soil is evaluated in the points, where the structure is connected to the ground. In Figure 3.9 and Figure 3.10, the maximum response of the soil is given as function of the frequency, with a reference point 8m from the center of the track.

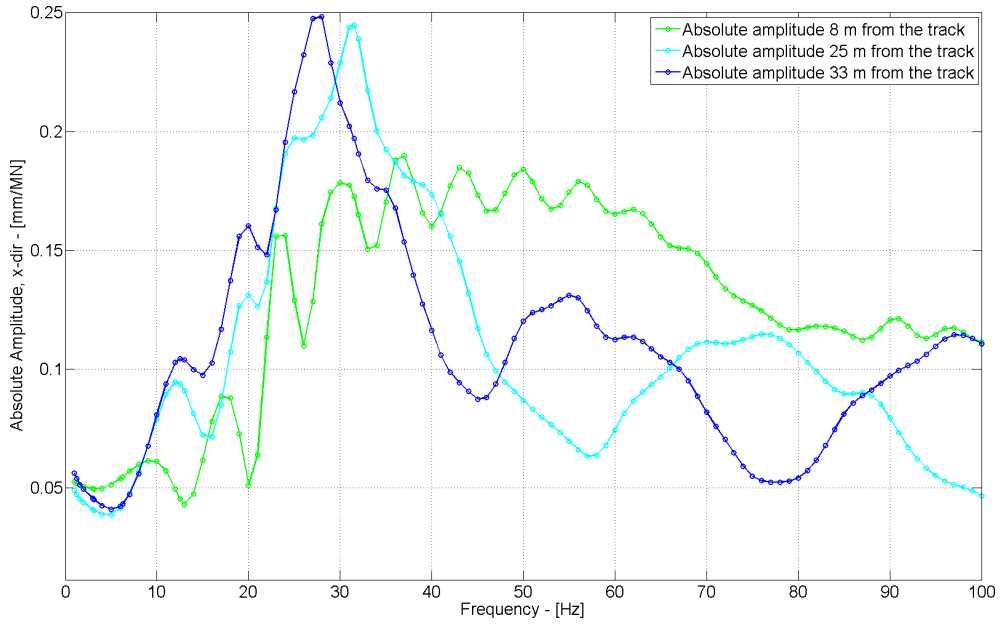

Figure 3.9 – *Absolute amplitudes in the x-dir on soil 1, at the base of the building (25 and 33m from the track) and at a reference point 8m from the track. The amplitudes are given as function of the load application frequency.*

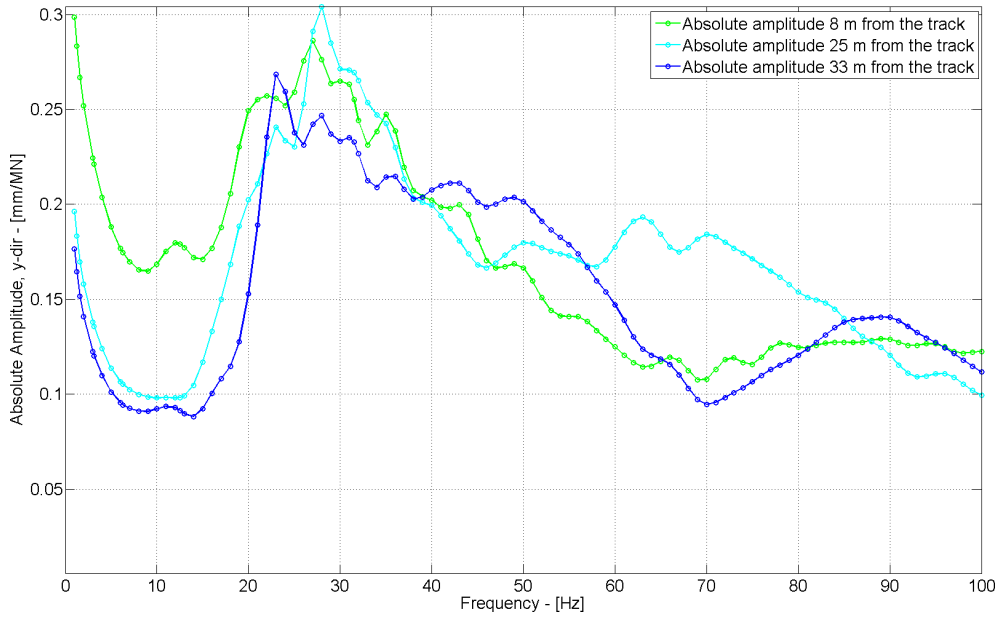

Figure 3.10 – *Absolute amplitudes in the y-dir on soil 1, at the base of the building (25 and 33m from the track) and at a reference point 8m from the track. The amplitudes are given as function of the load application frequency.*

The peak response, which occur for 22-28Hz, is achieved for a load of 1MN per meter in the depth, which is set a bit high (as this load correspond to the weight of a full 59m long IC3 train (DSB, 2011)). The absolute amplitude will therefore be significantly lower, than this value. But as the absolute amplitudes, are only considered relative to each other, this issue is not further addressed.
The response at a distance 25 and 33m from the track have three peaks between 0 and 100Hz. The first peak is observed furthest away, at the 33m point at a frequency of 27Hz. The same peak occurs for a slightly higher frequency at the 25m corresponding to a bit lower wavelength (and reflection length). The response 8m from the track is a bit more washed out, with no particular peaks, in contrast to the observed behavior of the two points 25 and 33m from the track. This washed out response occur, since this point lie relatively close to the load application, and response from the left side of the track and the right side of the track will be out of phase, at least for the horizontal response, as seen on Figure 3.9.
Both the horizontal and vertical response at 25 and 33m is relatively sensitive at and around 30Hz (20-40Hz), where the response is peaking and the absolute amplitude has even gained compared with the reference point 8m from the track. This can be visualized on a loss curve, where the loss of amplitude is given with respect to a reference point, which will be set to the 8m point. The loss is calculated in dB, via Equation (3.20).

$$Loss(x_1, f) = 20 \cdot log_{10}\left(\frac{U_{ref}(x_{ref}, f)}{U(x_1, f)}\right) \tag{3.20}$$

where f is the frequency, x_{ref} is the reference point and is set to 8m and x_1 is set to 25m and 33m respectively.

The loss is now expressed in dB, see Figure 3.11 and Figure 3.12.

While the peaks of the points at 25 and 33m, are well defined, the washed out response 8m from the track, lead to a significant loss peaking just below 60Hz at 25m and just below 80Hz for the x-direction. The loss in the vertical direction is mainly taken place at low frequencies, whereas the response in all points is of equal magnitude for the rest of the frequency band (except the response at 25m around 70Hz), see Figure 3.12.
For both the horizontal and the vertical response no (or little) loss occurs around the peak at (20-40Hz).

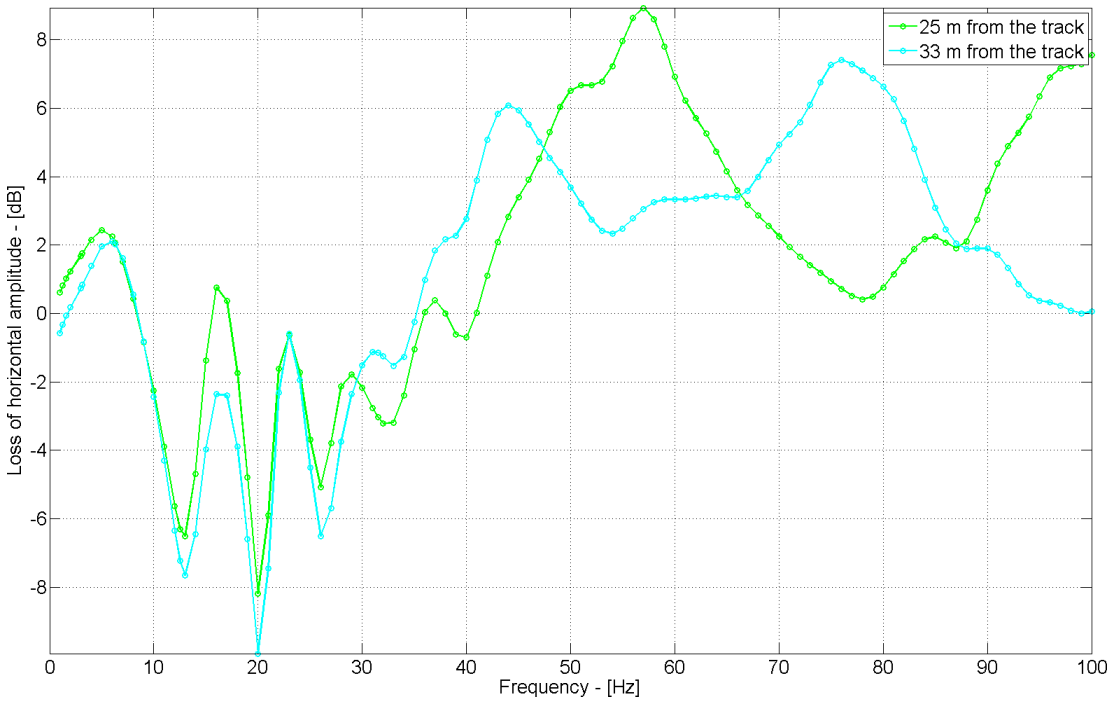

Figure 3.11 – *Loss of horizontal amplitude relative to $x_{ref} = 8m$ on soil 1, at the base of the building (25 and 33m from the track). The loss is measured in dB.*

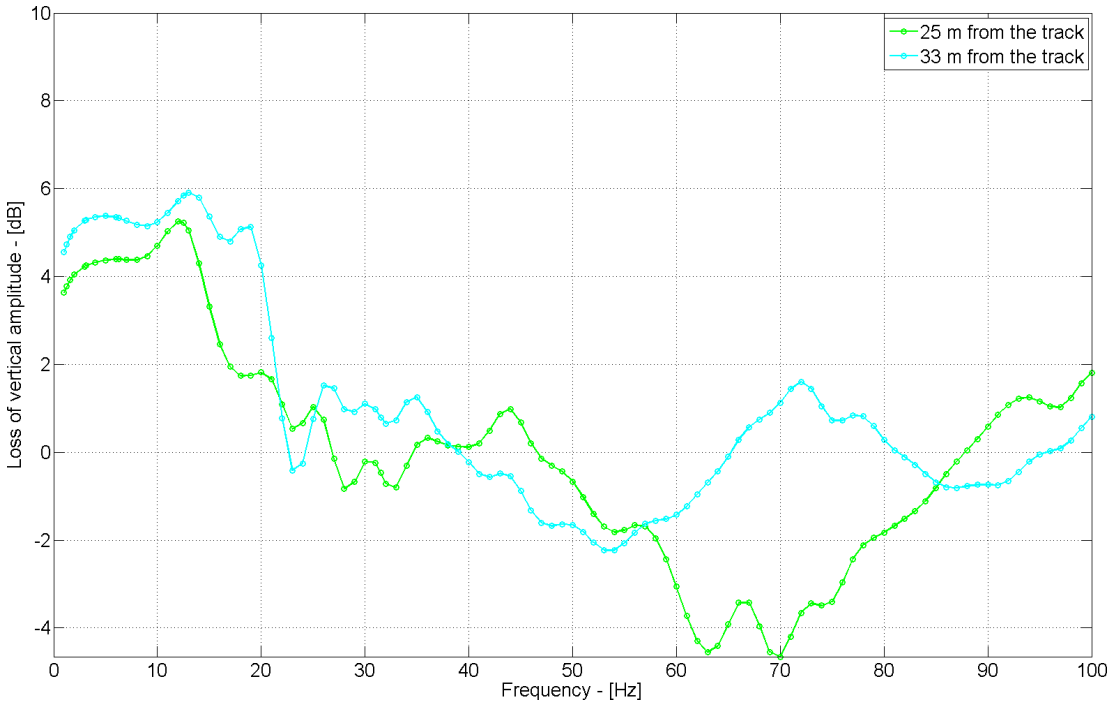

Figure 3.12 – *Loss of vertical amplitude relative to $x_{ref} = 8m$ on soil 1, at the base of the building (25 and 33m from the track). The loss is measured in dB.*

3.3.2 Soil 2

For soil number two, the amplitudes in the x- and the y-direction is shown in Figure 3.13 and Figure 3.14.

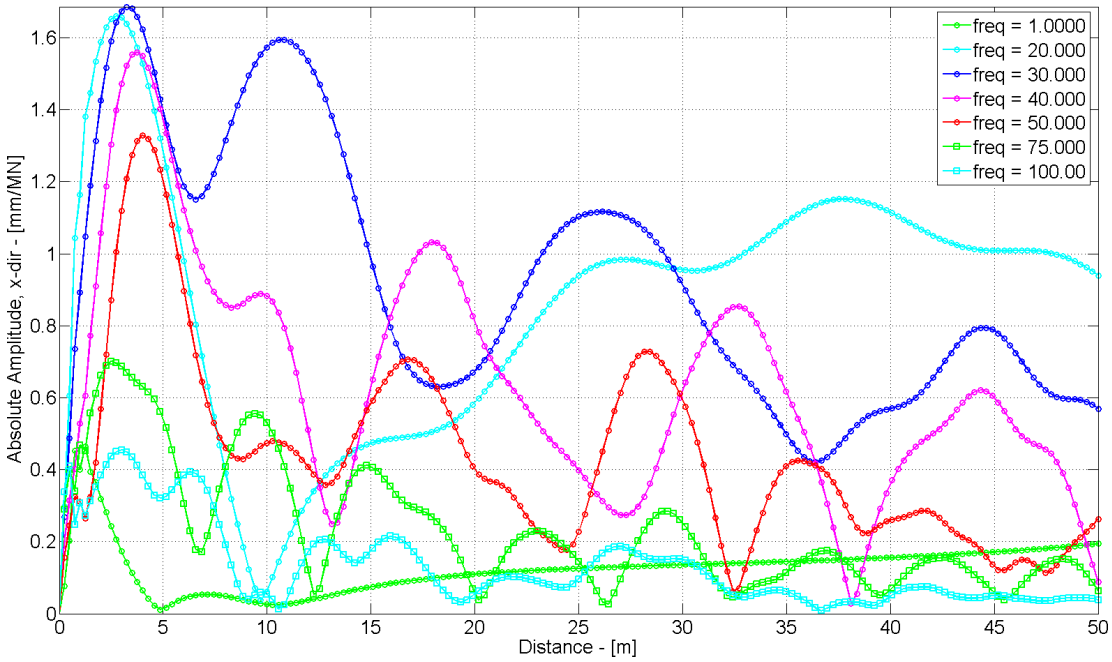

Figure 3.13 – *Absolute amplitudes for soil 2 as function of the distance to the track, in the x-direction.*

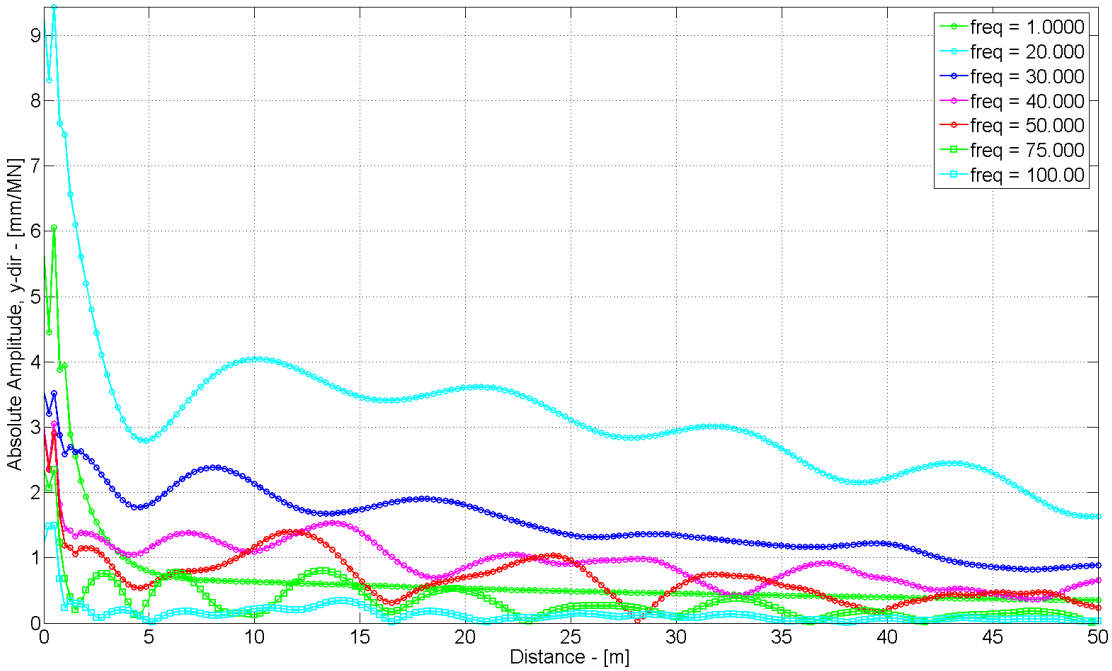

Figure 3.14 – *Absolute amplitudes for soil 2 as function of the distance to the track, in the y-direction.*

The response of the soil at the building site, is plotted against the frequency for the horizontal and the vertical response, in Figure 3.15 and Figure 3.16.

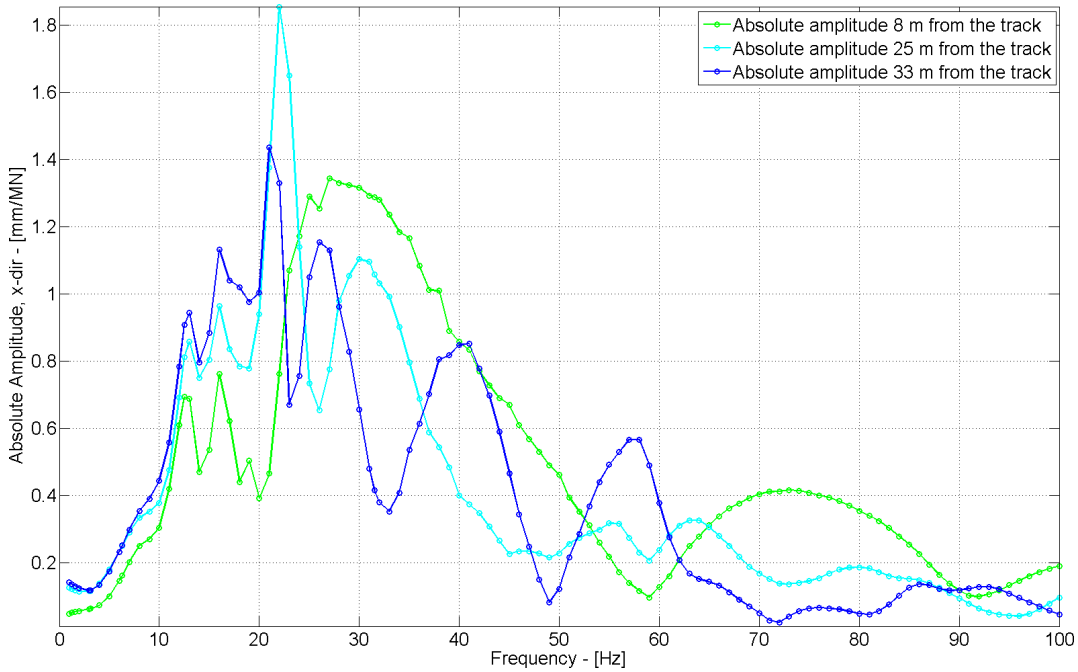

Figure 3.15 – *Absolute amplitudes in the x-dir on soil 2, at the base of the building (25 and 33m from the track) and at a reference point 8m from the track. The amplitudes are given as function of the load application frequency.*

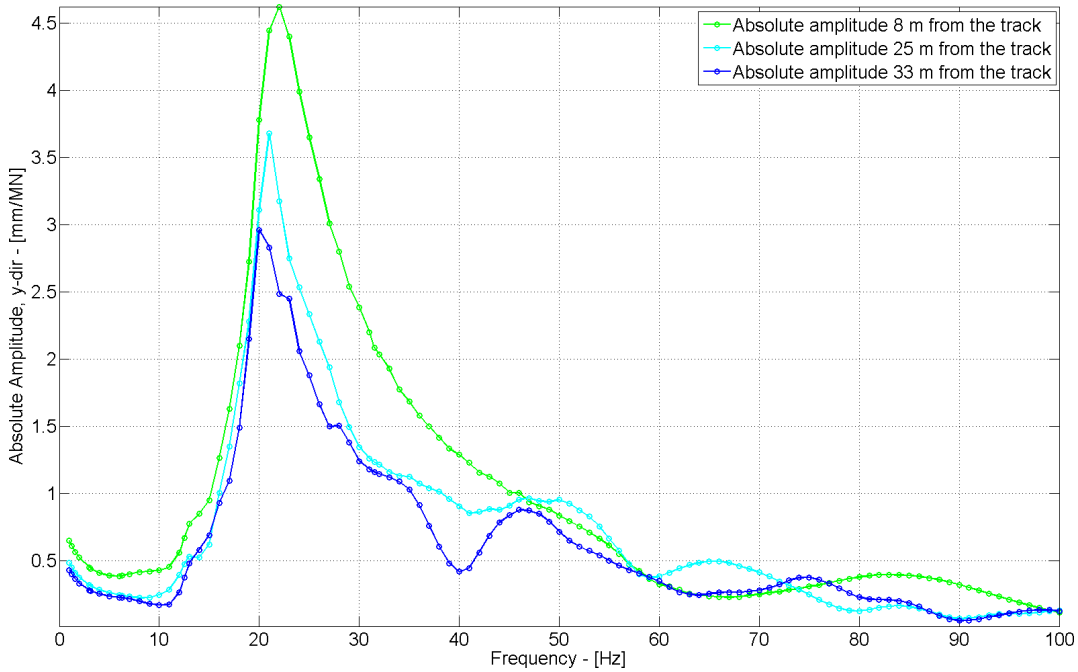

Figure 3.16 – *Absolute amplitudes in the y-dir on soil 2, at the base of the building (25 and 33m from the track) and at a reference point 8m from the track. The amplitudes are given as function of the load application frequency.*

The shape of the curve is somewhat similar to the curves for soil 1, but the peak frequency is a bit lower, peaking around 20Hz.
The order of magnitude of the response on soil 2 is 9-15 times larger than for soil 1. This increase of the responsiveness is due to the much softer materials, see Table 3.1.

The loss of amplitude at 25m and 33m is plotted in Figure 3.17 and Figure 3.18.

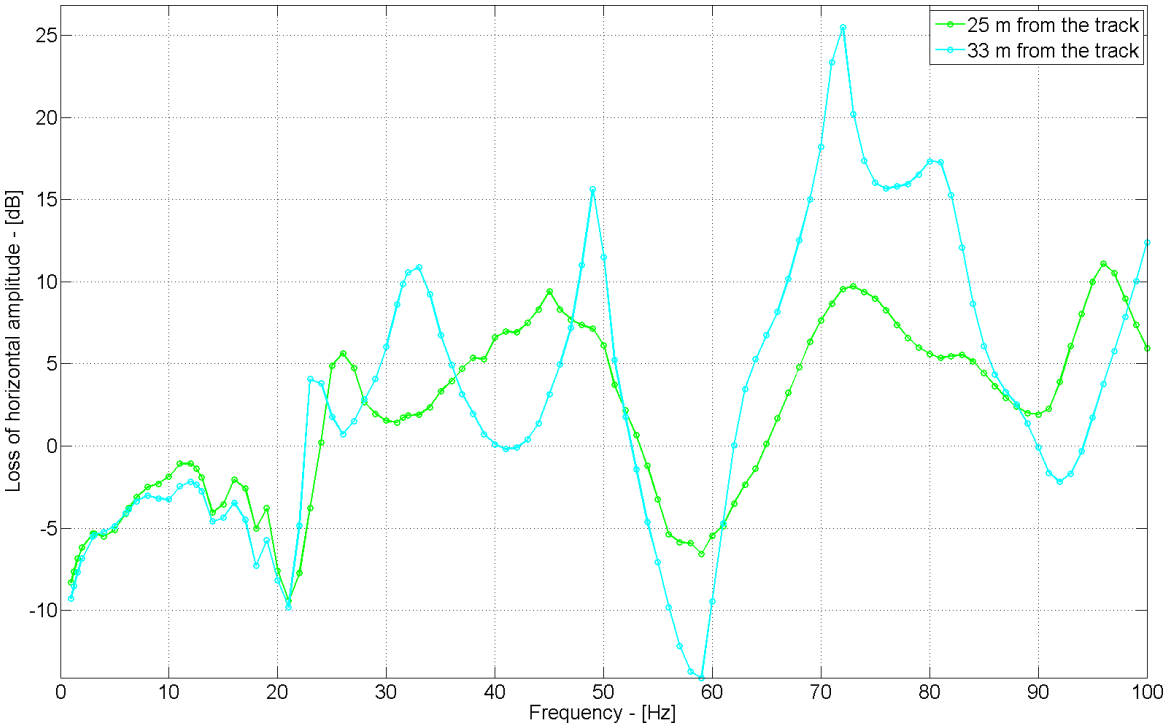

Figure 3.17 – *Loss of horizontal amplitude relative to* $x_{ref} = 8m$ *on soil 2, at the base of the building (25 and 33m from the track).*

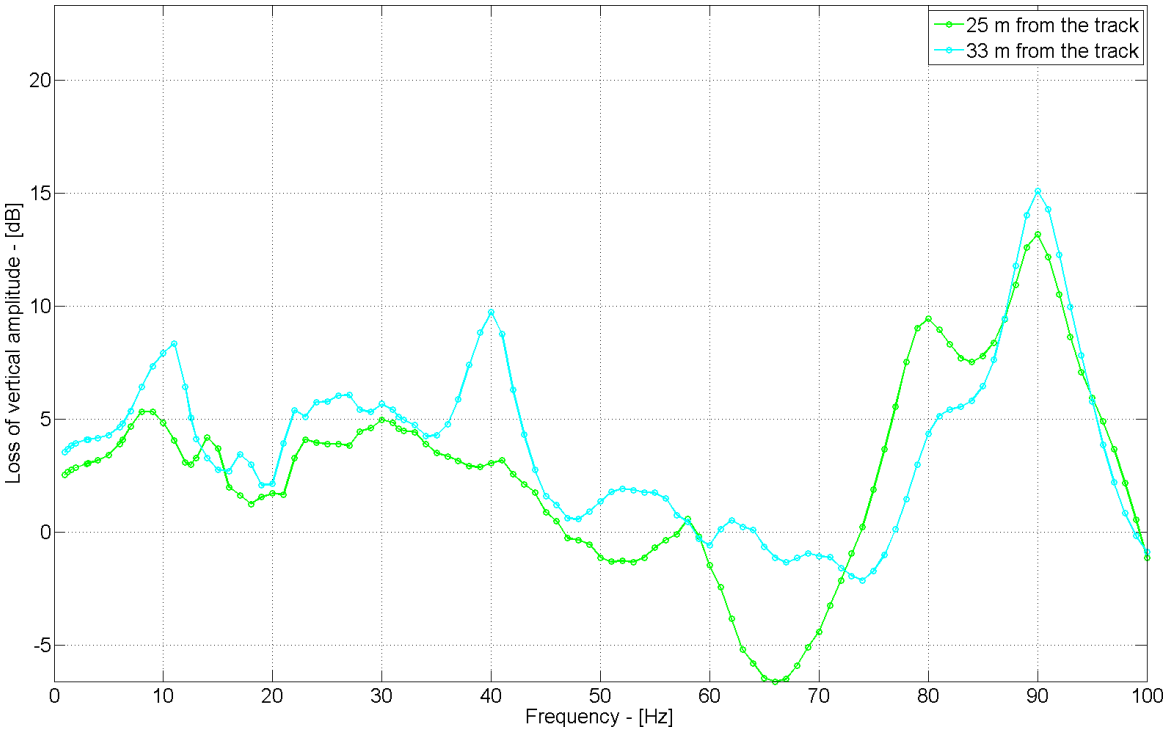

Figure 3.18 – *Loss of vertical amplitude relative to $x_{ref} = 8m$ on soil 2, at the base of the building (25 and 33m from the track).*

The loss of amplitude is a bit more distinct for soil 2; especially for frequencies around 70-90Hz, where the loss exceeds 15dB, for both the vertical and the horizontal response. This could be coincidental (as only two point are looked upon), or mean, that a higher amount of energy is dissipated in the interface between the soil layers.

Chapter 4

Finite Element Method

The waves traveling in the soil and along the surface, will hit the building which lies 25m from the center of the track. The building is 8m wide, which means that the back most wall will be placed 33m from the center of the track. The height of the building is set to 2.5m and is shown in Figure 4.1.

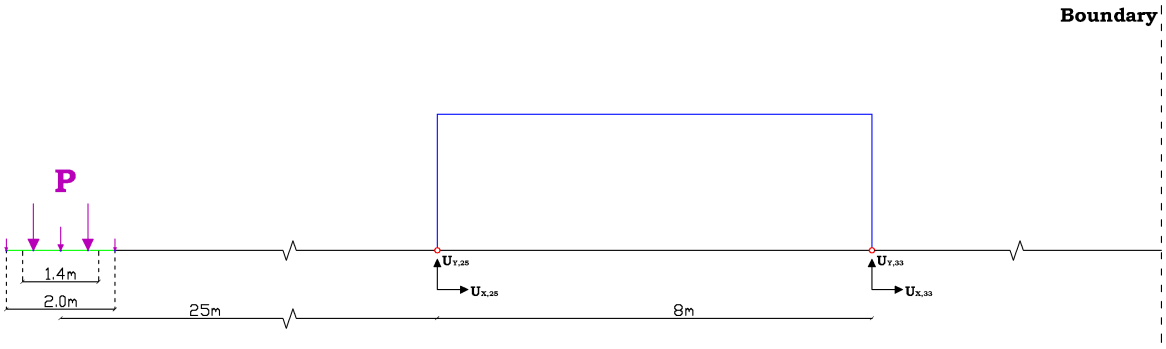

Figure 4.1 – *General model outline, (line) load application at the track, simple supported building with forced vibrations/deflections at the bases of the outer walls and boundary at the far right.*

The output from the BE model with the waves introduced by the train, will cause vibrations in the building as the building is coupled to the soil. However this coupling can be constructed in various ways. The most simple way of coupling the soil and the building is by forcing the building to move (x- and y-direction) as the soil do, at the two points where the wall of the construction meet the soil. This simplified coupling does not allow for any response from the building, to interact with the wave field in the sub-soils. This "back coupling", or lack of it, may or may not have a significant effect on the overall model, i.e. the wave field and the response of the structure. The building will counteract the forced movement from the soil with a force, which depends on the stiffness and the mass of the structure as well as the frequency of the load application (or equivalently the acceleration). The order of magnitude from the reaction forces from the FE structure, compared with the applied force at the track, will give an indication of the importance of the back coupling in the model at the given frequency. The reaction forces for the simple coupling, with no back coupling, is found in Section 4.3 further down and is compared with the response of a integrated BE-FE

model, which is conducted in the TEA software in Chapter 5. In this way the simple model can be compared with a model including the back coupling. (C. J. C. Jones, 1999a)

As a start, the simple model, with no back coupling is setup. This is done an external FE program, in (*FEM.m*) on the Appendix CD. The structure will be simply supported and the deflections of the soil will here be provided for the structure.
The construction will now be excited by the waves traveling in the soil, via the horizontal and vertical movements at the base of the building. Particular large movements of the building are expected at the eigenfrequencies of the construction itself.
The excitation of the building will, for the human body, be felt, via changes in the acceleration. The body expect an acceleration of 9.82m/s^2 in the vertical direction corresponding to gravitation and 0m/s^2 for the horizontal direction. From this it will be expected that small deviations in the horizontal acceleration will have a greater influence on the noticed disturbance inside the reference building. A deviation on a few percents, in the vertical direction might be unnoticeable in the vertical direction, while the same accelerations may be disturbing, if it is acting horizontally, where the body is used to no acceleration.

The movements of the building will be depending on the eigenfrequencies and the corresponding eigenmodes. This means, that even of the building is excited at or near one of its eigenfrequencies, it may not provide a large response, because the building could be excited in a way, where the mode shape is not possible for the given frequency, see Section 4.2.
In these cases, the building will just follow the movements of the soil.

The FE formulation used for the FE construction is described in the following section, where element as well as the global stiffness, mass and damping matrices are setup, loads and boundary conditions are applied and the global system of equations is solved.

4.1 Model setup

The general layout of a FE formulation has the following steps, which have to be gone through (Andersen, 2006, Chapter 2):

1. establish the strong formulation of the given problem
2. establish the weak formulation
3. discretize the continuous field into a finite number of nodal values
4. select the shape functions for the physical and virtual field
5. derive the element matrices and assemble them into a global system of equations
6. introduce boundary conditions and apply nodal forces
7. the global system of equations is solved

Since the construction which has to be model, is relatively small compared with the soil, which is evaluated in the already present BE model, it is chosen not to implement shape functions in the FE formulation. Instead a higher number of Degrees-of-freedoms (DOFs)

are used, which allows for a simple linear interpolation, between the individual nodes. Apart from this issue (item 4), the procedure is the same as listed above.

The problem considered is sketched in Figure 4.1.

The strong formulation is given by the Cauchy equation, see Equation (4.1).

$$\frac{\partial \sigma_{ij}(\mathbf{x},t)}{\partial x_j} + \rho(\mathbf{x}) b_i(\mathbf{x},t) = \rho(\mathbf{x}) \frac{\partial^2 u_i(\mathbf{x},t)}{\partial t^2} \tag{4.1}$$

where $\sigma_{ij}(\mathbf{x},t)$ is the Cauchy stress tensor, $u_i(\mathbf{x},t)$ is the displacement field, $\rho(\mathbf{x})$ is the mass density and $b_i(\mathbf{x},t)$ is the load per unit mass. The $\mathbf{x}$ vector is the position in space and t in time.
To save calculation resources, it is used that the considered problem can be simplified to a 2 dimensional beam problem, with forces and moments rather than stresses and strains, as output.
This means that the strong formulation can be rewritten, see Equation (4.2).

$$\begin{aligned} \frac{\partial^2}{\partial x^2}\left(EI(x)\frac{\partial^2 w(x,t)}{\partial x^2}\right) - \frac{\partial}{\partial x}\left(G(x)\frac{\partial^2 w(x,t)}{\partial x \partial t}\right) - \frac{\partial}{\partial x}\left(K(x)\frac{\partial w(x,t)}{\partial x}\right) \\ + m(x)\frac{\partial^2 w(x,t)}{\partial t^2} + \gamma(x)\frac{\partial w(x,t)}{\partial t} + \kappa(x) w(x,t) = f(x,t) \end{aligned} \tag{4.2}$$

The weak formulation is obtain by multiplication of the Cauchy equation with an arbitrary weight function (virtual field), $\delta w = \delta w(x,t)$ and then integrating over the element length. The first term is integrated by part providing the result given in Equation (4.3), where the subscript $beam^-$ and $beam^+$ denote the two end point of the beam.

$$\begin{aligned} \int_{x_{beam}^-}^{x_{beam}^+} \left[\frac{\partial^2 \delta w}{\partial x^2} EI(x) \frac{\partial^2 w}{\partial x^2} + \frac{\partial \delta w}{\partial x}\left(K(x)\frac{\partial w}{\partial x} + G(x)\frac{\partial \dot{w}}{\partial x}\right) \right. \\ \left. + \delta w(x,t)\Big(m(x)\ddot{w}(x,t) + \gamma(x)\dot{w}(x,t) - \kappa(x) w(x,t)\Big)\right] dx - \left[\delta w\left(G\frac{\partial \dot{w}}{\partial x} + K\frac{\partial w}{\partial x}\right)\right]_{x_{beam}^-}^{x_{beam}^+} \\ = \int_{x_{beam}^-}^{x_{beam}^+} \delta w(x,t) f(x,t) dx + \left[\delta w(x,t) Q(x,t) - \frac{\partial \delta w}{\partial x} M(x,t)\right]_{x_{beam}^-}^{x_{beam}^+} \end{aligned} \tag{4.3}$$

where $\dot{w}(x,t)$ and $\ddot{w}(x,t)$ are the second derivatives of the displacement with respect to the velocity and acceleration respectively.

Now the physical and the virtual field has to be discretized, which is done by introducing the shape and weight functions, $\mathbf{\Phi_e}(x)$ and $\mathbf{\Psi_e}(x)$, where the subscript e^- and e^+ refers to the end points of the element.

$$w(x,t) = \mathbf{\Phi_e}(x)\mathbf{z_e}(t), \quad \delta w(x,t) = \mathbf{\Psi_e}(x)\delta \mathbf{z_e}(t), \quad x \in [x_e^- x_e^+] \tag{4.4}$$

where x is defined within the bounds of the concerned element and $\mathbf{z_e}(t)$ and $\delta\mathbf{z_e}(t)$ stores the DOFs of the element.

As the shape functions are not introduced and used, the length of w and δw will be the same as the length of f $\mathbf{z_e}$ and $\delta\mathbf{z_e}$.

With inserting Equation (4.4) into Equation (4.3), the equation of motion in the finite element form is obtained, see Equation (4.5).

$$\mathbf{M_e}\ddot{\mathbf{z}}_\mathbf{e} + \mathbf{K_e}\mathbf{z_e} = \mathbf{f_e} + \mathbf{b_e} \tag{4.5}$$

where $\mathbf{M_e}$, $\mathbf{K_e}$ are the element mass and stiffness matrices and $\mathbf{f_e}$ and $\mathbf{f_e}$ are the element load vectors.

The building which has to be modeled is constructed by beam elements, which, for a prescribed geometry, have a given stiffness, a moment of inertia and a mass per unit length. It is chosen to use 30 cm thick concrete plates, which will be used both for the columns (the walls) and beams (the roof). The linear elastic material behavior implicit implies that the stiffness of the concrete, or the reinforced concrete, is given by a Young's modulus of 30GPa in both compression and tension.

Before the matrices are introduced a discretization of the continuous field must be done. As the problem have been rewritten to a plane 2 dimensional beam problem, the discretization of the field into a finite number of nodal values therefore becomes a discretization of the main beams into smaller sub-beams. This process is carried out in the program (*FEM.m*), when a set of master nodes, a topology and a maximum element length have been given.

The element matrices now have to be setup, which is done with use of the Galarkin approach. As the length dimension of the columns and beams, are relatively long compared with the width, the Bernoulli-Euler beam theory is used, allowing for a simplification of the strong/weak formulation. The element mass and stiffness matrix can in this way be written as in Equation (4.6).

$$\begin{aligned}
\mathbf{M_e} &= Le\frac{\mu}{420}\begin{bmatrix} 156 & 22L_e & 54 & -13L_e \\ 22L_e & 4L_e^2 & 13L_e & -3L_e^2 \\ 54 & 13L_e & 156 & -22L_e \\ -13L_e & -3L_e^2 & -22L_e & 4L_e^2 \end{bmatrix} \\
\mathbf{K_e} &= 2\frac{EI_z}{Le^3}\begin{bmatrix} 6 & 3L_e & -6 & 3L_e \\ 3L_e & 2L_e^2 & -3L_e & L_e^2 \\ -6 & -3L_e & 6 & -3L_e \\ 3L_e & L_e^2 & -3L_e & 2L_e^2 \end{bmatrix}
\end{aligned} \tag{4.6}$$

where L_e is the length of the element and μ is the mass per unit length.

With the inclusion of axial forces, the element mass and stiffness matrices become 6-by-6 matrices, see Equation (4.7). (Nielsen, 2004, Chap. 5)

$$\begin{aligned}
\mathbf{M_e} &= Le\frac{\mu}{420}\begin{bmatrix} 140 & 0 & 0 & 70 & 0 & 0 \\ 0 & 156 & 22L_e & 0 & 54 & -13L_e \\ 0 & 22L_e & 4L_e^2 & 0 & 13L_e & -3L_e^2 \\ 70 & 0 & 0 & 140 & 0 & 0 \\ 0 & 54 & 13L_e & 0 & 156 & -22L_e \\ 0 & -13L_e & -3L_e^2 & 0 & -22L_e & 4L_e^2 \end{bmatrix} \\
\mathbf{K_e} &= 2\frac{EI_z}{Le^3}\begin{bmatrix} \frac{ALe^2}{2I_z} & 0 & 0 & -\frac{ALe^2}{2I_z} & 0 & 0 \\ 0 & 6 & 3L_e & 0 & -6 & 3L_e \\ 0 & 3L_e & 2L_e^2 & 0 & -3L_e & L_e^2 \\ -\frac{ALe^2}{2I_z} & 0 & 0 & \frac{ALe^2}{2I_z} & 0 & 0 \\ 0 & -6 & -3L_e & 0 & 6 & -3L_e \\ 0 & 3L_e & L_e^2 & 0 & -3L_e & 2L_e^2 \end{bmatrix}
\end{aligned} \tag{4.7}$$

The element matrices have to be assembled, but before this can be done, the element matrices will have to be rotated in a way, which make them compatible with the global coordinate system. For this a transformation matrix is used, see Equation (4.8). (Robert D. Cook and Witt, 2002, Chap. 2), (Ottosen and Petersson, 1992)

$$\mathbf{T} = \begin{bmatrix} c & -s & 0 & 0 & 0 & 0 \\ s & c & 0 & 0 & 0 & 0 \\ 0 & 0 & 1 & 0 & 0 & 0 \\ 0 & 0 & 0 & c & -s & 0 \\ 0 & 0 & 0 & s & c & 0 \\ 0 & 0 & 0 & 0 & 0 & 1 \end{bmatrix} \quad where \quad \begin{aligned} c &= cos\beta \\ s &= sin\beta \end{aligned} \tag{4.8}$$

This transformation will, for the building frame, swop the first two DOFs in the columns (walls), which mean that the first DOF in each element matrices, will contain the bending contributions, while the second DOF will contain the axial mass and stiffness contributions. This means that the model, for a horizontal applied load in the roof, will be counter acted by the axial stiffness in the beam (DOF 1) and the bending moment in the columns (DOF 2). The element stiffness for a column will in this way be transformed via the transformation relation, see Equation (4.9).

$$\begin{aligned}
\mathbf{K_e}^{Glob\,Coor} &= \mathbf{T}\cdot\mathbf{K_e}^{Loc\,coor}\cdot\mathbf{T^T} = \\
&= 2\frac{EI_z}{Le^3}\begin{bmatrix} 6 & -0 & -3L_e & -6 & -0 & -3L_e \\ -0 & \frac{ALe^2}{2I_z} & 0 & -0 & -\frac{ALe^2}{2I_z} & 0 \\ -3L_e & 0 & 2L_e^2 & -3L_e & 0 & L_e^2 \\ -6 & 0 & -3L_e & 6 & -0 & -3L_e \\ -0 & -\frac{ALe^2}{2I_z} & 0 & -0 & \frac{ALe^2}{2I_z} & 0 \\ -3L_e & 0 & L_e^2 & -3L_e & 0 & 2L_e^2 \end{bmatrix}
\end{aligned} \tag{4.9}$$

With the transformed element stiffness and mass matrices, the global matrices can be constructed. This is simply done by starting with the element matrices in one end, then expand it by adding the contributions from the neighboring element at the one node they have in common. An example is shown in Equation (4.10), where the first two element stiffness matrices are assembled.

$$\mathbf{K} = \begin{bmatrix} k11^{(1)} & k12^{(1)} & k13^{(1)} & k14^{(1)} & k15^{(1)} & k16^{(1)} & 0 & 0 & 0 & \cdots \\ k21^{(1)} & k22^{(1)} & k23^{(1)} & k24^{(1)} & k25^{(1)} & k26^{(1)} & 0 & 0 & 0 & \\ k31^{(1)} & k32^{(1)} & k33^{(1)} & k34^{(1)} & k35^{(1)} & k36^{(1)} & 0 & 0 & 0 & \cdots \\ k41^{(1)} & k42^{(1)} & k43^{(1)} & k44^{(1)} + k11^{(2)} & k45^{(1)} + k12^{(2)} & k46^{(1)} + k13^{(2)} & k14^{(2)} & k15^{(2)} & k16^{(2)} & \\ k51^{(1)} & k52^{(1)} & k52^{(1)} & k54^{(1)} + k21^{(2)} & k55^{(1)} + k22^{(2)} & k56^{(1)} + k23^{(2)} & k24^{(2)} & k25^{(2)} & k26^{(2)} & \\ k61^{(1)} & k62^{(1)} & k63^{(1)} & k64^{(1)} + k31^{(2)} & k65^{(1)} + k32^{(2)} & k66^{(1)} + k33^{(2)} & k34^{(2)} & k35^{(2)} & k36^{(2)} & \\ 0 & 0 & 0 & k41^{(2)} & k42^{(2)} & k43^{(2)} & k44^{(2)} & k45^{(2)} & k46^{(2)} & \cdots \\ 0 & 0 & 0 & k51^{(2)} & k52^{(2)} & k53^{(2)} & k54^{(2)} & k55^{(2)} & k56^{(2)} & \\ 0 & 0 & 0 & k61^{(2)} & k62^{(2)} & k63^{(2)} & k64^{(2)} & k65^{(2)} & k66^{(2)} & \cdots \\ \vdots & & \vdots & & & & \vdots & & \vdots & \ddots \end{bmatrix} \tag{4.10}$$

Before the global system can be solved (with any useful output), the nodal load as well as boundary conditions have to be applied. As discussed earlier, the building will be force to move in the bottom of the wall in the x- and the y-direction. This means that the first and the second DOF in these two nodes will be forces to follow the motion of the soil, which is illustrated on Figure 4.1, where the arrows in the bottom of the columns represent the DOFs at which the deflection is prescribed. It is also possible to fix the structure to the soil (or a foundation in the BEM) by forcing the third DOF to be equal to the rotation from the BEM.
In the rest of the DOFs, the forces are specified to zeros, as no external non-zero loads are applied.

The stiffness and the mass matrices now have been set up, see Equation (4.7). With these, the global system of equations can be solved, either in time domain of in frequency domain. In time domain the motion of equation is given by Equation (4.5). With a damping model added, the equation of motion, for the global system, becomes:

$$\mathbf{M\ddot{u}} + \mathbf{C\dot{u}} + \mathbf{Ku} = \mathbf{f} \tag{4.11}$$

Obviously this implies a viscous damping model, as the damping is multiplied with the velocity, but alternatively e.g. a Rayleigh damping model could have been chosen ($\mathbf{C} = \alpha\mathbf{K} + \beta\mathbf{M}$).
As the time domain solution would be computational challenging with a model of this size, as the whole soil geometry as well as the structural geometry have to be evaluated for every time step, a solution in frequency domain is chosen. Here the system of equations is only evaluated once for every frequency, see further below. The equivalent frequency domain equation of motion, with a viscous damping model is given in Equation (4.12), where the derivatives with respect to time, t, is replaced by $i\omega$.

$$(-\omega^2\mathbf{M} + i\omega\mathbf{C} + \mathbf{K})\mathbf{u} = \mathbf{f} \tag{4.12}$$

But as the viscous damping model is expected to provide to high damping, at high frequencies, a hysteretic damping model is chosen, instead. In this hysteretic damping model, the damping matrix is chosen as a fraction of the stiffness matrix, see Equation (4.13).

$$\mathbf{C} = \eta\mathbf{K} \tag{4.13}$$

where η is a fixed value for the whole building, set to 0.02. Elimination of the frequency dependency and inserting the damping matrix into the equation of motion, provide the result, in Equation (4.14).

$$\begin{aligned} (-\omega^2\mathbf{M} + i\eta\mathbf{K} + \mathbf{K})\mathbf{u} &= \mathbf{f} \\ (-\omega^2\mathbf{M} + i\mathbf{C} + \mathbf{K})\mathbf{u} &= \mathbf{f} \end{aligned} \tag{4.14}$$

The term within the brackets on the left hand side of Equation (4.14), contains all the dynamic properties of the system. By assembling this "dynamic stiffness matrix" in $\widehat{\mathbf{K}}_\mathbf{j}$, the solution of the dynamic problem in frequency domain, is obtain in the same way as in time domain, i.e. a static solution method. The only difference is that the time domain solution is calculated for each time step, while the frequency domain solution is obtain for each frequencies, j. The dynamic stiffness matrix is written in Equation (4.15).

$$\widehat{\mathbf{K}}_j = -\omega_j^2\mathbf{M} + i\mathbf{C} + \mathbf{K} \tag{4.15}$$

The global system of equations is now solved, providing the unknown deflections and the unknown reactions (forces/moments) for each frequency. With the used of the dynamic stiffness matrix, the solution of the dynamic problem, is solved for via an equivalent static solution for each frequency, j, see Equation (4.16).

$$\widehat{\mathbf{K}}_j\mathbf{u}_j = \mathbf{f}_j \tag{4.16}$$

where $\mathbf{u}_j$ is the nodal displacements and $\mathbf{f}_j$ is the nodal forces for the $j'th$ frequency.
Before the system of equations is solved, the columns and rows are reordered, in such a way, that the DOFs where the known deflection is prescribed is at the top (the Dirichlet's boundary conditions). In this way the forces (reaction forces) are easily obtain for prescribed deflections and vice versa for the deflections, see Equation (4.17).

$$\begin{bmatrix} \widehat{\mathbf{K}}_{uu} & \widehat{\mathbf{K}}_{fu} \\ \widehat{\mathbf{K}}_{uf} & \widehat{\mathbf{K}}_{ff} \end{bmatrix} \begin{bmatrix} \mathbf{u}_u \\ \mathbf{u}_f \end{bmatrix} = \begin{bmatrix} \mathbf{f}_u \\ \mathbf{f}_f \end{bmatrix} \tag{4.17}$$

where $\mathbf{u}_u$ and $\mathbf{f}_f$ are the given deflections and forces respectively.

The Global system of equation is now solved in (*FEM.m*).

4.2 Structural response

In this section the structures shown in Figure 1.8 are shortly described and their eigenfrequencies are found. With these, the response of the structure is described, in Section 4.3 and Chapter 5.

The response of the FE structure is found the program (*FEM.m*), and can be found on the Appendix CD. The layout of the structure is shown in Figure 4.2, where the maximum element length is set to 250mm, which is the same order of magnitude, chosen for the combined FE-BE model in TEA. The undamped eigenfrequencies of the structure is found for a element division, which is ten times more refined than shown in the Figure 4.2, to get converging values.

Figure 4.2 – *Layout of structure 1, with element length's of 250mm. The node numberings are marked with black, while the line numberings are marked with red.*

The eigenfrequencies are determined in (*FEM.m*), and the values between 0 and 200Hz is given in Table 4.1. The eigenfrequencies are found for both at simply supported structure (or actually a pinned supported, as the deflection in the first two DOFs at the support is fixed) and a fixed supported structure. The pinned supports are chosen, as the building to a certain degree is locked by the opposite support, and the response of the structure is therefore expected to correspond to one of these two supports system (see Figure 4.1). In the pinned case, the deflections in both the x- and the y-direction is locked for the two supports and for the fixed structure, all three DOFs in each support is locked. The results presented below for the uncoupled model will be compared with the coupled model in Chapter 5, where the combined FE-BE model is discussed.

Structure 2 is visualized in Figure 4.3. The eigenfrequencies are given in Table 4.1, for both structures with both pinned and the fixed supports.

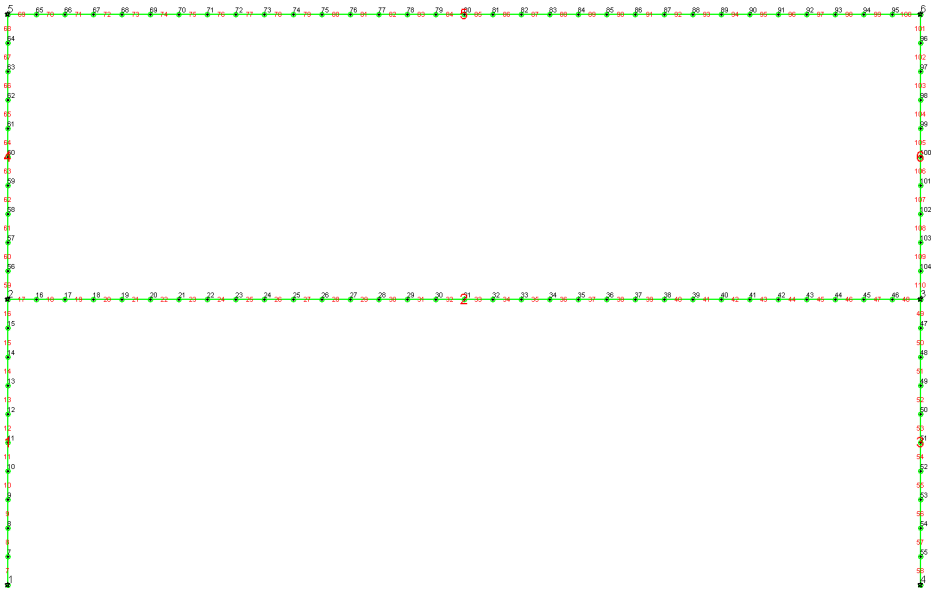

Figure 4.3 *– Layout of structure 2, with element length's of 250mm.*

Structure 1			Structure 2	
Simply supported	Pinned supported	Fixed supports	Pinned supported	Fixed supports
f - [Hz]	f - [Hz]	f - [Hz]	f - [Hz]	f - [Hz]
2.8	5.9	13.5	3.5	6.2
9.9	13.0	13.6	13.0	13.1
19.5	37.0	39.2	14.9	15.0
39.3	70.1	76.0	17.8	22.6
73.3	97.9	120.5	37.5	38.9
99.5	102.2	135.1	42.0	42.1
124.5	140.9	163.8	70.3	71.8
152.2	195.1	195.1	77.1	79.3
195.1	-	-	95.7	108.6
-	-	-	103.0	116.4
-	-	-	116.5	121.6
-	-	-	119.2	136.5
-	-	-	136.6	152.7
-	-	-	152.7	157.3
-	-	-	160.4	167.0
-	-	-	178.3	183.2
-	-	-	188.9	193.7

Table 4.1 *– Undamped eigenfrequencies of structure 1 and 2.*

Through the analysis, where the building is excited by the load acting at different frequencies, dynamic amplification will cause relatively large structural response.

The dynamic amplification will depend on the mode shape and will cause significantly large amplifications, for an excitation in phase/counter phase depending on the mode shape. Most of the excitations of the building will occur in a "mixed" phase, as an excitation in phase requires, an even amount of wavelengths between the front and the back of the building. Correspondingly, an excitation in counter phase requires one half wavelength or one and a half wavelength and so on ($L = 0.5$, $L = 1.5$, $L = 2.5$ ...).
For instance, a mode shape with a natural frequency around 80Hz would provide particular large response, if the mode is activated in phase, see Figure 4.4.

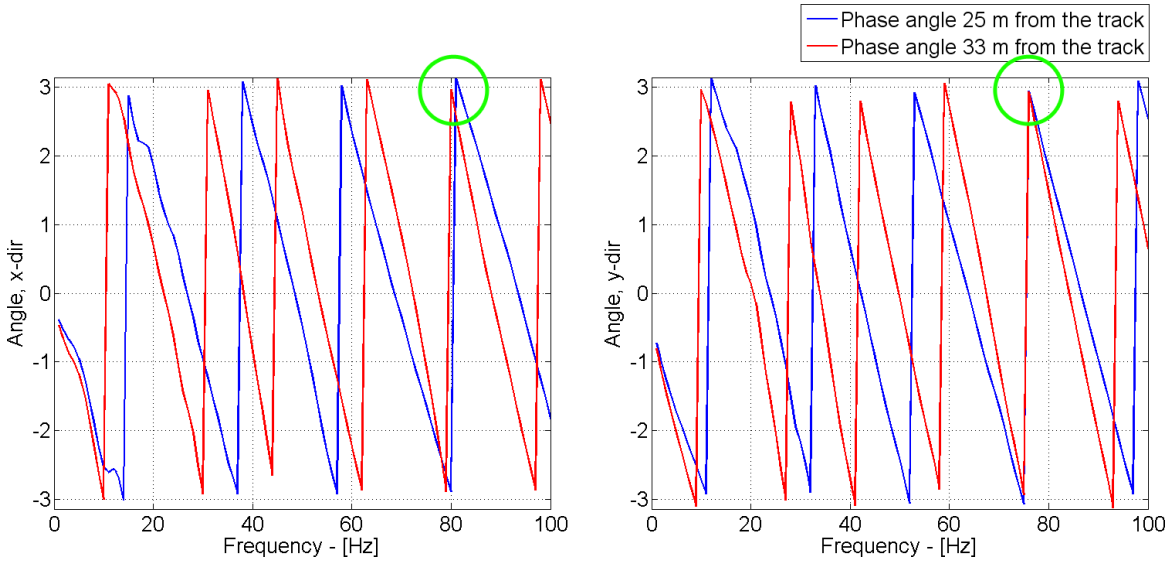

Figure 4.4 – *Phase angle of the waves 25 and 33m from the track in the x-direction (to the left) and the y-direction (to the right) for the reference soil number 1.*

The excitation is in phase, both regarding the horizontal and the vertical soil movements. This happens, as the width of the building fits, with the wavelength of a Rayleigh wave ($L_{Rayleigh} = c_{Rayligh}/f \approx 8$m). In this way, three wavelengths lie in between the source and the front wall, while the distance between the source and the back wall correspond to four wavelengths.
The opposite is seen for around 40Hz, where the phase angels are spaced with π, leading to an excitaton in counter phase.

The deflection of structure 1, excited in the first mode, is shown in see Figure 4.5, with the maximum response observed after approximately 0.19 period (see *FEM.m*),

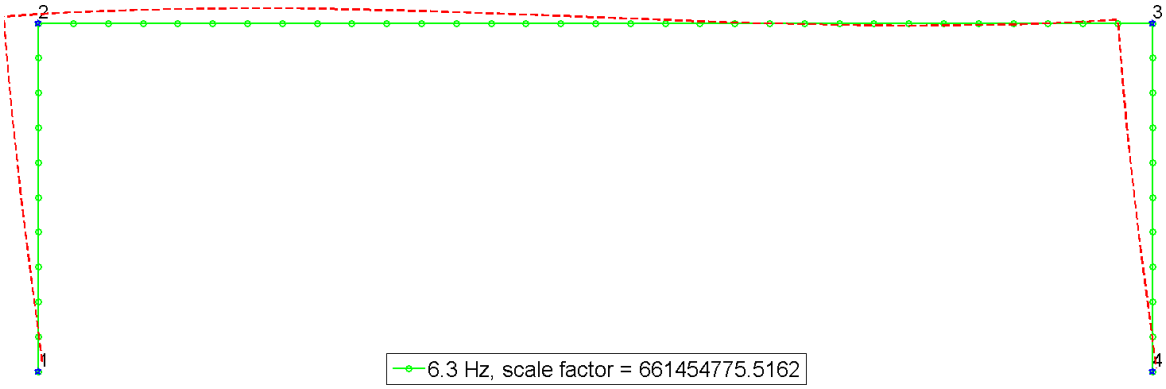

Figure 4.5 – *Maximum horizontal deflection of structure 1 excited in mode 1.*

This mode provide a relatively large response in the x-direction, and no particular response in the y-direction. The top beam is just making an s-shape, to ensure the right angle at the corners. The response in the x-direction is shown in Figure 4.6, where an example of the maximum structural response in the x- and the y-direction as function of the frequency is plotted for structure 1 on soil 1.

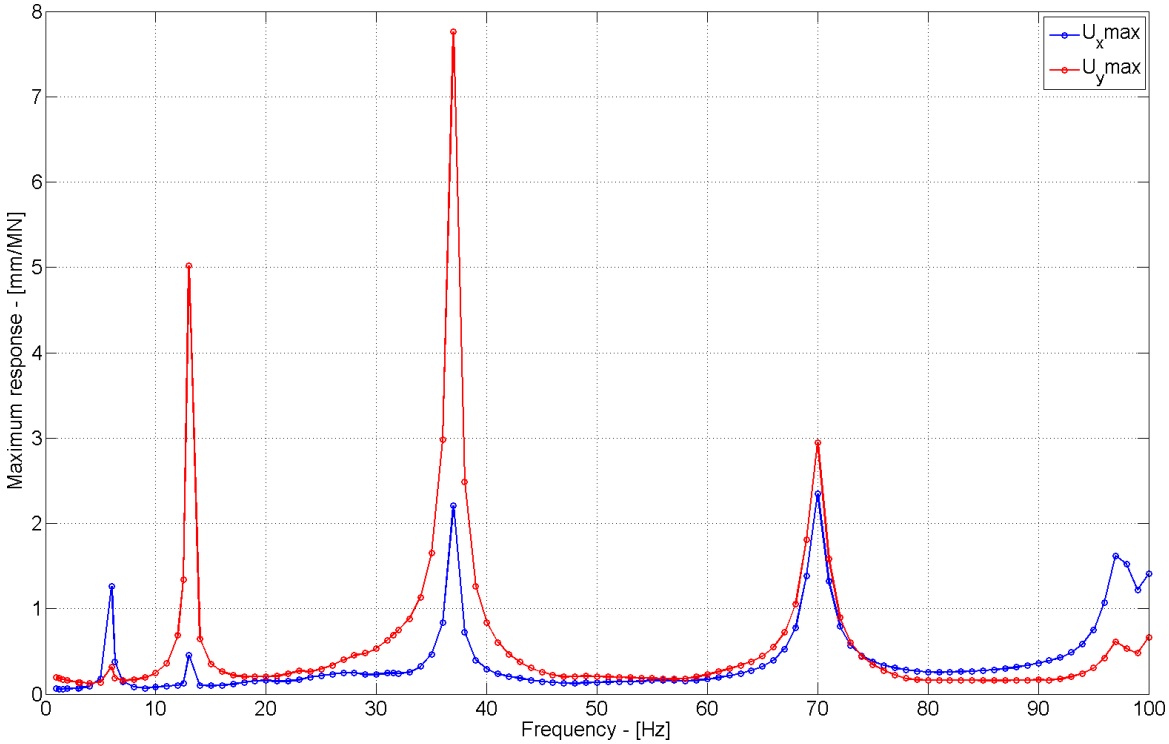

Figure 4.6 – *Maximum structural response of structure 1 on soil 1, in the x- and the y-direction as function of the frequency.*

The response of pinned structures 1 and 2, with the forced movements from the soil, providing no back coupling, will be discussed in Section 4.3. The model including soil-structure interaction, will be described in Chapter 5.

4.3 FE structure model results

The response of the structure, when the pinned structures are place on top of the soils modeled in the BE model, see Section 3.3, with no back coupling, is described in the following. First the structure number 1 on soil 1 and 2 respectively. Afterwards structure 2 on soil 1.

4.3.1 Structure 1 on soil 1

In Figure 4.7 the maximum response of the structure in both the x- and the y-direction is shown for soil number 1 with respect to the frequency.

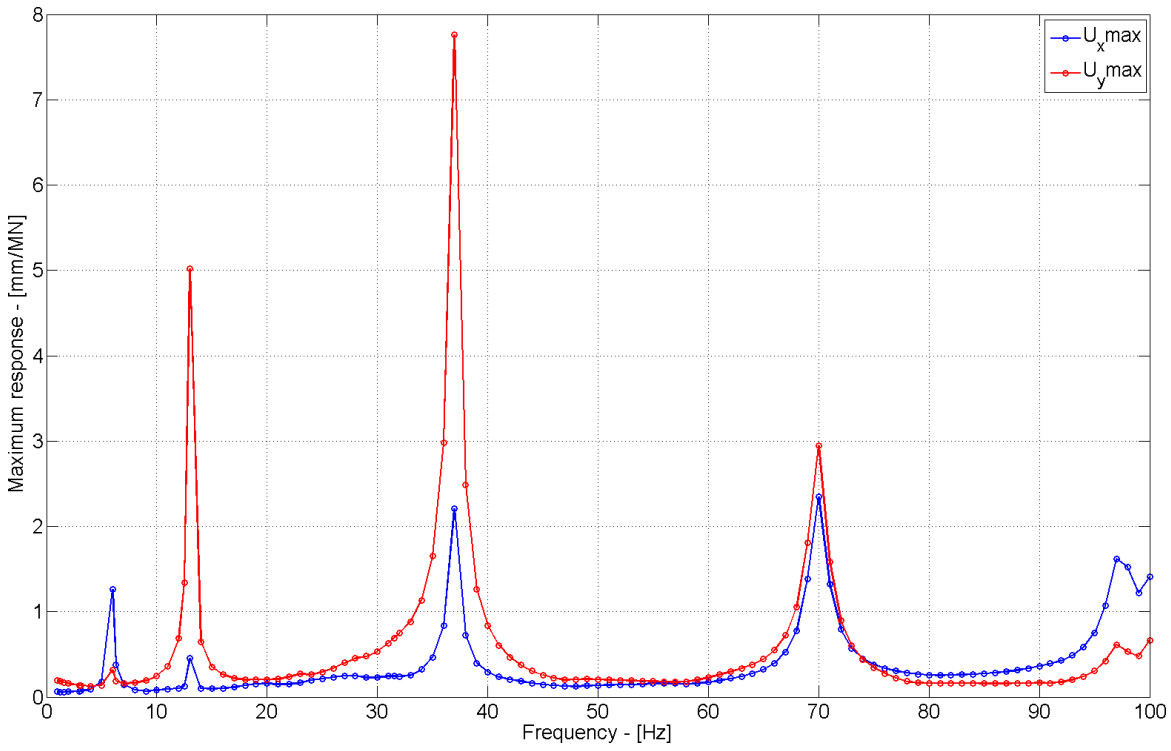

Figure 4.7 – *Maximum response of structure 1, on soil 1. The response is given in both the x- and the y-direction with respect to the frequency.*

As seen from Figure 4.7, the structure provide large response at the natural frequencies of the structure at 6.3, 13, 37 and 70Hz, where the peaks at 37Hz are amplified by the relative large soil response in frequency range 20-40Hz, see Figure 3.9 and Figure 3.10. As the response of the building depends on the response of the soil, see Section 3.3, a normalized plot is used to identify the dynamic amplification of the building only.

In Figure 4.8, the response is normalized with respect to the maximum response in the two connection points (at 25 and 33m from the track) in both the x- and the y-direction.

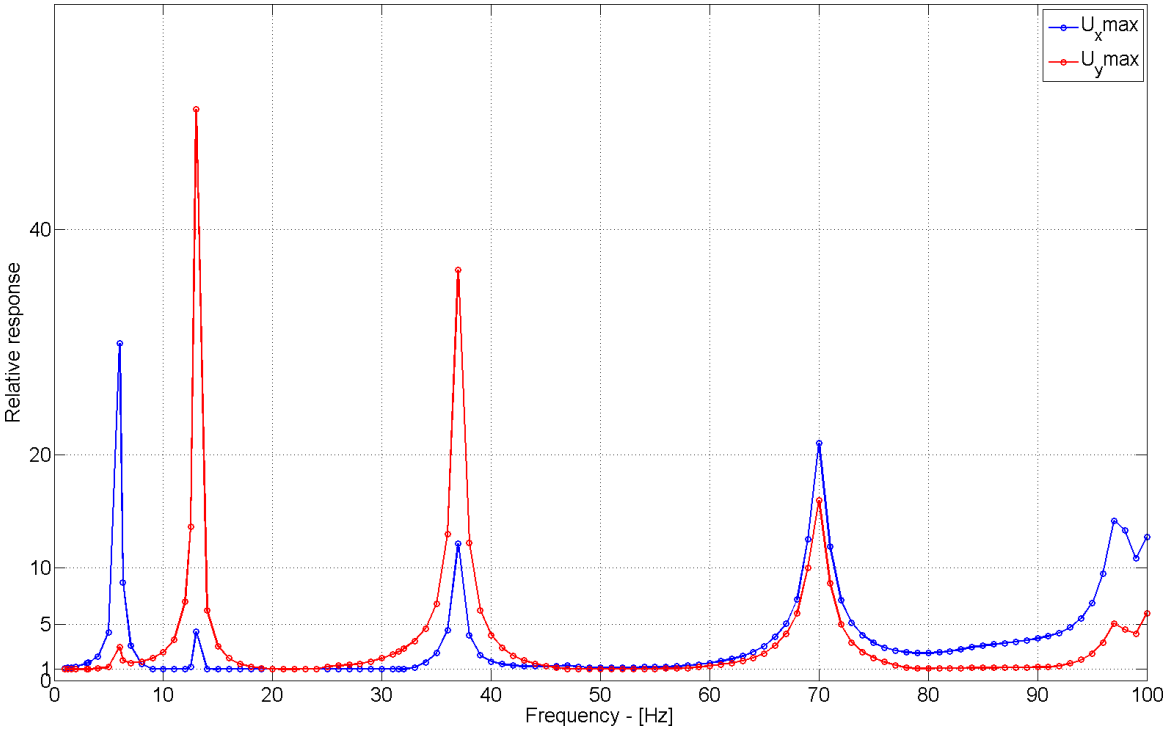

Figure 4.8 – *Normalized relative response of the structure 1 on soil 1, as function of the frequency.*

It here stands out, that the peaks experienced at 37Hz are not, where the building is experiencing the greatest dynamic amplification. The great peaks at Figure 4.7 arise, due to a combination of a dynamic amplification of the building and a large response of the soil at this specific frequency at the location of the building, see Figure 3.9.

4.3.2 Structure 1 on soil 2

In Figure 4.9 the response of the structure is shown for soil number 2.

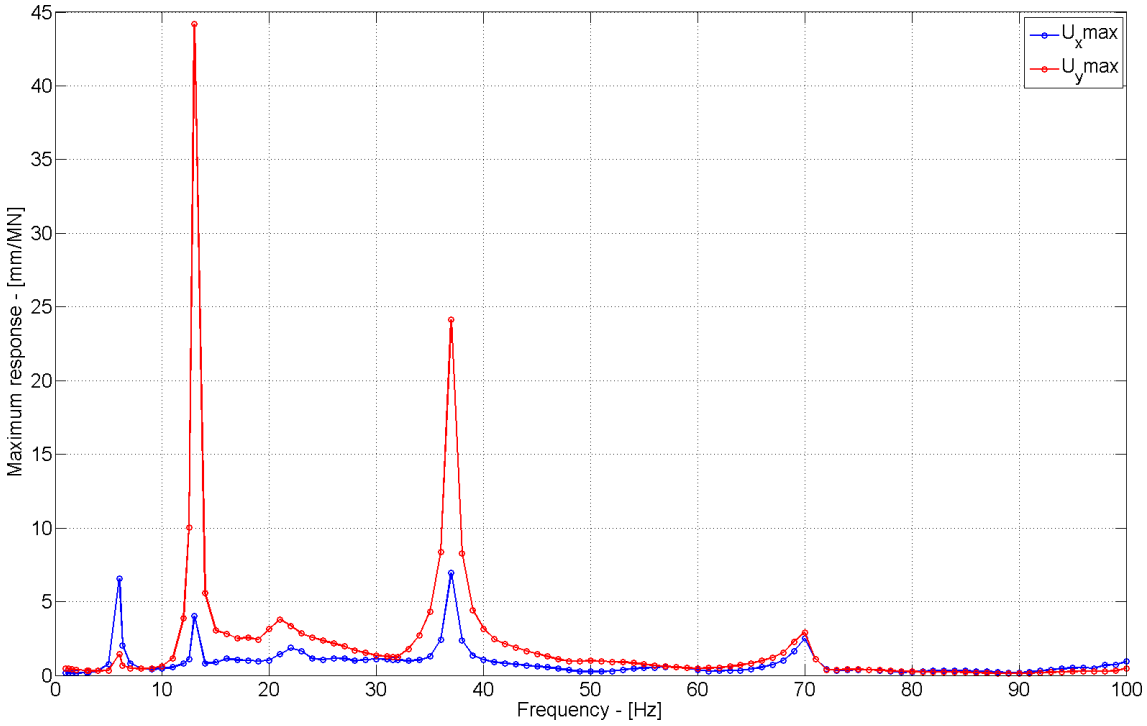

Figure 4.9 – *Maximum response of structure 1, on soil 2. The response is given in both the x- and the y-direction with respect to the frequency.*

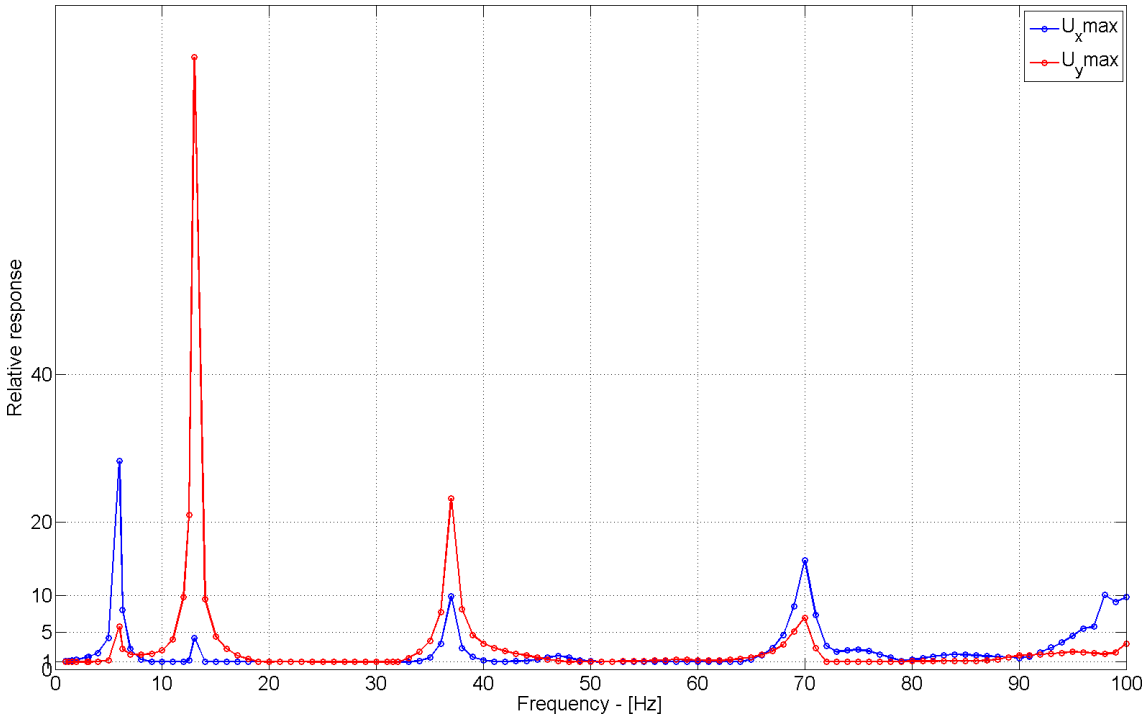

Figure 4.10 – *Normalized relative response of the structure 1 on soil 2, as function of the frequency.*

The peak response for soil 2 at 13Hz is significantly larger than for soil 1. This happens, even as the absolute amplitude of the soil is relatively low for this frequency. If the structure have had an eigenfrequency around 20Hz, the response of the structure could have been even bigger, due the the narrow peak response of soil 2, see Figure 3.15 and Figure 3.16.
The peak response for soil 2 at 13Hz is significantly larger than for soil 1. This happens, even as the absolute amplitude of the soil is relatively low for this frequency. If the structure have had an eigenfrequency around 20Hz, the response of the structure could have been even bigger, due the the narrow peak response of soil 2, see Figure 3.15 and Figure 3.16.

The relative response is shown in Figure 4.10.rge response is observed at 6.3 and 70Hz for both soil profiles in the horizontal direction.

These frequencies may have the biggest structural response, but this does not necessarily mean, that the vibrations steaming from these frequencies will be taken as the most disturbing vibrations. A large amplitude for a slow oscillating movement might not even be noticed, because the acceleration, and hereby the forces acting on the body, is low.
For this reason, the acceleration response, measured in dB, with a reference value of 1μ m/s^2 is plotted. For this Equation (4.18) is used.

$$A_{acc}(x_1, f) = 20 \cdot log_{10}\left(\frac{-\omega^2 U(x_1, f)}{1\mu\frac{m}{s^2}}\right) \tag{4.18}$$

where f is the frequency and x_1 is the distance from the track to the evaluated point(s) and is set to 25 and 33m respectively.

A plot of the acceleration response for structure 1 on soil 1, is shown in Figure 4.11.

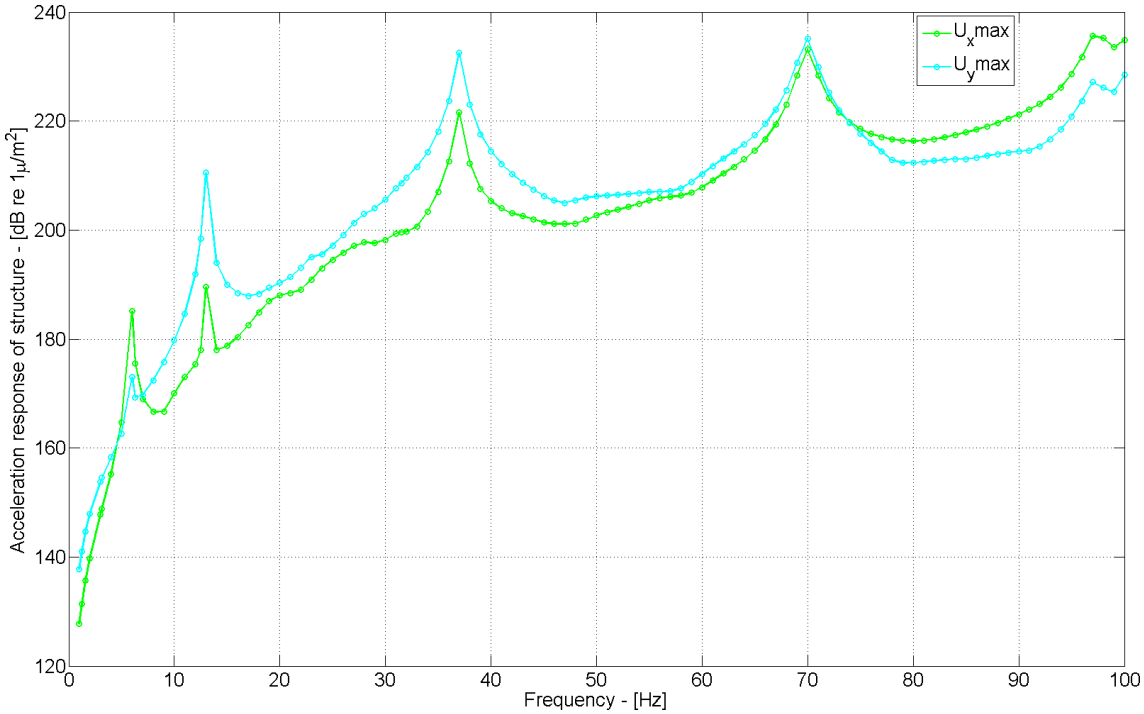

Figure 4.11 *– Acceleration response for structure 1 on soil 1.*

Figure 4.11 shows a weighting of the response as function of the frequency. As a higher frequency will create more disturbing response. This means, that even when the response of the structure is dropping for increasing frequency, see Figure 4.9, the vibrations at high frequencies will be noticed, due to the increased acceleration. As seen in the figure, the acceleration response is greatest for 70 and 97Hz, which is not directly noticeable from Figure 4.7.

The acceleration response for structure 1 on soil 2 is shown in Figure 4.12.

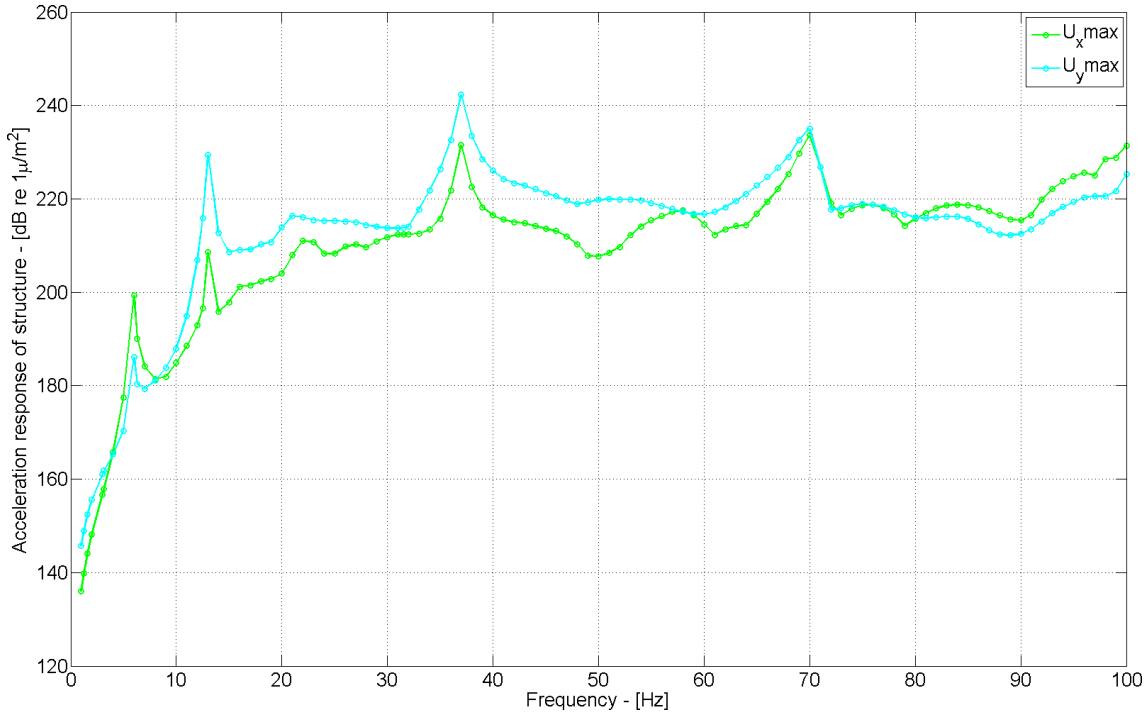

Figure 4.12 – *Acceleration response for structure 1 on soil 1.*

Here it is seen, that the most disturbing response is found for the 3rd mode at 37Hz. Most of the peak responses for the two soil profiles occur for a vertical movement, but as explained earlier, the horizontal accelerations might be much more disturbing than the vertical, even though they are slightly lower.

4.3.3 Structure 2 on soil 1

The response of the two storey building on top of the soil 1 is shown in Figure 4.13.

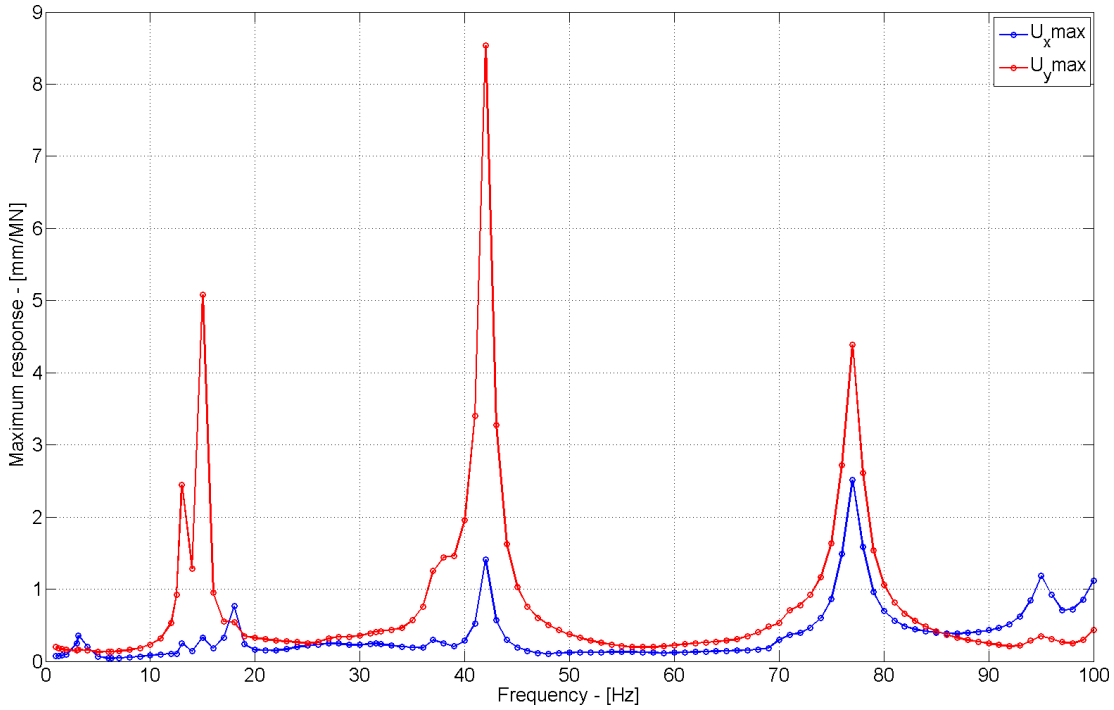

Figure 4.13 – *Maximum response of structure 2, on soil 1. The response is given in both the x- and the y-direction with respect to the frequency.*

The relative response of structure 2 on soil 2 is shown in Figure 4.14.
The response of the two-storey building, seem similar to the response of structure 1 on soil 1, with the exception of a higher response at mode 2-4, which occur, due to the larger structure.

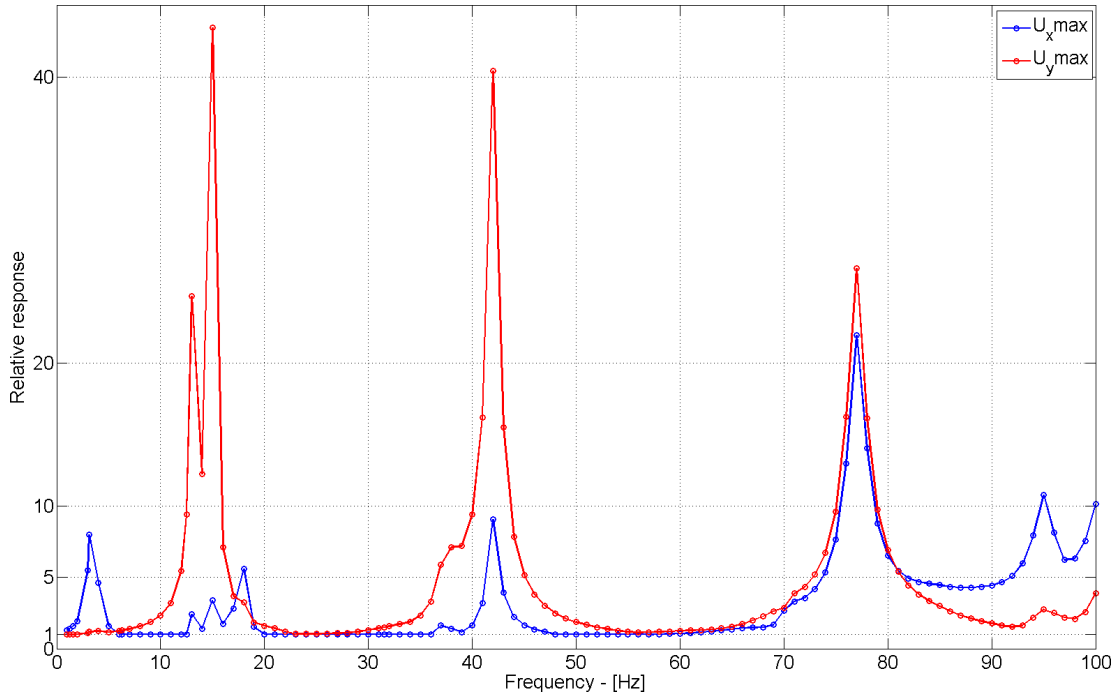

Figure 4.14 – *Normalized relative response of the structure 2 on soil 1, as function of the frequency.*

Chapter 5

Combined FE-BE model

In this chapter, the results obtain in the soil (BE) model and the FE model will be discussed in relation to the combined FE-BE model evaluated in TEA. The reference model is structure 1 consisting of a one-storey, pinned supported structure (see Section 4.2), at the ground surface and soil number one, which consists of 10m of normal consolidated moraine with a stiffness of $E = 2340$MPa on top of a stiffened moraine with a stiffness of $E = 6760$MPa. The reference model is marked with red in Figure 5.1.

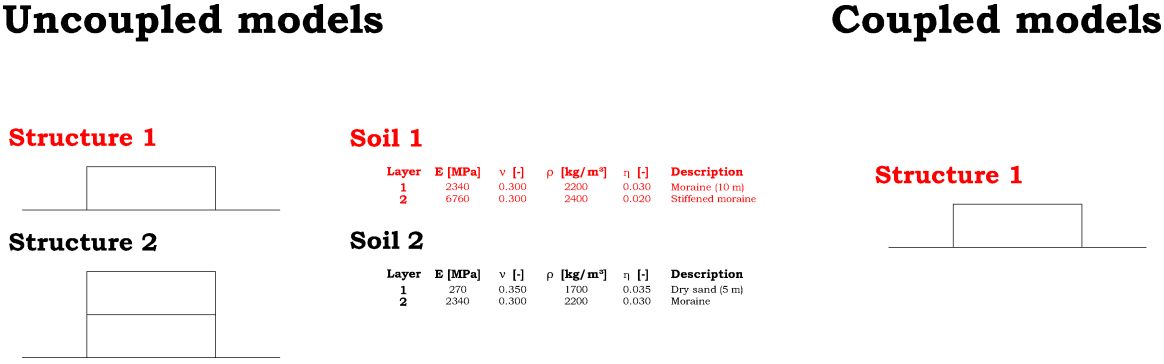

Figure 5.1 – *Model matrix, with the structural systems of the uncoupled model listed to the left, the structural system of the coupled model to the right and the soil strtifications in the middle.*

5.1 Soil structure interaction

The simple models, with forced displacements of the structure, have been discussed in the previous chapters in relation to the soil response and the structural response. This will be the starting point, when the importance of the back coupling, allowing the structure to interact with the soil, will discussed in the following.
When the soil is moving, caused by the oscillating load from the rails, the soil will excite the building, forcing it to move. If the mass of the building is zero, the building will follow the soil anywhere it moves, but as the building have a certain mass, the building will counter act the movements from the soil, due to the inertia of the construction, as the moving soil has to change the inertia of the building. The mass of the moving soil determines the order of magnitude of the force acting on the structure relative to the reaction force encountered by

the structure, f_{rel}, as the acceleration of the soil is equal to the acceleration of the building (at least in the point of application), see Equation (5.1).

$$\begin{aligned} F_{soil} &= F_{structure} \\ M_{soil} \cdot a_{soil} &= m_{structure} \cdot a_{soil} \\ &\Downarrow \\ f_{rel} = \frac{F_{soil}}{F_{structure}} &= \frac{M_{soil}}{m_{structure}} \end{aligned} \tag{5.1}$$

It is here noted, that the mass of the building will be dependent on the activated modal mass at the given frequency. This means, that the building will provide largest reaction forces, at the natural frequencies, where the corresponding modal mass is high.
If it is assumed, that the soil mass affecting the structure lie within one wavelength, the mass interacting with the structure will be greatest for low frequencies and smaller for higher frequencies. This means, that the wave field is easiest affected by the structure at high frequencies, where the soil interacting with the structure is smallest, see Figure 5.2.

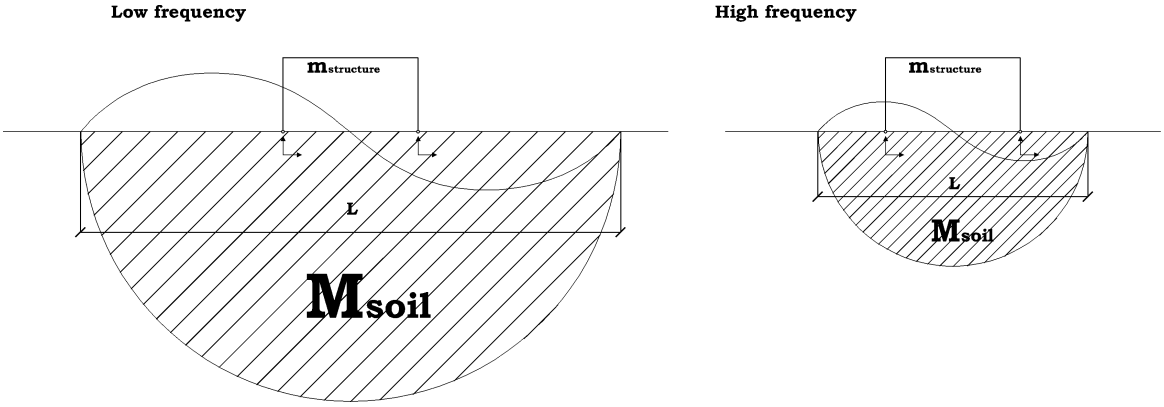

Figure 5.2 – *Principal sketch of large soil mass with corresponding low frequency waves (left), and a small soil mass with corresponding high frequency waves (right).*

In the uncoupled model, where the soil and the structural response is found in separate models, the reaction force from the structure, as function of the frequency, is given in Figure 5.3, for a pinned supported structure 1.

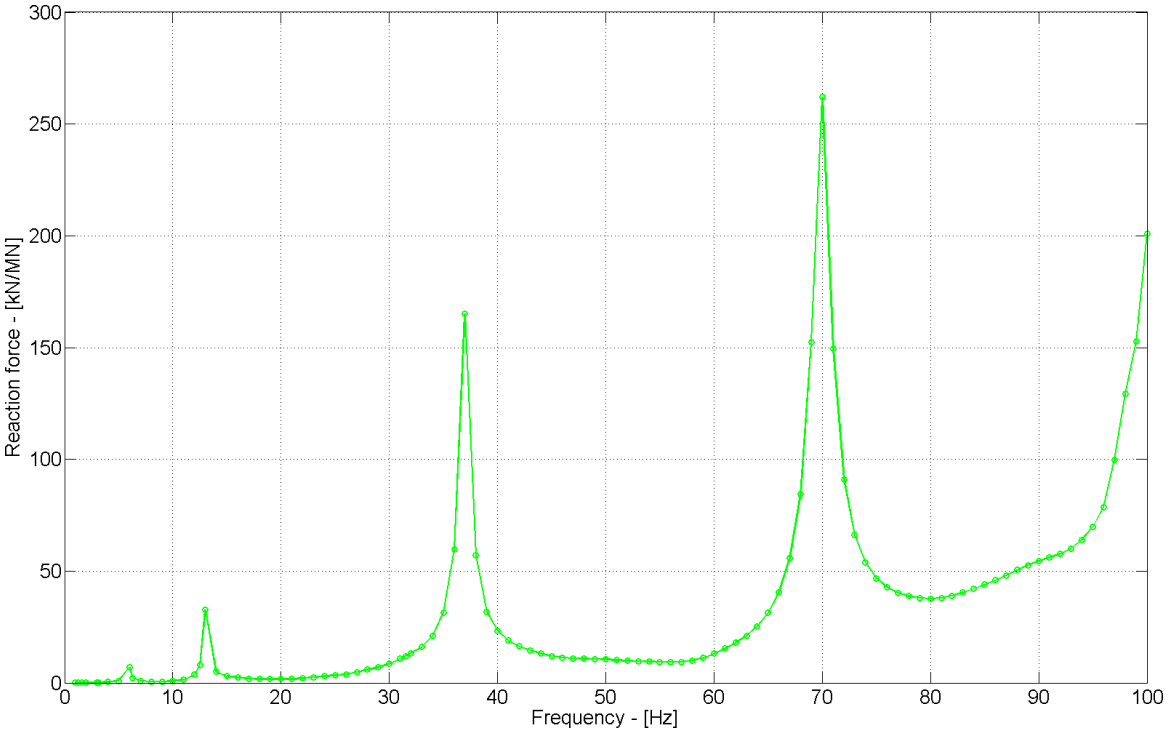

Figure 5.3 – *Reaction forces from structure 1 (pinned supports) on soil 1, from the simple model in Section 4.3. The reaction force is expressed in kN per MN applied at the track.*

The change in the wave field might be insignificant, depending on the order of magnitude of the reaction force from the building, compared with the load of the train. The geometrical position of the considered structure will in this relation play a role, as geometrical damping occurs. But it is hard to judge the influence directly, as the waves might be trapped in the top layer, creating a relatively high response even far away from the track. Opposite the case where the energy could dissipate rather quickly, if no or low reflection takes place in the interface between the two soil layers. The wave field changes, with an increasing reaction force from the structure. As the mass of the soil interacting with the structure decrease, the acceleration increases, strengthening the reaction force from the building, particularly at the natural frequencies of the structure, see Figure 5.3, where a high mass participation factor is expected.
In Figure 5.3, the reaction forces, expressed in kN per MN, are applied at the track for structure 1 on soil 1 in the uncoupled model. As seen the reaction forces exceed 250kN per MN applied at the natural frequencies of the structure. This causes a significant change of the wave field near the building.

5.1.1 Structure 1 - combined FE-BE model

Structure 1 is now included in the BE model in the TEA software, which has the ability of combining the BEM and the FEM. The structure is via the geometry file (*geolayfig14fem.m*), modeled as a FE structure, where eight noded quadrilateral elements, with quadratic shape

functions, are used. Even though these elements converge, for a lower amount of elements, than for the FE model (where linear interpolation is used), the division of the structure into elements, is done with the same order of magnitude, as for the separate FE program. The element length's is no longer than 320mm, see Figure 5.4. The material properties of the structure, is the same as for the FE structure modeled in (*FEM.m*), as well as the material damping is set to 0.02.

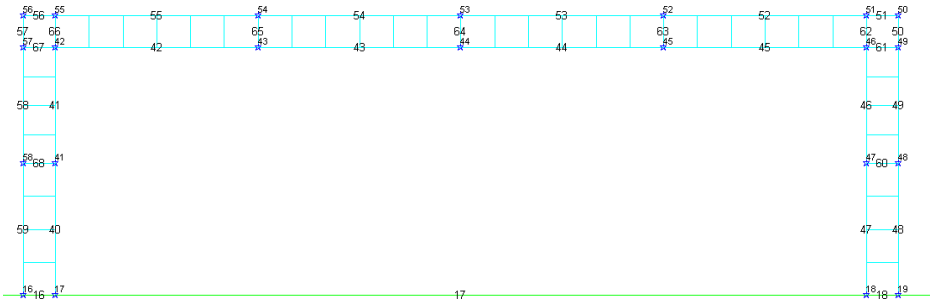

Figure 5.4 *– Combined FE structure 1, inside the BE soil model. Master nodes are marked with blue stars, with line numbers in between.*

As seen from Figure 5.4, the columns are placed directly on the ground, creating a 30cm wide interface. This support will act as a fixed support, or possible as a pinned support, if a charnier is developed, due to yielding locally around the support.

The absolute amplitude at the surface is plotted in Figure 5.5.

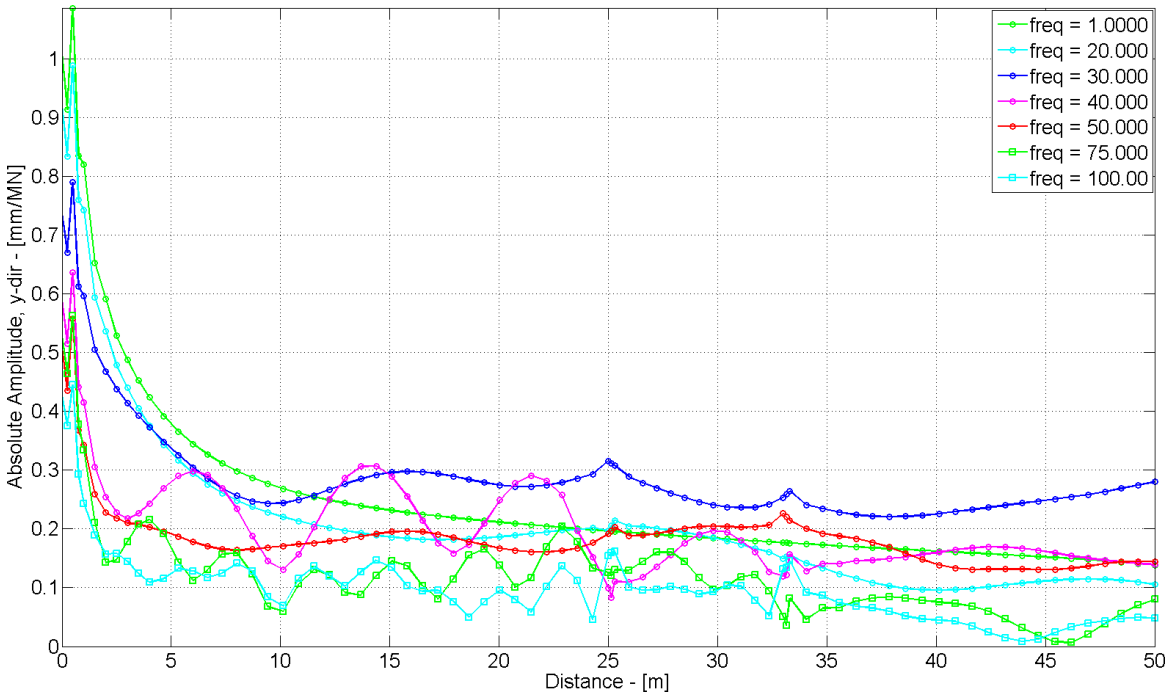

Figure 5.5 *– Absolute amplitudes for soil 1 with FE-BE building on soil 1.*

As seen from Figure 5.5, the wave field is influenced by the presence of the building, compared with the BE model of the soil, with no building, see Figure 5.6.

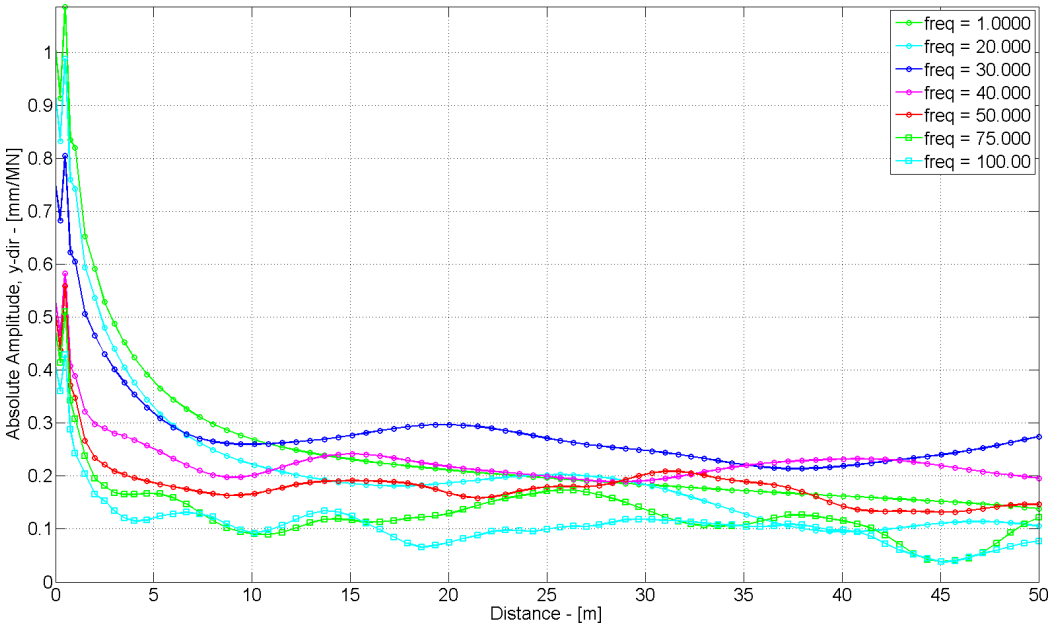

Figure 5.6 *– Absolute amplitudes for soil 1 with no coupled structure.*

In Figure 5.7, the relative amplitude of the soil response in the uncoupled BE model relative to the response of the coupled BE model is shown.

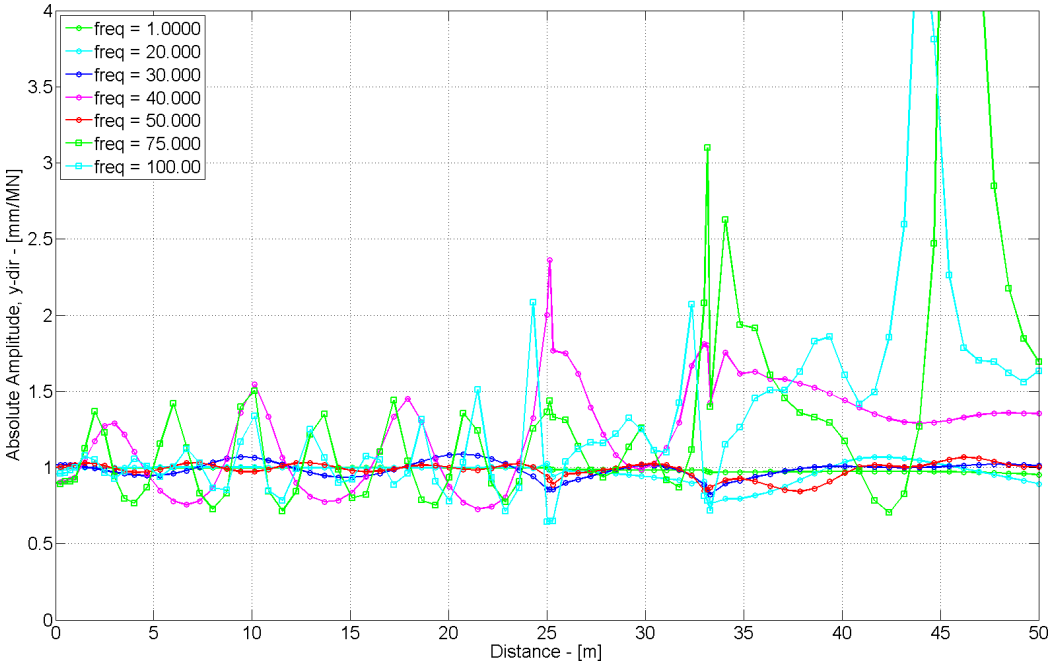

Figure 5.7 *– Relative amplitude of the soil response in the uncoupled BE model, relative to the coupled FE-BE model.*

As seen in Figure 5.7, the response of the soil is especially influenced at the natural frequencies of the building and for high frequencies, where the high frequent oscillation of the soil creates a relatively large reaction force from the building, see Figure 5.3. The uncoupled model shows a response, which is almost 2.5 times greater at 40Hz near the wall 25m from the track. This deviation arises, since 40Hz is close to one of the structures eigenfrequencies, see Figure 4.7. It is further noticed, that the building tend to change the wave pattern for the waves behind the building and even act as a wave shield for high frequent waves, see for instance the 75Hz curve, where the uncoupled response is more than 10 times greater, than the response of the coupled model. The low frequent waves get past the building without any significant change (see the 1Hz wave), as the soil mass interacting with the building is much greater.

The amplitudes in the y-direction at the surface of the soil are plotted in Figure 5.8 at 8, 25 and 33m, corresponding to Figure 3.10.

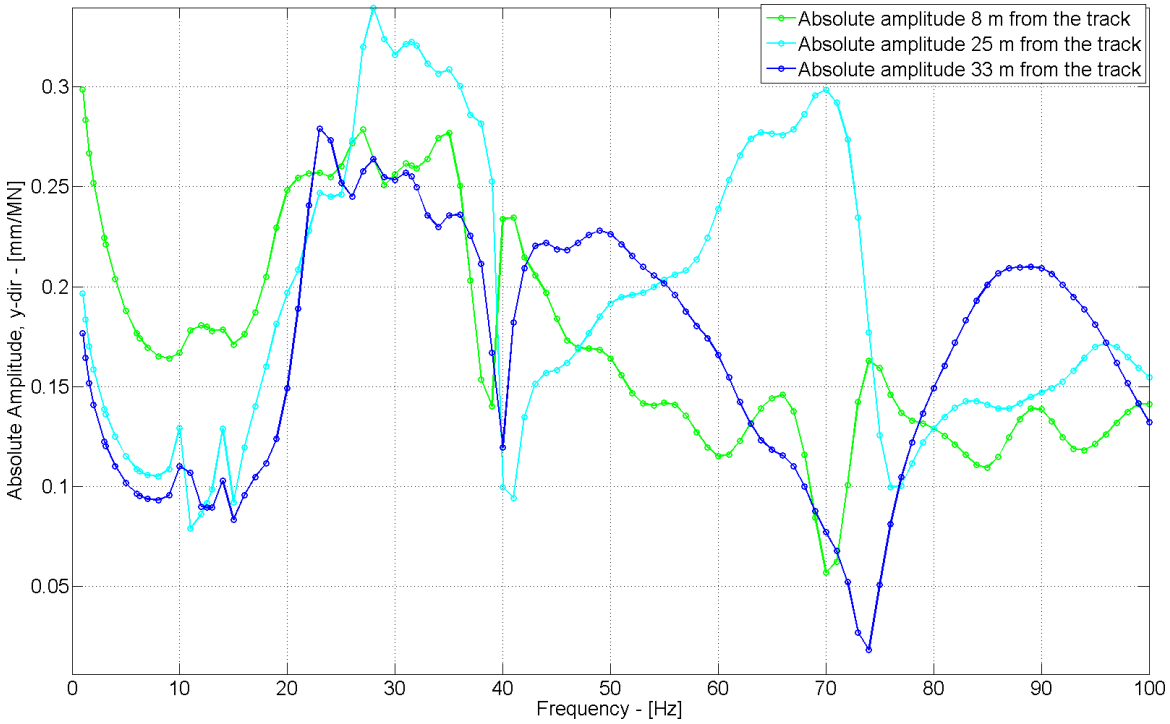

Figure 5.8 – *Absolute amplitudes of soil 1 in the y-direction with structure 1 included in the BE model, at the base of the building (25 and 33m from the track) and at a reference point 8m from the track. The amplitude is given as function of the load application frequency.*

The response of the coupled model seems to decrease at the structures natural frequencies, compared with the response of the uncoupled soil model on Figure 3.10. The decrease occur at 12 and 15, 40 and 74Hz, where the maximum response of the structure is experienced, see Figure 5.10. The decrease can be identified on Figure 5.9, where the response of the uncoupled soil 1 is plotted relative to the coupled response of soil 1 (the combined FE-BE model).

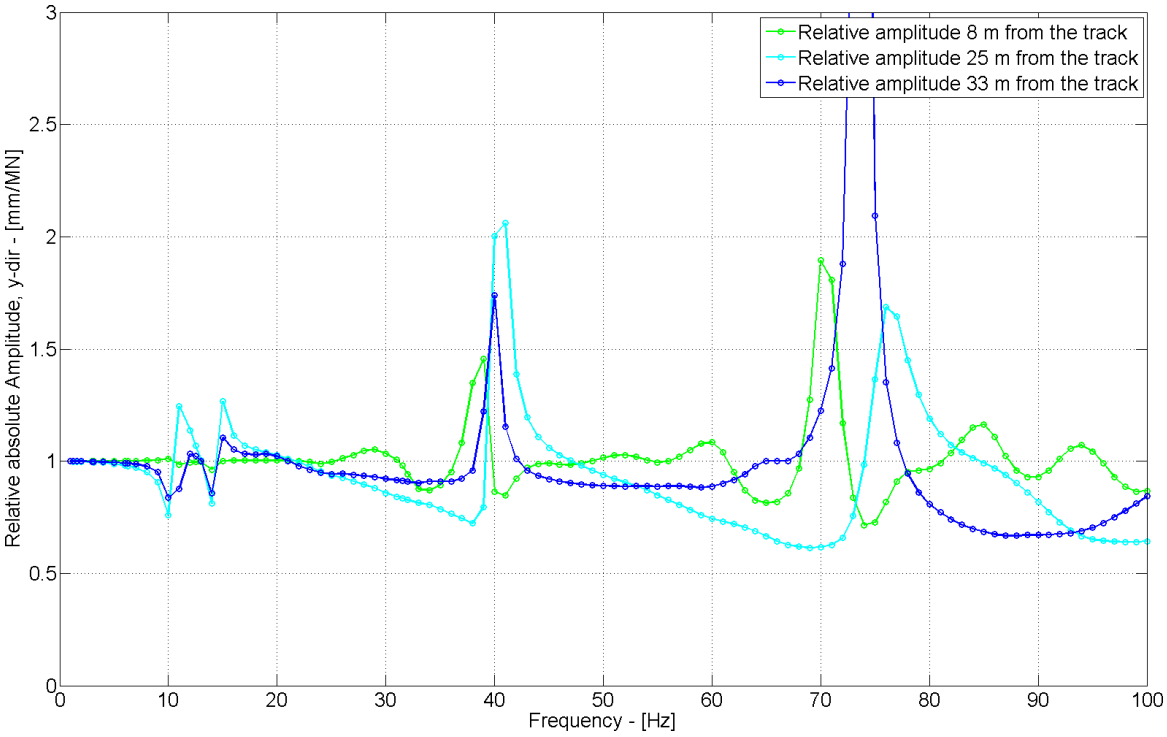

Figure 5.9 *– BE response of soil relative to FE-BE response.*

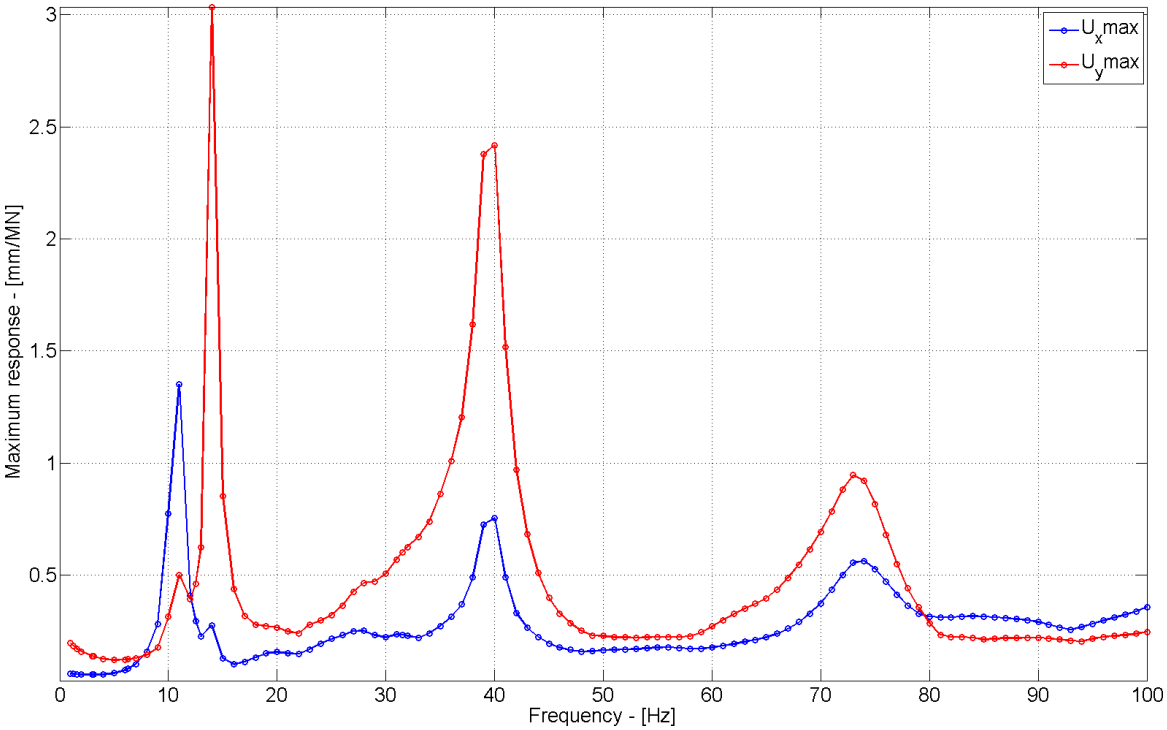

Figure 5.10 *– Maximum response of FE-BE structure 1 on soil 1.*

The sudden drops and peaks observed in Figure 5.9 of the relative soil response occur, since the building is excited at its natural frequency. This means, that the mass of the structure will act as a tuned mass damper, creating a reaction force approximately equal to the excitation load from the soil (with an opposite sign definition), leading to a steady soil response at the natural frequency of the building, as the structure is oscillating on top, see Figure 5.11. This is seen as, the response of the uncoupled soil relatively large, compared with coupled soil. The differences are increasing as the eigenfrequencies increase, since the reaction forces (accelerations) is increasing. The relative soil movements of the uncoupled model are approximately 2 times great at 40Hz, and almost 6 times greater at 70Hz.

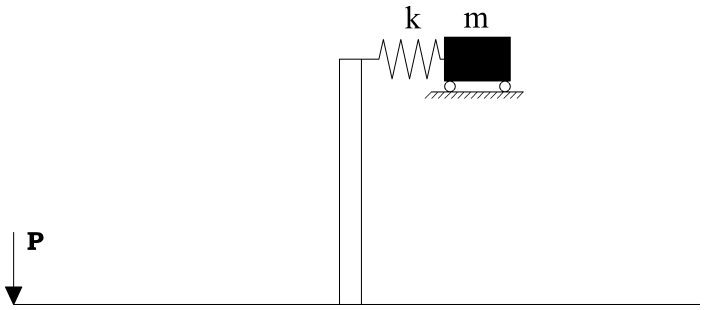

Figure 5.11 – *Principle sketch of tuned mass damper effect. The mass at the top represent the moving structure, creating a steady chimney and hereby a steady soil.*

Before the peaks at Figure 5.9 occur, the relative response is below 1, meaning that the response in the coupled soil model is greater than the response in the uncoupled model. This happens as the phase of the soil and the structure is changing phase (phase shift of π), as the frequency gets closer to the natural frequency of the structure, where the oscillations at the natural frequencies are out of phase, see Figure 5.11.
Another interesting thing observed is the influence of the reference point 8m from the track. Not much disturbance is observed before 25Hz, due to the low acceleration. Here the two model start to drift apart. A large response is observed at the reference point at and around the natural frequencies of the structure, but apart from this, some disturbance is observed at 52Hz and a more noticeable response at 84 and 95Hz. This disturbance could be caused by either constructive or destructive interference, as the reaction forces at the supports of the structure will create reflected waves. The largest deviation between the two models in the reference point, is found at 70Hz, which is an eigenfrequency of the structure, where the response of the uncoupled model compared to the coupled model approach a factor 6.

The acceleration response of the soil is plotted in Figure 5.12.

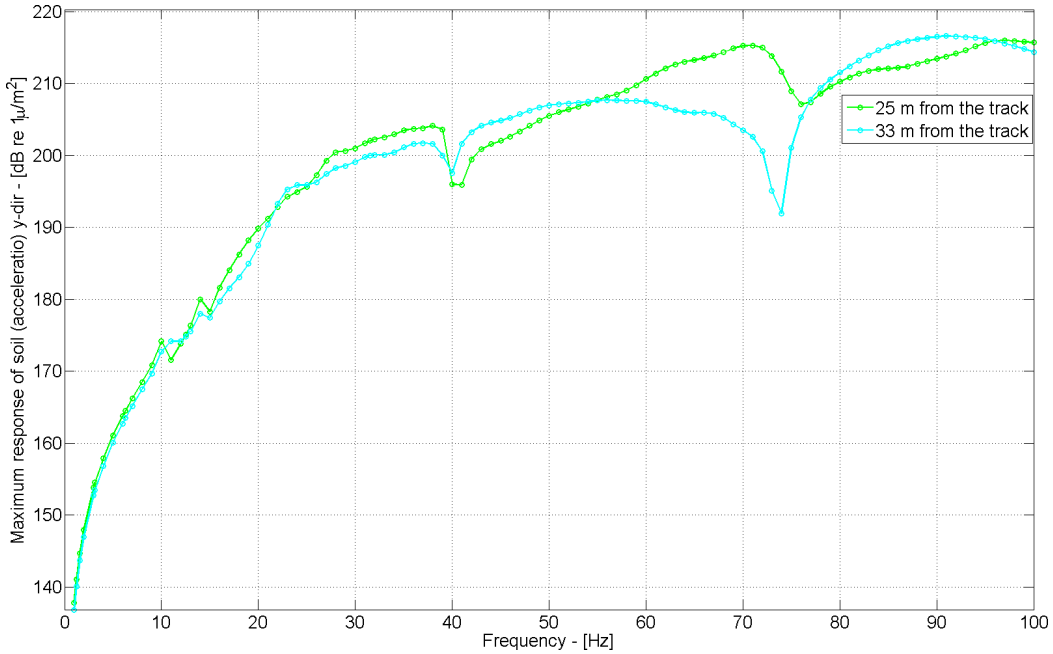

Figure 5.12 – *Acceleration response of soil 1, in the coupled model, with structure 1 on soil 1.*

The same drops in response of the soil is here notices as in Figure 5.8 and Figure 5.9.

Correspondingly the maximum acceleration of the structure will appear as seen in Figure 5.13.

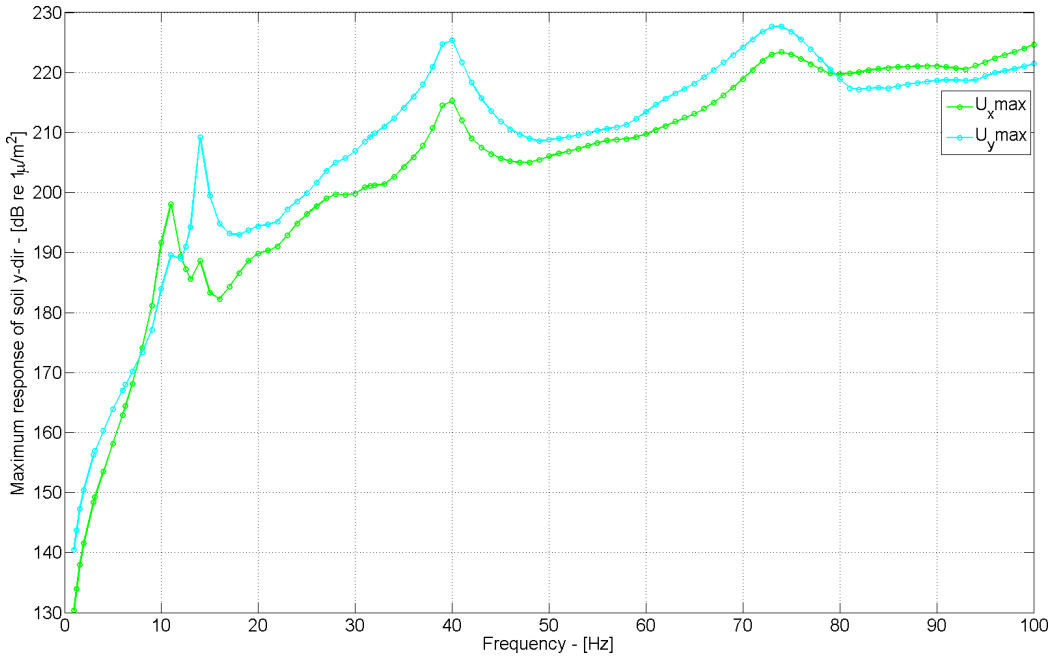

Figure 5.13 – *Acceleration response of structure 1, in the coupled model, with structure 1 on soil 1.*

From Figure 5.13 it is seen, that at the natural frequencies of the structure the building is vibration strongly.

The greater response create a larger reaction force as seen on Figure 5.3, depending on the mode shape.

The peak responses of the uncoupled model, see Figure 4.7, for structure 1 on soil 1, is plotted together with the structural response of the coupled model in Figure 5.14.

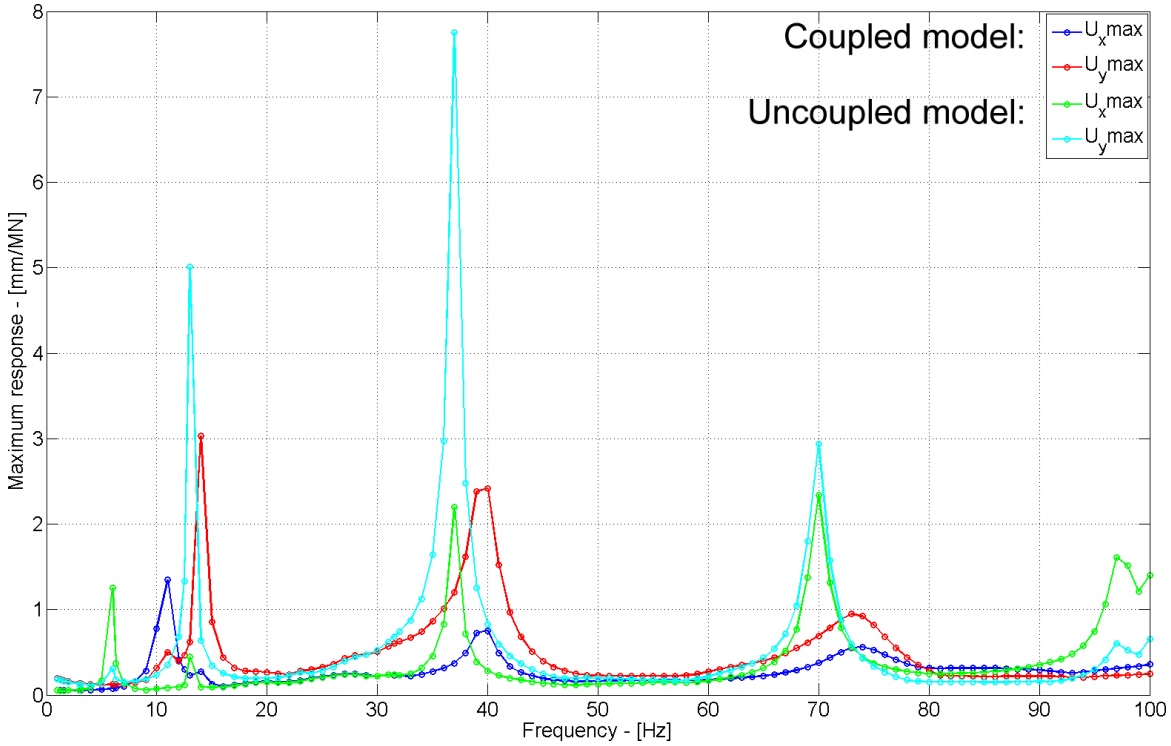

Figure 5.14 – *Maximum response of coupled model, with structure 1 on soil 1 (red and dark blue). Maximum response of uncoupled structure 1 (pinned supports) on soil 1 (green and blue).*

As seen, the peaks are not exactly at the same frequencies, which might be due to deviating boundary conditions. The peaks of the uncoupled structure occur for lower eigenfrequencies, than the peak response experienced by the coupled FE-BE model. The response of the uncoupled (pinned) model is also significantly larger, which again is due to the supports. The peaks of the coupled FE-BE model, occur in agreement with the natural frequencies of the fixed structure, see Table 4.1. This indicates, that the fully connected walls in the coupled BE model, will make the structure act as a fully fixed structure.
In Figure 5.15, the same plot is shown, with the response of the uncoupled structure, where the supports have been fixed (DOF_3 =0; independent of the soil rotation). It is here seen that a much closer fit is obtained.

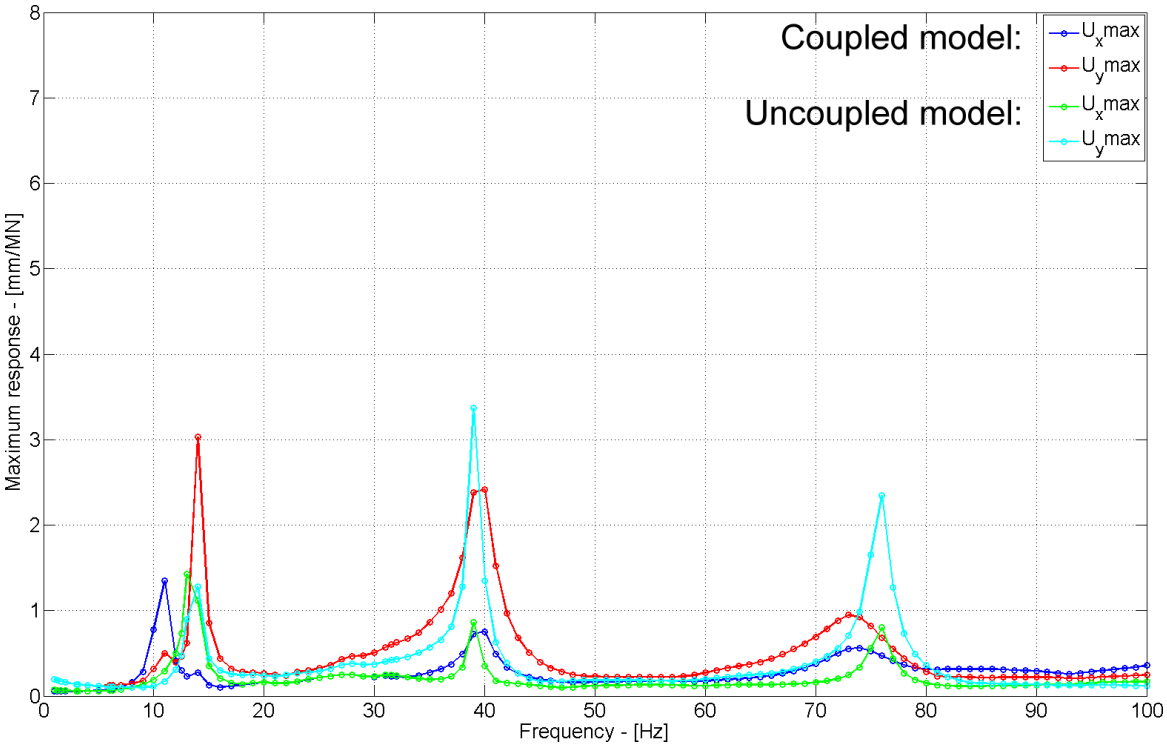

Figure 5.15 – *Maximum response of coupled model, with structure 1 on soil 1, with maximum response of uncoupled structure 1 (fixed supports) on soil 1.*

Not only are the peaks at or near the same frequencies, but the order of magnitude of the response is comparable, which strengthens, that the supports in the coupled model will act as fixed supports.

The coupled structure is now modeled with a modified support, where only a point of the structure is touching the soil. In this way, a charnier is created, and it becomes possible to see if the structure will act as a pinned or as a simply supported structure, see Figure 5.16.

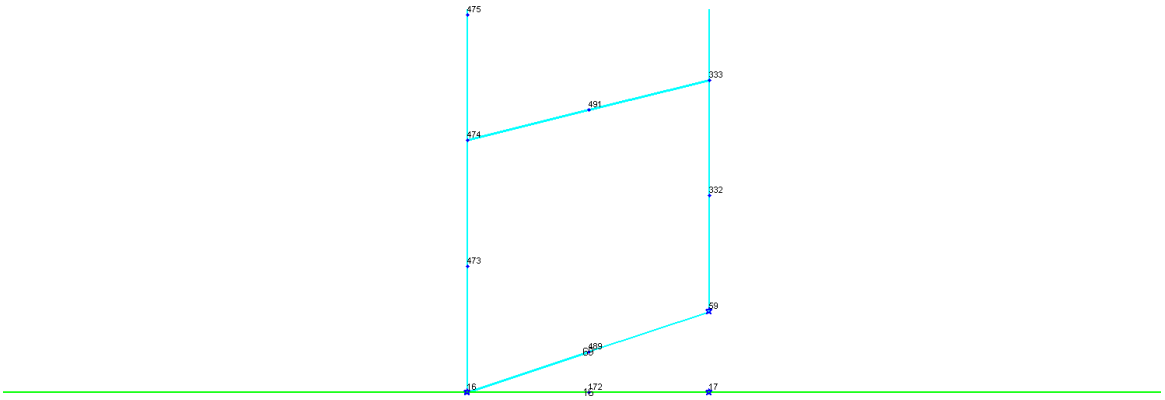

Figure 5.16 – *Illustration of support of building 25m from the track. The corner node in the lower right corner is raised 100mm.*

The response of the coupled FE-BE structure is plotted in Figure 5.17.

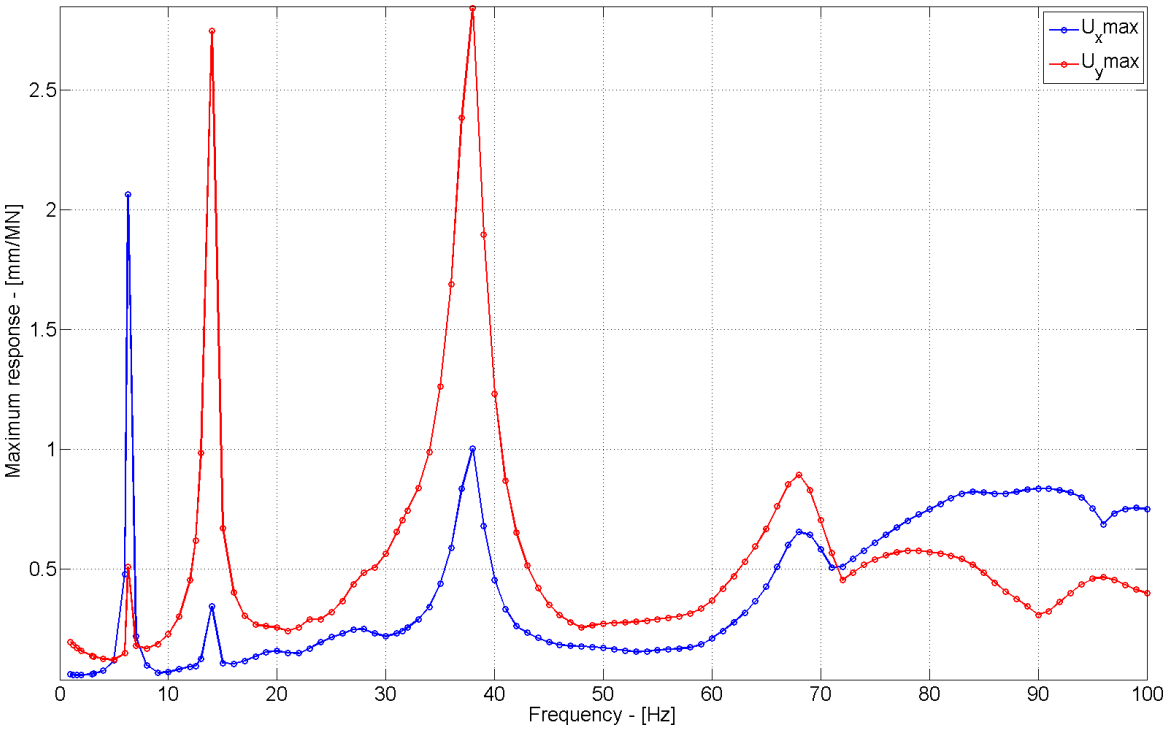

Figure 5.17 – *Maximum response of combined FE-BE structure 1 with charniers in the connections to soil 1*

As seen, the response is peaking at the eigenfrequencies of the pinned structure at the natural frequencies 6, 13, 37 and 70Hz. The coupled structure with charnier at the support, will hereby act as a pinned structure. It is however noted, that the response of the coupled model, is considerably lower, than the uncoupled model. The order of magnitude for the two coupled models with the pinned supports and the fixed supports does not change, while the order of magnitude for uncoupled system drops by a factor 2.

Chapter 6

Conclusion

In this chapter, the findings of this thesis are summarized. The vibrations emanating from passing trains are analyzed in relation to a reference building place 25m from a new planned railway in connection to the planned Femern Belt Link. The amplitudes of the waves are evaluated on two soil profiles, as well as the response of two different structures, with different boundary conditions. The amplitudes are evaluate with respect to distance from the source (the track) to the reference building and frequency of the train load application. Especially the transmission of waves originated in the soil into the reference building is analyzed.

Two different approaches are used to find the response of the soil and the structure; an uncoupled model, with no soil-structure interaction, and a coupled model. The uncoupled model, requires an external finite element model, which is made by the author.
The soil is modeled in an existing two dimensional plane strain boundary element program. In the soil model, deflections are found for a given domain, corresponding to a surface load applied at the railway, imitating the oscillating train load.

The response of the program is validated in a convergence analysis, where the necessary element length for the investigated frequency band is determined; the overall extent of the model is determined, leading to converging accurate results in a limited inner domain, undisturbed by the bounds of the model.
The deflections found in the soil model are used as forced displacements at the supports of the finite element structure in the uncoupled model. In this way, the response of the structure is found with no interaction.
By implementing the finite element model of the building in a combined finite element/boundary element model, the coupling between the soil and the structure is taken into account. In this way, the structure is allowed to interact with the soil, creating reaction forces in return for the displacements, due to the inertia of the building.

By comparing the response of the uncoupled model with the results from the coupled model, it is found, that the reaction forces from the building are balancing the response of the soil around the natural frequency of the building acting as a tuned mass damper system, where the structure is oscillating, while the response of the soil is reduced by up to 80%. However, if the excitation frequency is slightly beside this frequency, the reduction may change to an amplification of the soil response, if the soil and the structure are acting in phase.
Regarding the order of magnitude of the structural response, it is observed that the response first and foremost depend on the support system. Especially a significant change in response is found for the uncoupled FE structure, where the order of magnitude, drops by a factor 2, from the pinned system to the fixed system.

It is found, that it is extremely important to carefully select a reference point, if for instance field measurements should provide estimates of a vibrations level at a certain distance on a specified soil profile. Care most taken, as constructive and destructive interference can create peak responses relatively far away from the track, and large responses will occur at different places, depending on the load application frequency.

Part I

Appendix

Appendix **A**

European railway Map

In Figure A.1, a map of the train speeds used in Europe is shown.

Figure A.1 – *European map of railroad speeds. (Media, 2009)*

Currently the fastest stretch in Europe is between Paris and Strasbourg, where the speed goes towards 350km/h, which is archived by the German Intercity-Express (Wikipedia, 2011a). Among other fast trains operating above 300km/h the French TGV is worth mentioning, which is connecting France to Switzerland, Italy, Germany and Belgium (Wikipedia, 2011b).

Appendix **B**

TEA results files

In the report, five different geometry files are used throughout the report. The geometry files generate a .dat-file, which via the TEA software (*TEA.bat*), is processed into a result file. The different geometry and their corresponding results files (.res), are listed in Table B.1, under the sections where they belong.

Convergence	**analysis**	Geometry file	Results file
	Element length	*geosimmod.m*	*110322geosimmod.res*
			110322geosimmod.res
			110323geosimmod.res
			...
			110323geosimmod_4.res
	Boundary	*geosimmodbc.m*	*110324geosimmodbc.res*
			...
			110324geosimmodbc_2.res
	Boundary (multiple layers)	*geolayfig14.m*	*110507geolayfig14.res*
			110509geolayfig14_4.res
			...
			110509geolayfig14_4.res
BEM			
	Soil 1 (uncoupled)	*geolayfig14.m*	*110531geolayfig14.res*
	Soil 2 (uncoupled)	*geolayfig16.m*	*110530geolayfig16.res*
	Soil 1 (coupled)	*geolayfig14fem.m*	*110605geolayfig14fem.res*
	Soil 1 (coupled (pinned))	*geolayfig14femss.m*	*110605geolayfig14femss.res*

Table B.1 *– Overview of the models used throughout the report.*

Both the geometry files and the TEA program, can be found in the main MatLab folder on the Appendix CD. Here the data file (.dat) as well as the results file (.res), will be acceable in the sub-directory "data".

Bibliography

Andersen, **2006**.
Lars Andersen.
Linear Elastodynamic Analysis.
Department of Civil Engineering, Aalborg University, 2006.

Andersen, **2010**.
Lars Andersen.
Vibrationer fra jernbane til den ny Femern Bælt forbindelse.
Aalborg University, 2010.
DCE Contract Report No. 98.

C. J. C. Jones, **1999a**.
D. J. Thompson & M. Petyt C. J. C. Jones.
TEA - A Suite of Computer Programs for Elastodynamic Analysis Using Coupled Boundary and Finite Elements.
University of Southhampton, 1999a.
Institute of Sound and Vibration Research - Technical Memorandum No. 844.

C. J. C. Jones, **1999b**.
D. J. Thompson & M. Petyt C. J. C. Jones.
Ground-borne Vibration and Noise from Trains: Elastodynamic Analysis using the Combined Boundary Element and Finite Element Methods.
University of Southhampton, 1999b.
Institute of Sound and Vibration Research - Technical Memorandum No. 840.

Clausen, **2009**.
Johan Clausen.
Finite Element Analysis.
http://people.civil.aau.dk/~i5jcc/7sem_finite_element/lecture_notes/FEAI_lec3_4.pdf, 2009.
Lecture notes, Downloaded: 19-05-2011.

DSB, **2011**.
DSB.
Intercity-Express.
DSB, http://www.dsb.dk, 2011.
Downloaded: 01-06-2011.

F. Kirzhner, G. Rosenhouse, **2005**.
Y. Zimmels F. Kirzhner, G. Rosenhouse.
Attenuation of noise and vibration caused by underground trains, using soil replacement.
Science Direct, 2005.

Media, **2009**.
Bernese Media.
High Speed Railroad Map Europe 2009.
Wikipedia, http://upload.wikimedia.org/wikipedia/commons/9/9f/High_Speed_Railroad_Map_Europe_2009.gif, 2009.
Downloaded: 19-05-2011.

Nielsen, **2004**.
Søren R. K. Nielsen.

Vibration Theory, Vol. 1.
Aalborg Teknisk Universitetsforlag, 2004.

Ottosen and Petersson, 1992.
Niels Ottosen and Hans Petersson.
Introduction to the finite element method.
ISBN: 0-13-473877-2. Prentice Hall International, 1992.

P. Galvín, 2007.
J. Domínguez P. Galvín.
High-speed train-induced ground motion and interaction with structures.
Science Direct, 2007.

Robert D. Cook, David S. Malkus and Witt, 2002.
Michael E. Plesha Robert D. Cook, David S. Malkus and Robert J. Witt.
Concepts and applications of finite element analysis.
ISBN: 978-0-471-35605-9. Wiley, 2002.
Fourth edition.

Wikipedia, 2011a.
Wikipedia.
Intercity-Express.
Wikipedia, http://en.wikipedia.org/wiki/InterCityExpress, 2011a.
Downloaded: 19-05-2011.

Wikipedia, 2011b.
Wikipedia.
TGV.
Wikipedia, http://en.wikipedia.org/wiki/TGV, 2011b.
Downloaded: 19-05-2011.

X. Sheng, C.J.C. Jones, 2003.
D.J. Thompson X. Sheng, C.J.C. Jones.
A comparison of a theoretical model for quasi-statically and dynamically induced environmental vibration from trains with measurements.
Science Direct, 2003.